Title
Genetic analysis of morphological and functional synpase growth at the Drosophilia NMJ

Author
Heckscher, Elizabeth

Publication Date
2007-04-02

Peer reviewed|Thesis/dissertation

Genetic analysis of morphological and functional synapse growth

at the Drosophila NMJ

By

Elizabeth Heckscher

DISSERTATION

Submitted in partial sastisfaction of the requirement for the degree of

DOCTOR OF PHILOSOPHY

in

Cell Biology

in the

GRADUATE DIVISION

of the

UNIVERSITY OF CALIFORNIA, SAN FRANCISCO

ACKNOWLEDGEMENTS

My dissertation is dedicated to my late father, Ledyard Heckscher II.

I would like to thank my family for their love and support. Pips, Pants and Chris—I love you! Interactions and scientific discussions with Anne Wehman, Max Heiman and Peter Clyne helped shape me as a scientific thinker and as a person. In addition, I'd like to acknowledge my thesis committee, Rob Edwards, Holly Ingraham, and Cori Bargmann as well as my thesis advisor, Grae Davis. Finally, I would like to thank the following people for technical assistance: Gama Ruiz, Gina Vittore, Mollie Biewald, Kurt Marek, Rick Fetter, Jack Roos, Emit Jolly, Ben Eaton, Kira Poskanzer and Stephanie Albin.

ABSTRACT

Genetic analysis of morphological and functional synapse growth

at the Drosophila NMJ

Elizabeth S. Heckscher

Advisor: Graeme Davis, Ph.D.

Nerve cells contact each other at synapses and communicate via synaptic transmission. Once they form synapses are not static, but continue to grow during development, plasticity and disease. Combining genetic and cell biological tools at the Drosophila neuromuscular junction (NMJ), I isolated a number of mutations and signaling pathways regulating morphological and functional synapse growth. In my introduction I define the terms morphological and functional synapse growth as well as review our current knowledge of these topics. In the first chapter, I characterize the *nerve-wracked* mutation, which disrupts synaptic bouton formation. Second, I describe *bad hair day*, a novel gene encoding a chromatin-remodeling factor that is involved in suppression of satellite bouton formation. Next, I demonstrate that the Drosophila NF-kappa B pathway regulates GluR abundance via a novel, cytoplasmic mechanism. Finally, I suggest that cytoplasmic NF-kappaB/Dorsal acts upstream of Pelle kinase, which regulates insertion of GluR into the synaptic membrane. These findings reveal some of the molecular mechanisms in place during synapse growth, and may have implications for understanding synaptic plasticity and disease.

TABLE OF CONTENTS

List of Tables

List of Illustrations

INTRODUCTION

The brain is composed of individual nerve cells, interconnected into networks of communicating neurons that ultimately construct perception and action. A first step to understand the brain is to study how neurons are organized and how they communicate. Nerve cells are connected to each other via synapses and signal to each other using synaptic transmission. In general a synapse consists of a presynaptic, neuronal axon terminal apposed to a postsynaptic cell, (e.g. a neuron, in the central nervous system (CNS), or a muscle, in the peripheral nervous system). A model synapse is the neuromuscular synapse of the Drosophila larval neuromuscular junction (NMJ). This synapse is a typical chemical synapse: a cleft separates the neuron and muscle. Communication between these cells is initiated after an electrical potential travels down the presynaptic axon, leading to the release of neurotransmitter. The neurotransmitter in the cases of the Drosophila NMJ and vertebrate CNS is glutamate. It diffuses across the synaptic cleft and binds to glutamate receptors on the postsynaptic muscle membrane. Upon binding to glutamate the receptors open, allowing an electrical current to flow. If enough current passes across the membrane, the sarcoplasmic reticulum releases calcium causing the muscle to contract; through coordination of many such contractions the larva crawls.

Once they form most synapses are not static but continue to grow during development and plasticity. The Drosophila NMJ serves as an example of this phenomenon. During embryonic stages, which in Drosophila are characterized by rapid patterning in the absence of growth, synapses form (Budnick et al., 1990). Initially glutamate receptors are expressed homogeneously on the muscle surface (Broadie and Bate, 1993a, 1933b, Saitoe et al., 1997). Nerve contact and neuronal activity induces

rapid clustering of receptors at the site of inneravation, followed by synthesis and insertion of new synaptic receptors (Broadie and Bate, 1993a, 1933b, Saitoe et al., 1997). Within hours of the initial contact between the motoneurons and the proper muscle target, the motoneuron's axonal growth cone transforms into a synaptic bouton (Rheuben et al., 1999; Schuster et al., 1996b; Yoshihara et al., 1997). A bouton, the fundamental unit of any synapse, is a swelling of the neuronal membrane that contains the cellular machinery needed for release of neurotransmitter; this includes mitochondria, glutamate-filled synaptic vesicles, and active zones, the sites at which synaptic vesicles fuse with the plasma membrane and release glutamate. At the end of embryogeneis all of the NMJ's synapses are fully formed and fully functional. In Drosophila, almost all of the animals' growth occurs during larval stages. Consequently once formed, the synapses of the Drosophila NMJ continue to grow throughout larval development (Atwood et al., 1993; Schuster et al., 1996b; Zito et al., 1999). The Drosophila larval NMJ is a system ideally suited for studies of synaptic growth, and indeed in studying this system much progress has been made in elucidated the molecular mechanisms controlling synaptic growth.

Morphological Synapse Growth

Fruit flies grow rapidly during the four days of larval development. By the end of the third and final larval instar body wall muscles have increased an approximate100 fold in surface area (Atwood et al., 1993). The basic morphological shape of the synapse, which is relatively invariant, is laid down at the start of the first larval instar (Zito et al., 1999; Rasse et al., 2005). And this morphological shape does not vary greatly between first and third larval instars despite a large increase in morphological synapse growth.

Boutons increase in size (~20-fold increase in bouton surface area), and boutons are added to the synapse (~10-fold increase in bouton number) (Schuster et al., 1996b). As the muscle grows, boutons stretch apart and new boutons insert between them, or boutons are added to the end of a string of boutons. In addition, new branches can form when more than one bouton buds off from an existing bouton (Zito et al., 1999). Using the Drosophila NMJ as a model synapse, molecular studies have revealed three distinct cellular mechanisms involved in regulation of morphological synapse growth.

Promoting synaptic growth—communication from neuron to muscle

Because motoneuron targets are continuously growing, synapses are structurally plastic, undergoing constant expansion. This kind of structural plasticity can be regulated by neuronal activity. The first clue that this was the case came from studies of mutants with altered neuronal activity that identified a correlation between increased activity and morphologically larger, more complex synapses (Budnik et al., 1990). Now a molecular network of three proteins, CaMKII, Dlg and FasII are thought to link increased neuronal activity to morphological synapse growth. A general model can be drawn as follows: Due to increased neuronal activity, there is increased calcium influx into the postsynaptic muscle. Ca 2+/Calmodulin-Dependent Protein Kinase II (CaMKII) relays these changes by phosphorylation of target substrates. One such substrate is a postsynaptic, scaffolding molecule, Discs large (Dlg) (Lahey et al., 1994, Kho et al., 1999). Dlg binds to, and regulates the abundance of a cell adhesion molecule, FasII (Thomas, et al. 1997). FasII, which is both necessary and sufficient to cause increases in bouton number, is downregulated (Schuster et al., 1996b), and indeed, such a downregulation is detected in activity mutants (Schuster et al., 1996a). In addition, Dlg is required during normal

development to determine the synaptic size (Guan et al., 1995). Thus, not only is this the mechanism by which structural plasticity is achieved in activity mutants, it is also likely to be a mechanism by which structural plasticity is achieved in normally developing synapses.

Promoting synaptic growth—communication from muscle to neuron

TGFβ/BMP signaling positively regulates synaptic growth. In addition, one attractive hypothesis is that BMP acts as retrograde signaling system: emanating from the muscle, causing the synapse to grow. A general molecular model for such as system follows: The BMP ligand, Glass bottom boat (*gbb*) is thought to be the retrograde signal that passes from muscle to neuron (McCabe et al., 2003). Gbb is received in the muscle by Wishful thinking (*wit*), a type II BMP receptor (Aberele et al., 2002; Marques et al., 2002), in association with a type I receptor, in this case either Thickviens of Saxophone (Sweeney et al., 2002; Rawson et al., 2000). Ligand binding initiates intracellular signaling that is mediated by the SMAD proteins, Mothers against dpp and Medea (Rawson et al., 2002; McCabe et al., 2004). These intracellular signaling molecules are transported to the nucleus by the Dynactin complex, which mediates cargo binding to the molecular motor Dynein (Eaton et al., 2002; McCabe et al., 2003). Presumably once in the nucleus, these proteins initiate a transcriptional program necessary synaptic growth. Failure to attenuate the TGFβ pathway can lead to overgrown synapses (Sweeney et al., 2002; McCabe et al., 2004). For example, mutation of the TGFβ inhibitor, Daughters against dpp results in synaptic overgrowth (Sweeney et al., 2002). In addition, the late endosome/lysosomal protein, Spinster (*spin*) is thought to shut off TGFβ signaling, and perturbation of *spin* causes synaptic overgrowth (Sweeney et al., 2002). Thus, the TGFβ

pathway is both necessary and perhaps sufficient to promote morphological synapse growth.

Inhibiting synaptic growth

Ubiquitination in the neuron is required to downregulate signals that promote synaptic growth. This has been shown in variety of ways including neuronal overexpression of deubiquitnating enzymes, such as Fat facets and UBP2 (DiAntionio, et al., 2001). Attention was initially focused on ubiqutination when mutations in *hiwire* were identified in a two-part screen that assayed walking behavior and neuromuscular anatomy (Wan et al., 2000). *hiwire,* a putative E3 ubiquitin ligase, is required in the neuron to negatively regulate synaptic growth (Waikar et al., 2005). This finding lead to the hypothesis that Hiw degradaded a growth-promoting signal, and to the search for the singal regulated by *hiw*. For example, a genetic suppressor screen identified *wallenda* as the target for *hiw* in morphological synapse growth. Identification of *wallenda*, which encodes a MAPKKK homologous to vertebrate DLK and LZK, upstream of JNK and Fos (Collins et al., 2006), demonstrated that MAPK signaling is involved in synaptic growth. This MAPK pathway, however, is not the only target of ubiquitination in the neuron. Mutations that perturb another E3 ubiquitin ligase, Anaphase Promoting Complex (APC) also lead to synaptic overgrowth (van Roessel et al., 2004). Although the growth-supressing activity of the APC is presynaptic, the APC targets are thought to be distinct from those regulated by *hiwire* (van Roessel et al., 2004). Thus, downregulation of a variety of signaling pathways by ubiquitination balances the action of growth-promoting pathways at the NMJ (McCabe et al., 2004).

Open questions

Although there has been much progress in understanding the pathways involved in regulation of morphological synapse growth, there are still a large number of questions about the pathways highlighted above. For example, although regulation of FasII is both necessary and sufficient to drive synapse growth, how does manipulating the levels of a cell adhesion molecule translate into altered synapse size? If Gbb represents a retrograde signal coming from the muscle signaling neuronal growth, then what regulates gbb expression? When Smad transcription factors enter the nucleus, what proteins do they interact with to find genetic targets specific for neuronal growth, and what are those the downstream genes? For ubiqitination, what regulates the expression or activity of ubiquitin ligases? In addition, there are a number of more general questions about synapse growth for which we do not yet have answers. Have we identified all of the growth programs, or do more exist, perhaps a hormonal signal acting as a global regulator for animal growth? How are all of the growth-regulating pathways intertwined? How is stereotyped synapse morphology maintained in the face of such a large amount of synaptic growth? Growth cones are guided by soluble guidance factors, and the extracellular environment; are there analogous diffusible or substrate cues that guide morphological synapse growth?

Functional Synapse Growth

As the muscle grows the synapse must keep pace, both morphologically and functionally, and morphological synapse growth occurs concurrently with functional synapse growth. Conceptually, functional synapse growth could occur either by

increasing the amount of neurotransmitter released from the presynaptic neuron, or by increasing the sensitivity of the postsynaptic muscle to neurotransmitter release. Both occur at the NMJ over larval development. Increased neurotransmitter release is accomplished by increasing the number of active zones; between synapse formation and late third instar there is an approximate 200-fold increase in number of presynaptic neurotransmitter release sites (about 20-fold increase in active zones per bouton together with a 10-fold increase in bouton number) (Schuster et al., 1996b). At regularly spaced intervals, apposing active zones GluR clusters are inserted into the postsynaptic muscle membrane (Atwood, et al., 1993; Rasse et al., 2005); during larval development insertion of a GluR cluster may actually precede the development of a new active zone (Rasse et al., 2005). Increased sensitivity to neurotransmitter release occurs by increases in size, and possibly density, of glutamate receptor clusters (Saitoe et al, 1997). Newly formed GluR clusters continue to grow until they reach a particular size, but then the individual cluster size platoes (Rasse et al., 2005). Of note is that many studies have used fluorescent microscopy measuring GluRIIA abundance, and electrophysiology monitoring the muscles' response to release of a single synaptic vesicle. Although these assays do not distinguish between insertion of new active zones apposed by new GluR receptor clusters, growth of existing GluR clusters, or changes in GluR receptor density within clusters, overall they can be used as a postsynaptic read out for functional growth.

Translational control of synaptic GluR abundance

One mechanism involved in regulation of synaptic GluR abundance is local translation. Large aggregates of eIF4E, the translation initiation factor, and poly(A) binding protein (PABP) as well as GluRIIA mRNA were found in a subsynaptic

compartment of the NMJ (Sigrist et al., 2000). Genetic manipulations that increase the aggregates of eIF4E and PABP correlate with increases in synaptic GluRIIA abundance and basal synaptic transmission (Sigrist et al., 2000; Sigrist et al., 2003; Menon et al., 2004). In addition, one study, which correlated the amount of larval locomotor activity with increased numbers of eIF4g aggregates, showed that this manipulation resulted increased numbers of GluR clusters. Many studies of the initial GluR clustering event during synaptogenesis in the embryo demonstrate that neuronal activity is required for this process (Broadie and Bate, 1993; Saitoe et al., 1997). Thus, it is tempting to speculate that neuronal activity via local translation acts in as positive regulator of GluR abundance during larval development.

Coordinate regulation of functional synaptic growth with postsynaptic development

As functional growth occurs over larval development, specifically increasing GluR abundance and active zone size, other aspects of the postsynaptic specializations develop. For example, at the beginning of first instar the muscle membrane apposing synaptic boutons begins to infold, and by the end of the third instar it is a highly reticulated structure called the subsynaptic reticulum (SSR) (Guan et al., 1996, Schuster et al., 1996b). What are the molecular mechanisms which control each of these aspects of growth, and how are this growth coordinately regulated? Molecules have been identified that individually regulate either active zone size, such as the receptor tyrosine phosphotase, Dlar and its intracellular effector, Dliprin (Kaufmann et al., 2002), or SSR development, such as Dlg (Lahey et al., 1994). Coordinate regulation of GluR abundance, and SSR development can be mediated by dPix. *dPix*, encoding a rho type guanine nucleotide exchange factor, was recovered in a screen for genes controlling

synaptic structure (Parnas et al., 2001). In *dPix* mutants the SSR is almost completely lacking, and GluR abundance is significantly reduced; however, active zone size is normal (Parnas et al., 2001). dPix largely exerts its effects through p21 associated kinase (Pak), which it localizes to synapse (Parnas et al., 2001). Pak is involved in coordinating postsynaptic development because signaling diverges downstream of Pak. Through physical association with the adaptor protein, Dreadlocks (Dock), Pak control GluRIIA abundance; however, mutation of *dock* has no effect on SSR development (Albin et al., 2004). The dPix/pak/doc pathway is only one mechanism by which functional synaptic growth is coordinated with other aspects of postsynaptic development. Thus, there are molecular pathways that individually regulate functional synapse growth and act to coordinately regulate this growth with other aspects of postsynaptic growth.

Questions

Although there has been some advancement our understanding of functional synapse growth, surprisingly little is understood about this fundamental aspect of synapse biology. For the molecular pathways and mechanism identified thus far there are a large number of important and outstanding questions. For example, does neuronal activity regulate local translation, and if so, how? Are the mechanisms used to create active zones and GluR clusters during synaptogenesis the same mechanisms that are used later during synapse growth? Thus far the dPix/Pak/Dock pathway is the only intracellular signaling cascade that is know to regulate GluR abundance; Dock is usually associated with a receptor tyrosine kinase,-- what is the idenity of such a receptor and its ligand? In addition, what the downstream molecular targets of Pak-mediated phosphorylation and what cellular process are consequently impacted to regulate GluR cluster abundance? In

addition there are a host of fundamental phenomenonological questions for which we do not yet have answers. For example, we know that GluR cluster size increases over development; does the size of active zones also increase? Does the density of GluR within a cluster change over development? Are there pathways that act to specifically regulate GluRs without changing other aspects of development? And finally how are morphological and functional synapse growth related and coordinately regulated?

Overall the ultimate goal, in understanding the brain is to link molecular regulation of individual nerves, to changes in neuronal networks and then to relate this to observable behavior. The Drosophila NMJ has been a useful model system to characterize some of these links. In the next chapters I present the work that I have done during my Ph.D., which represent a few small steps towards attaining this ultimate goal.

CHAPTER ONE

nerve-wracked perturbs syanaptic bouton formation: links between synaptic growth and nuclear hormone receptors

Elizabeth S. Heckscher, Richard D. Fetter, Jack Roos, and Graeme W. Davis

SUMMARY

All chemical synapses, including the Drosophila neuromuscular junction, are organized into boutons. Boutons are varicosities in the neuronal membrane that contain synaptic vesicles and active zones. We have isolated a mutation, *nerve-wracked (nwak)* in which the synapse is not organized into boutons. Specifically, bulging varicosities of the neuronal membrane are lacking, and rather than concentrated into boutons presynaptic proteins are diffusely localized throughout the synapse. In addition, postsynaptic glutamate receptor clusters underlie the entire synapse rather than localizing beneath distinct bouton structures. Perhaps as a secondary consequence to lack of synaptic boutons, *nwak* synapses are significantly overgrown. *nwak* is caused by insertion of *EP(2)2490* into a putative regulatory region *DHR39*, and this insertion causes upregulation of *DHR39*. Analysis of *DHR39* null mutants, show no synaptic phenotype; however a closely related hormone receptor, FTZ-F1 is required for synaptic growth. Taken together these data begin to relate synaptic growth and morphogenesis to nuclear hormone receptor function.

INTRODUCTION

Communication between neurons and target cells, e.g. other neurons, muscles, occurs at chemical synapses. Although size and strength varies among different types of chemical synapses, one characteristic feature of synapses that they are organized into boutons (Rollenhagen and Lubke, 2006). Boutons are swellings of the neuronal membrane that contain mitochondria, neurotransmitter-filled synaptic vesicles, and active zones (Figure 1A, D). Despite the fact that boutons are the fundamental organizational unit of the synapse, there is a paucity of information about the molecular mechanisms used in bouton formation.

The Drosophila neuromuscular synapse is a genetic model system, ideally suited for study of synaptic bouton morphogenesis. As development proceeds, a growth cone transforms into a mature neuromuscular synapse in a process that involves the formation of boutons (Broadie et al., 1993, Schuster et al., 1996). Synaptic boutons are added to the growing neuromuscular synapse, and existing boutons expand in size as new active zones are inserted into the presynaptic membrane (Zito et al., 199). By the third larval instar each synapse is composed of 40-100 boutons, which can be easily visualized by fluorescent confocal microscopy (Johansen et al., 1989, Keshishian et al., 1996). At the Drosophila neuromuscular junction (NMJ) membrane associated markers highlight varicosities in the neuronal membrane, each of which is a bouton. Synaptic vesicle associated proteins and periactive zone proteins are concentrated into these bouton structures, while the same proteins are largely absent from interbouton spaces within the synapse. Using these characteristic features of a bouton, we show that the mutant, *nerve-wracked, (nwak)* has a profound disruption of normal bouton development.

On a molecular level *nwak* seems to be associated with misregulation of a nuclear hormone receptor, Drosophila Hormone Receptor 39 (DHR39). DHR39 (also called FTZ-F1beta) expression and biochemical activity have been characterized. In embryos *DHR39* is expressed in many regions including the ventral chord and brain (Ohno and Petkovich, 1992); in larva DHR39 is regulated by the insect molting hormone, ecdysone (Horner et al., 1995, Heut et al., 199e), and in the third larval instar DHR39 comes on only late in this developmental stage (Horner et al., 1995). Biochemical analysis of DHR39 shows that it binds to FTZ-F1 binding sites (Ohno et al., 1994, Horner et al., 1993), where it acts as a repressor of transcription (Ayer et al., 1993, Ohno et al., 1994). Another nuclear hormone receptor, FTZ-F1, which is closely related to DHR39, binds to FTZ-F1 binding sights and activates transcription (Ayer et al., 1993, Ohno et al., 1994). Thus, it is hypothesized that FTZ-F1 and DHR39 act antagonistically to regulate gene expression of common target genes. Although DHR39 has been characterized on the molecular and biochemical levels, there are no known phenotypes associated with loss of function mutations in *DHR39* (Horner and Thummel, 1997). I find that a published null mutation in *DHR39* has no obvious synaptic phenotypes, but has severe axon pathfinding defects. In addition I show that FTZ-F1 is required for normal synaptic growth. These data establish a role for the nuclear hormones, DHR39 and FTZ-F1 in the development of the Drosophila nervous system.

Lack of Synaptic Boutons in *nerve-wracked*

nerve-wracked (*nwak*) mutants have a striking and dramatic phenotype: lack synaptic boutons. Lack of presynaptic bouton structure can be seen at the light level using markers, which are usually confined to boutons, such as a synaptic vesicle associated protein, Cystine String Protein (CSP) and a periactive zone marker, Dynamin Assoicated Protein 160 (DAP-160). In controls, staining is concentrated into boutons and is absent from interbouton regions (Figure 1B, top panels). In *nwak*, however, there is an even distribution of staining throughout the synapse, as if there is no distinction between bouton and interbouton regions (Figure 1B, bottom panels). Next, to visualize the contours of the presynaptic membrane, I stained with a cell adhesion molecule, Fasiclin II (FasII). Using this method, varicosities in the neuronal membrane are easily identified in controls (Figure 1C, left panels, yellow arrow). In contrast, in *nwak* synapses, FasII staining shows a wide, flat, almost two-dimensional neuronal contour (Figure 1C, right panels). To confirm these observations, we preformed electron microscopy (done by Rick Fetter). We find that wild type synapses contain large neuronal varicosities (Figure 1D left panel), which are lacking in *nwak* synapses (Figure 1D right panel). Thus we see lack of bouton structure using both light and electron microscopy. Finally, we visualized the distribution of active zones, by muscle expression of a myc tagged glutamate receptor, which apposes presynaptic sites of release. In wild type we see myc stained GluR clusters grouped beneath presynatpic boutons (Figure 2A, gray bars). In contrast, in *nwak*, the GluR clusters are smaller, more numerous and no longer grouped beneath

boutons (Figure 2B,C). Taken together these data demonstrate that in *nwak* mutants the fundamental organizational unit of the synapse, boutons are disrupted.

In addition to of lack of synaptic boutons, *nwak* synapses are overgrown. *nwak (EP(2)2490)* synapses usually appear in one of two morphologies: a long unbranched synapse (Figure 3A-B), or an unbranched synapse with several finger like projections coming off the distal end of the synapse (Figure 3C, D). In either configuration, *nwak* mutants are overgrown (Figure 2E). In addition *nwak* synapses have lower average fluorescence of synaptic antigens including DAP-160 (wild type = 85+/-2.6, *nwak* = 42 +/- 1.2 relative fluorescence units) and the synaptic vesicle marker, Synapsin (data not shown). This is consistent with the paucity of synaptic vesicles seen ultrastructurarlly (Figure 1D, right panel). One possible explanation for this observations is that total amount of synaptic protein could be similar between wild type and *nwak;* however, in *nwak* these proteins may be distributed diffusely over a longer synapse, giving the appearance of lower fluorescence. It is an open and interesting question to determine whether synaptic overgrowth is a secondary consequence of lack of synaptic boutons.

To determine whether the *nwak* mutation was of any consequence to the overall health of the animals, I examined survival of *nwak* mutants in comparison to controls. While 99% of control larvae (wild type n=251) reached third instar, only 67% of *nwak* larvae were at the same developmental time point (*nwak* n=260). When examining survival to adulthood, I find16% lethality in wild type versus 41% lethality in *nwak* mutants. Thus, although *nwak* animals are homozygous viable, they are not as healthy as wild type counterparts. Again it would be interesting to know whether this is a consequence of lack of synaptic boutons or due to another aspect of the *nwak* phenotype.

Next, I asked whether there was an embryonic phenotype associated with *nwak*, by examining motoneuron axon pathfinding. Staining with FasII in wild-type at stage 17, highlights the segmental nerves (SN) including SNb, which branches into three distinct paths (Figure 4A, and B blue arrows). At the same stage in *nwak* embryos, however, I see two phenotypes: either the axons fail to grow out along the right path (as in the left most segment, Figure 4C), or the axons overshoot their targets (as in the central segment, Figure 4C). These embryonic defects are presumably corrected later in development, because by third instar each muscle is enervated by motoneurons. Taken together, these analyses demonstrate that in *nwak* neuronal development is affected in both embryonic and larval stages.

As a side note *nwak* was originally pulled out of a screen looking for molecules that interfere with the process of synaptic homeostasis (Davis et al., 1996, Davis 2006, Petersen et al., 1997). I asked why *nwak* was isolated in this screen. The screen was based on synthetic lethal interactions between EP elements (Rorth et al., 1998) and a genetic background in which homeostatic compensation had been triggered (Davis et al. 1998). It is likely that *EP(2)2490* (*nwak*) was not synthetically lethal, rather just lethal with the driver used in this screen (G14, Table 1), and therefore represented a false positive result. In addition, experiments with *EP(2)2490* in other genetic backgrounds in which homeostatic compensation had been triggered (Paradis et al., 2001) showed no role for *EP(2)2490* in regulation of synaptic homeostasis (data not show).

Molecular Analysis of *nwak* Reveals an Upregulation of *DHR39* in *EP(2)2490*

Next I turned to a molecular analysis *nwak*. Two lines of evidence show that *nwak* phenotypes are caused by the insertion of an EP element, *EP(2)2490* into chromosome 2R. First, even after 15 generations of outcrossing to wild type, *nwak* phenotypes are associated with *EP(2)2490*, showing a strong correlation between this P-element insertion and the *nwak* phenotype. Second, precise excision of *EP(2)2490* reverts the *nwak* to wild type (*EP(2)2490*^{21}, done by Jack Roos, data not shown), showing that insertion of *EP(2)2490* causes *nwak* phenotypes.

EP(2)2490 sits in a gene-rich region of the genome. It inserts between the first and second intron of *DHR39*, a Drosophila nuclear hormone receptor. It also potentially sits in the 3' UTR of *CG8677* and in the putative promoter region for *CG31626* (Figure 5). I turned to Northern analysis of all three of these genes to determine which, if any were affected by *EP(2)2490*. I see wild type levels of both *CG8677* and *CG31626* in *EP(2)2490* (data not shown). When I look at *DHR39* transcripts I see no reduction, rather I find two new bands in this genetic background compared to controls (Figure 6, right panels). This observation raised the possibility that the *nwak* phenotype is caused by overexpression of *DHR39*.

Because I wanted to know whether the *nwak* phenotype could be caused by either of these new mRNA species, first I addressed whether the larger band (~12kb in size, Figure 6, top right panel) correlated with the *nwak* phenotype. Further northern analysis shows that this 12 kb band is an *DHR39-EP* fusion (data not shown). To determine whether this chimeric mRNA correlated with the *nwak* phenotype I took advantage of another *nwak* allele, made by excision of *EP(2)2490* (done by Jack Roos). *EP(2)2490*^{145},

which is an insertion of 30 nt, has the *nwak* phenotype, and is allelic with *EP(2)2490* (Figures 3A-E, 5). However, this allele should not make a 12 kb chimeric mRNA with *DHR39*. Thus, it is unlikely that this large, chimeric *DHR39* species is correlated with the *nwak* phenotype.

Next, I turned to an analysis of the other *DHR39* band in *nwak* (>5.1kb, Figure 6 center right panel). *DHR39* has at least three published isoforms: *DHR39-RC*, a 3.5 kb transcript expressed only early in development, and two longer isoforms *DHR39-RA*, and *DHR39-RB* (Figure 5). *DHR39-RA* and *DHR39-RB* encode identical proteins and differ only in their UTRs. To determine whether *DHR39-RB* was selectively up regulated in *EP(2)2490*, I turned to RT-PCR analysis of the different splice forms. I find evidence for both *DHR39-RB* and *DHR39-RA* expression in wild type and *nwak* cDNA libraries prepared from third instar larvae (data not shown). Becuase, both isoforms are expressed at some level in wild type and *nwak*, a more detailed analysis to determine the exact tissue, time and amount of transcript upregulated in *EP(2)2490* could be helpful.

I performed a genetic analysis to determine whether the *nwak* phenotype could be associated with overexpression of *DHR39*. This would predict that the *nwak* phenotype would not act as a classical loss of function allele. When I examine *EP(2)2490* in trans to *DHR39* null, *k13215* (Horner and Thummel, 1997) (Figure 9E) or deficiency (*Df(2R)TW1*, data not shown), the synapses look no different from controls. In contrast, when I put *EP(2)2490* in trans to a duplication (*Dup 2,2*), I am able to recapitulate some aspects of the phenotype (data not shown). This genetic analysis is consistent with the idea that overexpression of *DHR39* causes the *nwak* phenotype.

How could insertion of *EP(2)2490* cause an upregulation in *DHR39-RB*? The most parsimonious explanation for such a finding is that *EP(2)2490* landed in a enhancer element that normally represses the transcription of *DHR39-RB* in third instar larvae (Figure 7A-B). One prediction of such a model is that the sequence into which *EP(2)2490* inserts should be highly conserved among Drosophila species. I blasted the intronic sequence between exon1 and exon2 of *DHR39* against all Drosophila species. Within the *melanogaster* group of Drosophilid flies (*Drosophila melanogaster, simulans, sechellia, erecta and yakuba*), I found a highly conserved 43 nt block of sequence (Figure 7C), into which *EP(2)2490* inserts. This represents a highly significant block of homology, because even the UTRs of many glutamate receptor genes are not this well conserved within the *melanogaster* group (data not shown). Thus, this data suggests that *EP(2)2490* inserting into a cis-regulatory element.

Overexpression of *DHR39*

I next directly addressed the question of whether overexpression of *DHR39* could cause the *nwak* phenotype. First, because *EP(2)2490* is a UAS-containing element, I crossed *EP(2)2490* to several different tissue specific Gal4 driver lines (Table 1). Neither neuronal expression, nor muscle expression was sufficient to recapitulate the *nwak* phenotype by driving *DHR39* with *EP(2)2490*. However, using the G14-gal4 driver, which drives in both muscles and neurons (data not shown), I was able to recapitulate some aspects of the *nwak* phenotype (Table 1). This finding suggested that upregulation of *DHR39* was causing the *nwak* phenotype.

It was formally possible that *EP(2)2490* drives expression of another gene, or that a perturbation caused by *EP(2)2490* in synergistic combination with expression of *DHR39* causes the *nwak* phenotype. To directly determine whether overexpression of DHR39 protein alone was sufficient to cause *nwak* phenotypes, I constructed a *UAS-GFP-DHR39* transgene. This transgene localizes to nuclei (Figure 8), and when expressed ubiquitously kills the animal (Table 1), suggesting that it is functional. When I crossed this transgene to a variety of drivers, including G14 (Table 1, Figure 8), I was unable to recapitulate the *nwak* phenotype. Currently, I favor the possibility that I did not identify the correct time, place or amount of *DHR39* to be supplied to create the *nwak* phenotype; however many alternative explanation for this negative result exist.

Normal synapses in *DHR39* null mutants

Given that missexpression of *DHR39* could potentially affect the synapse, I wanted to determine whether loss of DHR39 was of any consequence to the synapse. To ask this question I turned to a published null in *DHR39*, *k13215* (Horner and Thummel, 1997). In contrast to *EP(2)2490*, *k13215* sits between the second and third exons of *DHR39* (Figure 5). Northern analysis confirms a previous finding that only a truncated *DHR39* mRNA is produced in *k13215* (Figure 9A, Horner and Thummel, 1997). In addition, I find no *CG31626* mRNA is produced (Figure 9A). When I examine the synapses of *k13215* mutants, I see normal synaptic growth (Figures 9B-C, 10C) and morphology (Figure 9B-C). In addition, expression of a variety of synaptic markers (i.e. DAP-160, Synaptotagmin, nc82, FasII and Discs Large) is normal in this background

(data not shown). Thus, although *k13215* is a double mutant in both *DHR39* and *CG31626*, these mutant synapses are no different from wild type.

Next, I turned to an analysis of the embryonic role of DHR39. When I examined the axon pathfinding in *k13215* embryos (Figure 4D) I find a pronounced phenotype; axons fail to grow out of the SNb nerve. This is an interesting finding for two reasons: first, because of the *nwak* also has pathfinding defects (Figure 4C), and second because there is no known phenotype for *DHR39* (Horner and Thummel, 1997). However, we must approach this finding with caution since *k13215* is mutant in *DHR39* and *CG31626*.

To determine the likelihood that *CG31626* causes the axon guidance phenotype in *k13215*, I did preliminary characterization of *CG31626*. *CG31626* is likely a secreted protein, because it has an N-terminal signal sequence (data not shown). It contains five repeated units, similar to P-rich extensin motifs that are found in plant cell wall proteins and in proteins used by mussels to adhere to wet surfaces. These motifs can be found in a large number of Drosophila proteins, all with unknown function (data not shown); there are no obvious vertebrate homologues of *CG31626*. Finally, in situ hybridization shows that *CG31626* is expressed after stage 13 of embryogenesis in epidermal structures (BDGP). This last finding makes *CG31626* an unlikely participant in axon pathfinding.

FTZ-F1 involved in synaptic growth

DHR39 is highly related to another nuclear hormone receptor, FTZ-F1. FTZ-F1 and DHR39 compete for binding to the same DNA sequences (Ohno et al., 1994). I wanted to know if misexpression of DHR39 (the potential cause of *nwak* phenotypes) could be interfering with FTZ-F1 by out competing FTZ-F1 for DNA binding sites. This

model predicts that *FTZ-F1* should share phenotypes with *nwak*. Thus, I undertook an analysis of the synaptic *FTZ-F1* phenotypes. Several alleles for FTZ-F1 are available including *FTZ-F1*^{ex19}, a loss of function mutation (Fortier et al., 2003), and *FTZ-F1*^{ex17}, a deletion of the regulatory region which specifically disrupts the adult splice form of *FTZ-F1*, *beta-FTZ*-F1 (C. Woodard personal communication). With lack of *FTZ-F1,* I find statistically significant synaptic undergrowth (Figure 10). This undergrowth maps specifically to loss of *beta-FTZ-F1*. This analysis demonstrates that *FTZ-F1* loss of function phenotypes do not phenocopy *nwak*, and does not support a model in which *nwak* interferes FTZ-F1 function. Interestingly, however, this analysis shows that the nuclear receptor, FTZ-F1 is required for normal synaptic growth. As an interesting side note, recently FTZ-F1 was identified in a unbiased genome wide screen seeking to identify molecules involved in synaptic growth (Liebl et al., 2006). Taken together these data begin to define a role for nuclear hormone receptor function in neuronal growth and morphogenesis.

DISCUSSION

We have isolated a mutation, *nerve-wracked (nwak*) that eliminates synaptic bouton structures and has significantly overgrown synapses. *nwak* is caused by insertion of *EP(2)2490* into a putative regulatory region of the nuclear hormone receptor, *DHR39*. Molecular analysis of *EP(2)2490* reveals an upregulation of *DHR39*, however overexpression of an *DHR39* transgene is not sufficient to recapitulate *nwak* phenotypes. Analysis of *DHR39, CG31626* double mutants, reveals an axon outgrowth defect. This finding may identify the first known *in vivo* requirement for DHR39. Finally, genetic analysis of a hormone receptor closely related to *DHR39, FTZ-F1* shows synaptic undergrowth. Taken together these data highlight a role for nuclear hormone receptors in neuronal growth and synaptic morphogenesis.

Why Are Synapses Organized into Synaptic Boutons?

Lack of synaptic boutons is a remarkable phenotype, and to date, *nwak* is the only mutant with such a phenotype. Perhaps this explains why there is so little understood about why neurons organize synapses into boutons. One attractive hypothesis about the function of boutons is that they create biochemically-distinct sections of the synapse. If this is the case, then active zones in different boutons should release transmitter-filled synaptic vesicle independent of each other. A recent study in the Drosophila NMJ using calcium imaging suggests that indeed, strength of synaptic transmission varies greatly from bouton to bouton within an individual synapse (Guerrero et al., 2005). It would be interesting to perform such calcium imaging analysis along with electrophysiology in the

nwak background, to determine whether synaptic bouton structures are sufficient to account for heterogeneity of release among boutons.

Molecular Cause of *nwak* Phenotype

Currently, the molecular root of *nwak* phenotype is unclear. *nwak* is caused by insertion of the *EP(2)2490* P-element into a putative regulatory region of *DHR39*. And I show that this insertion causes upregulation of *DHR39*. Additionally, the *nwak* phenotype acts as if it stems from a gain of function mutation, consistent with this upregulation of *DHR39* being involved in generating the *nwak* phenotype. However, I cannot recapitulate the *nwak* phenotype with overexpression of *DHR39*. There are three possible reasons for this result. First, the *nwak* phenotype may have nothing to do with overexpression of *DHR39*. To test this possibility I could perform RNAi- mediated knock down of *DHR39* in *EP(2)2490*. If this rescues the *nwak* phenotype, then I would favor either of the following possibilities. Second, overexpression of *DHR39* alone may be sufficient to cause the *nwak* phenotype. In this case, perhaps I did not resupply *DHR39* to the animal using the correct set of variables (i.e., splice variant, time, place, amount) to recapitulate the *nwak* phenotype via overexpression. Thrid, the *nwak* phenotype may stem from the overexpression of *DHR39*, and another, unidentified molecular change in the *EP(2)2490* mutant background.

Hormone Receptors in Synapse Growth

We observe that along with lack of bouton structure, *nwak* synapses are overgrown. How are these phenotypes related? Lack of synaptic boutons in *nwak* is not

likely to be a secondary consequence of driving synaptic growth, because all other overgrown mutants (Wan et al., 2000, Sweeney and Davis, 2002), have synaptic boutons. Two possibilities remain. First, to compensate for the labk of bouton structure, synapses may overgrow. Second, the molecular perturbations in *nwak* may regulate synaptic bouton structure and synaptic growth independently.

In *Drosophila melanogaster* a majority of the animals' growth is accomplished in the four days of larval development. During this time the animal goes through three larval instars that are induced by spikes in the insect hormone, ecdysone. Over this period muscles increases 20 fold in volume, and to depolarize the enlarged muscle fiber the neuron must also grow in size and strength (Schuster et al. 1996). During this period of rapid growth, how is the size of the synapse coordinated with the size of the muscle? There are two general models by which this could be accomplished. One model implicates a retrograde signal emanating from the muscle that would trigger neuronal growth. At the Drosophila NMJ, a TGF-beta signaling cascade has been invoked as such a retrograde signaling system (McCabe et al., 2003). While there is a dramatic lack of growth in TGF-beta signaling mutants, the synapse is still able to grow somewhat, raising the possibility that additional mechanisms contribute to synaptic growth. An alternative model does not require direct communication between the nerve and muscle, and instead would posit that an organism-wide signal regulates growth in many different tissues. In support of this model the insect hormone, ecdysone is required for proper synapse growth at the larval NMJ (Li and Cooper, 2001). However, there is little other molecular information about how such a mechanism could work. Implicating nuclear receptors, FTZ-F1 and DHR39 in a hormonal regulation of synapse growth is an attractive prospect.

The activity of both receptors is known to be regulated by the insect hormone, ecdysone (Horner et al., 1995). And our finding that FTZ-F1 is required for proper synapse growth, places it as a possible downstream effector of ecdysone in the neuron. To test this possibility double mutants between *FTZ-F1*, and the *ecdysoneless* mutant could be constructed. Overall this would provide a molecular mechanism by which neuronal growth is linked to not only to the growth of the muscle, but also to the overall developmental status of the larva. In addition the finding that *DHR39*, *CG31626* double mutants have axon outgrowth defects brings up the possibility that this class of nuclear hormone receptor could have a broader role in neuronal growth.

Table 1. Overexpression of DHR39

Driver name	Tissue expression	Phenotype	Lethality
Using EP2490			
elaV c155	post mitotic neurons	no synaptic phenotype	viable
d42	neurons	no synaptic phenotype	viable
BG57	muscle	no synaptic phenotype	viable
24B	muscle	no synaptic phenotype	viable
MHC	muscle	no synaptic phenotype	viable
G14	muscle, neurons	may phenocopy lack of boutons	lethal
Engrailed	wing	wing blisters	viable
1096	wing	wing vein phenotype	viable
ey	eye	no eye phenotype	viable
GMR	eye	no eye phenotype	viable
Using UAS-GFP-DHR39			
elaV c155	post mitoic neurons	none	n.d
G14	muscle, neurons	none	viable
da	everywhere	none	lethal

Figure 1. *nerve-wracked* mutants lack synaptic boutons.

A) Schematic diagram of the Drosophila neuromuscular junction shows the synapse is organized into boutons. A single bouton is enlarged. The bouton is shown rotated 90° with respect to the X-axis pictured above to demonstrate that boutons are neuronal varicosities that project into the muscle and contain synaptic vesicles (white circles) and active zones (under T structures). **B)** Control (top panels) and *nerve-wracked* (*nwak*) synapses (bottom panels) are stained with a synaptic vesicle marker, CSP (left panels) and a periactive zone marker, DAP-160 (right panels). Note these markers are absent from interbouton areas in control synapses, but distributed throughout *nwak* synapses. **C)** We made 3D-reconstructions of control (left panels) and *nwak* (right panels) synapses co-labeled with anti-FasII, a cell adhesion molecule, which highlights the contours of the neuronal membrane. Top panels show neuronal staining in the plane of the muscle surface. The middle panels show a 45° rotation, and the bottom panels show a 90° rotation (muscle surface represented by a red line). Note the neuronal varicosity in control synapses (yellow arrow) and the lack of varicosities in *nwak* synapse. **D)** Electron microscopy of control (left panel) and *nwak* (right panel) show the lack of neuronal swelling in *nwak*.

Figure 2. Postsynaptic GluR clusters disrupted in *nwak.*

A-B) wild type (A) and *nwak* (B) synapse that express a myc-tagged GluR receptor are stained with anti-myc. In wild type GluR clusters are concentrated beneath synaptic boutons (white bars) and absent from interbouton regions; however in *nwak* synapses GluR clusters are distributed evenly. **C)** Active zone area as inferred by the size of GluR puncta is significantly smaller in *nwak* mutants in comparison to wild type.

Figure 3. *nwak* synapses are overgrown.

A-D) Synapses are labeled with the neuronal membrane marker, HRP. (A) wild type synapses are organized into synaptic boutons. *nwak* (*EP(2)2490*) synapses are either long and unbranched (B), or have many long finger-like structures projecting off the terminus of the synapse (C and D). Note that two alleles of *nwak* show the same phenotype, *EP(2)2490* and $EP(2)2490^{145}$**. E)** Quantification of synapse length, values shown as % wt synaptic length.

Figure 4. *nwak* and *DHR39, CG31626* double mutant synapse have axon pathfinding defects.

A) A schematic of motoneuron projections is shown for reference. The SNa nerve is shown in red, and the SNb nerve is shown in blue, which makes three branches (blue arrows). **B-D)** Stage 17 embryos stained with anti-FasII to highlight motoneuron axonal projections. In wild type (B) all three SNb projections can be seen, at the stage where SNa is projecting into a fork like structure. In *nwak*, (*EP(2)2490)* embryos at the same stage (C), axons either fail grow out (left most segment, marked by *), or are projecting too far (center segment, marked by *). In *DHR39, CG31626* double mutant embryos (D) axons fail to grow out (marked by *) in each segment.

Figure 5. The genomic region surrounding the insertion of *EP(2)2490*

EP(2)2490 and the imprecise excision of this P-element, $EP(2)2490^{145}$ sit in the first intron of *DHR39*. Another P-element, *k13215* sits in the second intron of *DHR39*. *DHR39* has at least three isoforms, *DHR39-RA*, *DHR39-RB* and *DHR39-RC*. Two other genes, *CG8677* and *CG31626* are found close to the insertion site of *EP(2)2490* as well.

Figure 6. Northern analysis reveals two new *DHR39* species in *EP(2)2490*.

Nothern analysis was done using whole, wandering third instar larvae. In control larvae, the *DHR39* probe recognizes a single 5.1 kb band. The same 5.1 kb band is found in *EP(2)2490* larvae. In addition, the *DHR39* probe detects an equally abundant, slightly larger species, as well as faintly detecting an approximately 12 kb species in *EP(2)2490*. *RP49* is a housekeeping gene, shown as a loading control.

Figure 7. A model for regulation of *DHR39* expression

A) In wild type a hypothetical enhancer element (gray box) sits between exon1 and exon2 of *DHR39*. This hypothetical element represses the transcription of *DHR39-RB*.

B) In *EP(2)2490* a P-element inserts into the hypothetical enhancer element, disrupting the repression mediated by this element, and thus allowing transcription of *DHR39-RB*.

C) Comparative analysis of the DNA between exon1 and exon 2 of *DHR39* from *Drosophila melanogaster* reveals a highly conserved, 43 nt block of sequence into which *EP(2)2490* inserts. An alignment is shown with members of the *melanoaster* group of Drosophilid flies.

Figure 8. GFP-tagged *DHR39* transgene localizes to the nucleus.

A-B) wild type (A) and flies expressing *UAS-GFP-DHR39* in the muscle were costained with anti-GFP antibody (green) and the synaptic membrane marker HRP (red). GFP-tagged *DHR39* localizes to the muscle nuclei. Note the synaptic morphology is similar in both genetic backgrounds.

Figure 9. *k13215*, a double mutant in *DHR39* and *CG31626,* has normal synapses.

A) Nothern analysis of wandering third instar larva with *DHR39, CG31626* and *RP49* probes show that in *k13215 DHR39* is truncated and expressed at a lower level. In addition there is no expression of *CG31626* in *k13215*. **B-C)** Synapses stained with the neuronal membrane marker HRP, show normal synapse growth and morphology in wild type (B) and *k13215* (C) synapses.

Figure 10. FTZ-F1 is required for synaptic growth.

A-B) wild type (A) and *FTZ-F1* (B) synapses stained with synaptic vesicle marker (Synapsin). FTZ-F1 is significantly undergrown. **C)** Quantification of bouton number in *k13215* and *FTZ-F1* mutants. *FTZ-F1*^{ex17} specifically disrupts the beta-FTZ-F1, adult isoform of FTZ-F1

Figure 1. *nerve-wracked* mutants lack synaptic boutons.

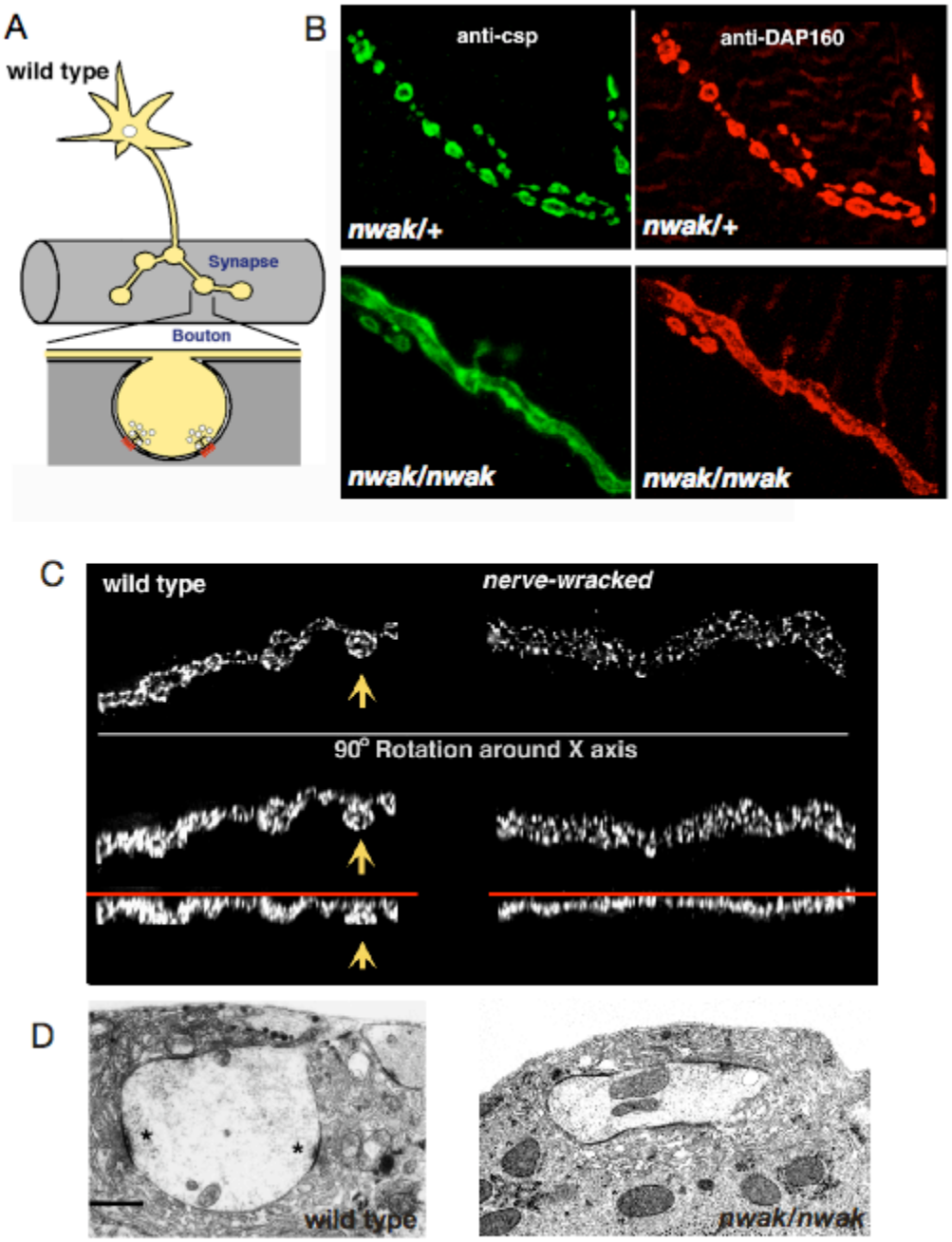

Figure 2. Postsynaptic GluR clusters disrupted in *nwak*.

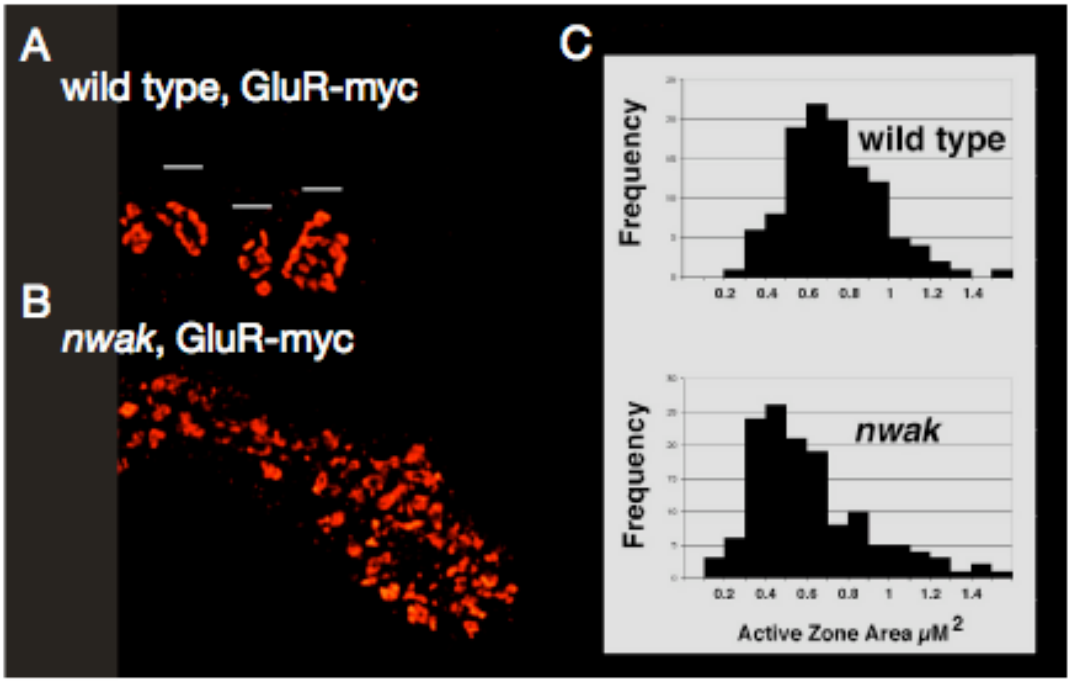

Figure 3. *nwak* synapses are overgrown.

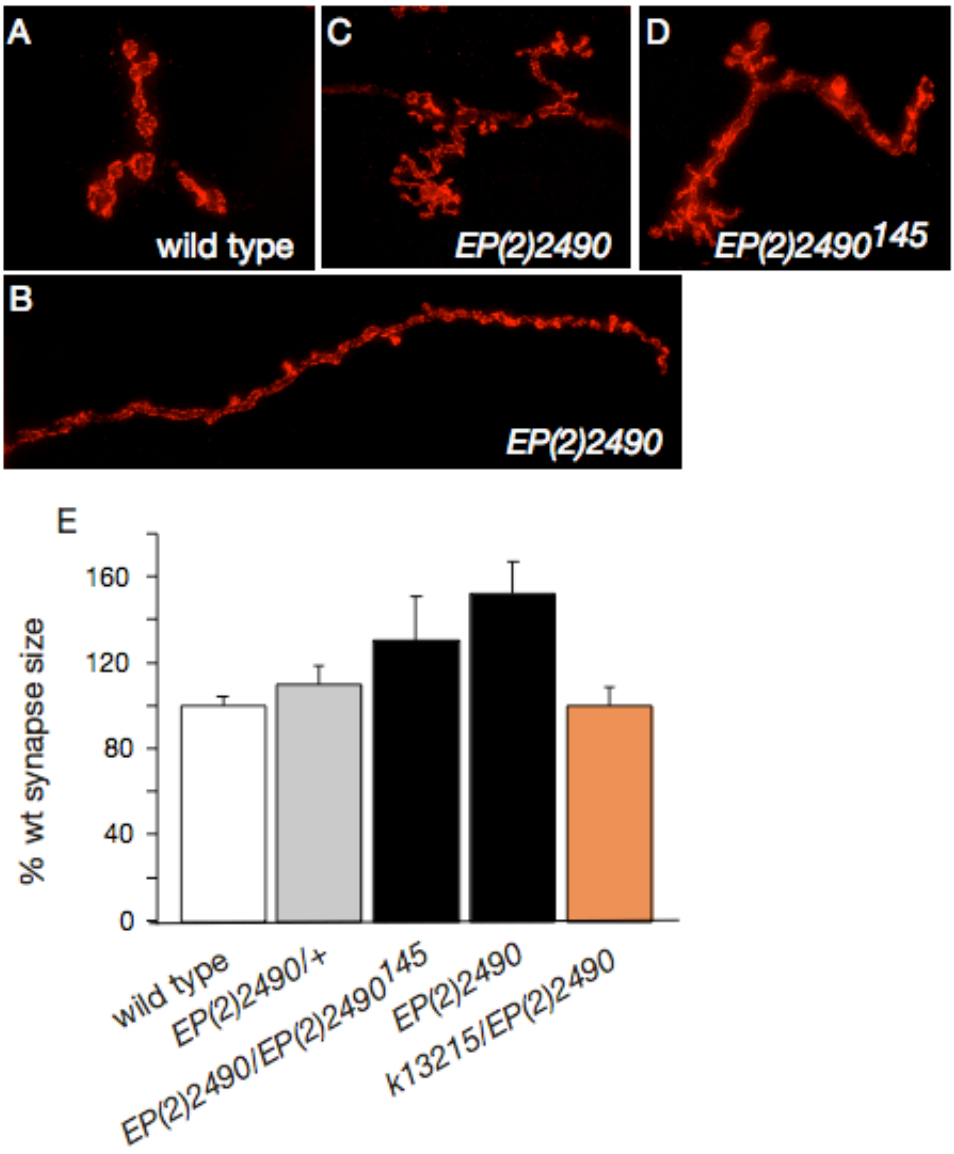

Figure 4. *nwak* and *DHR39, CG31626* double mutant synapse have axon pathfinding defects.

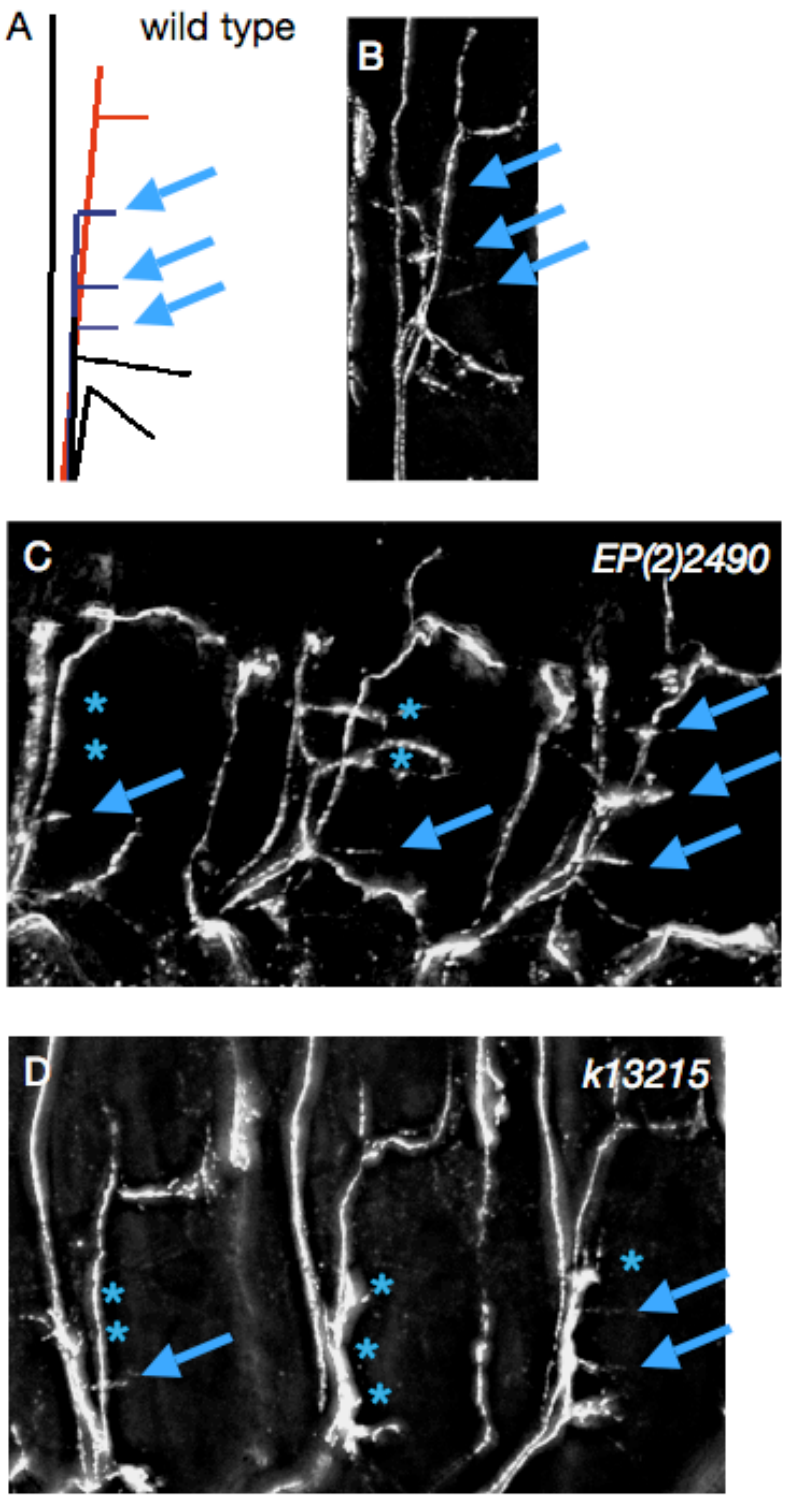

Figure 5. The genomic region surrounding the insertion of *EP(2)2490*

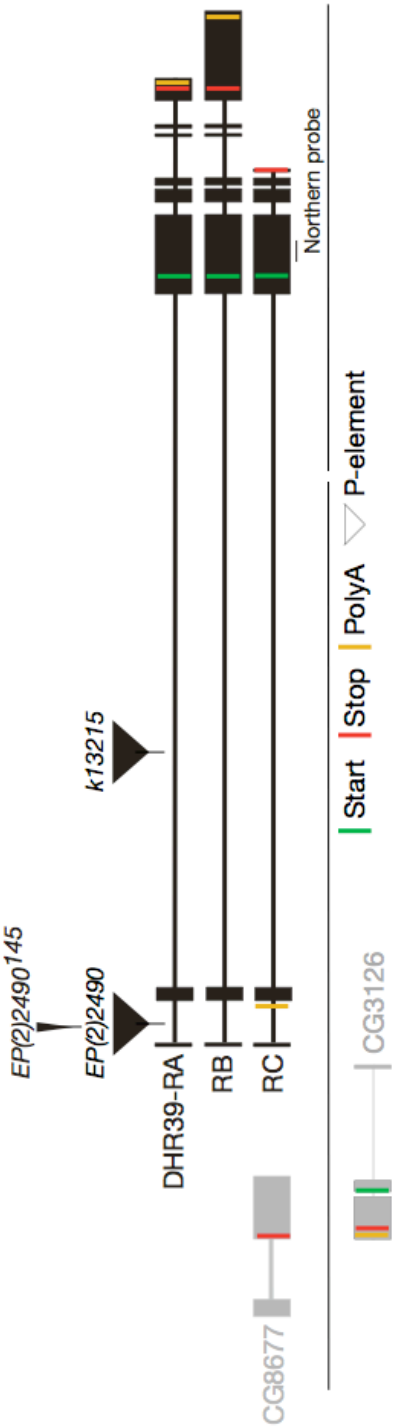

Figure 6. Northern analysis reveals two new *DHR39* species in *EP(2)2490*.

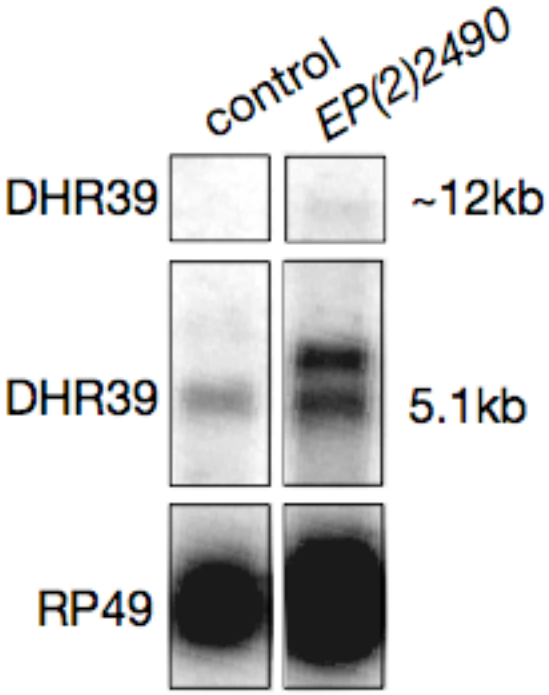

Figure 7. A model for regulation of *DHR39* expression

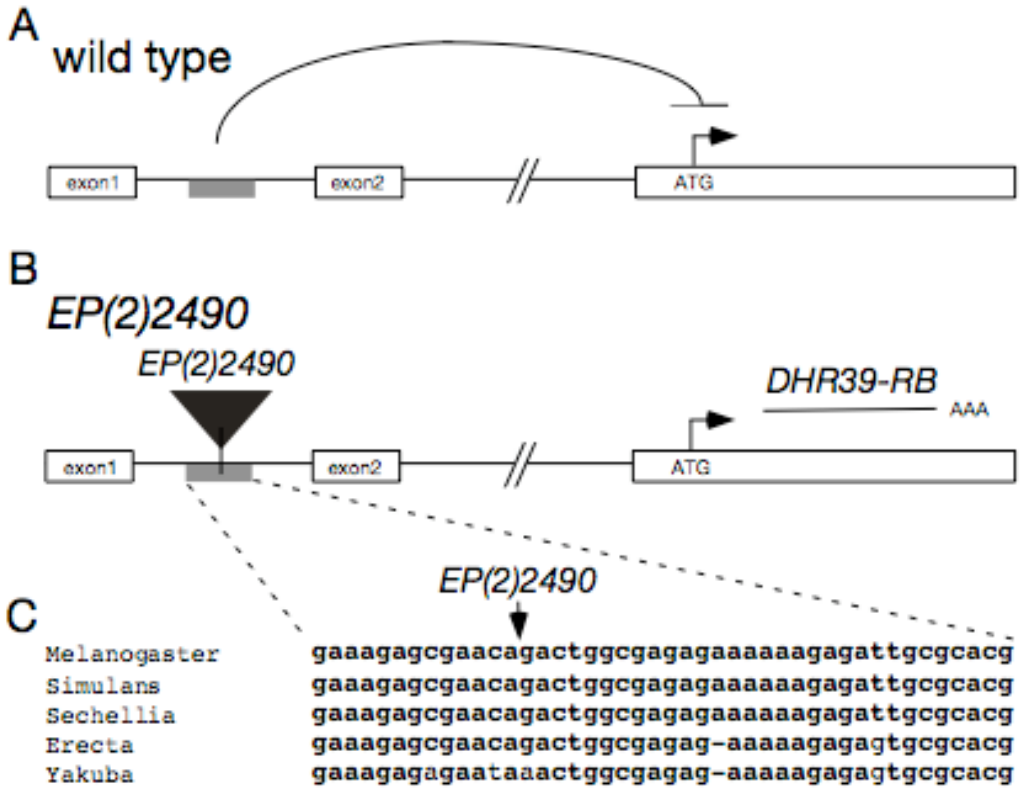

Figure 8. GFP-tagged *DHR39* transgene localizes to the nucleus.

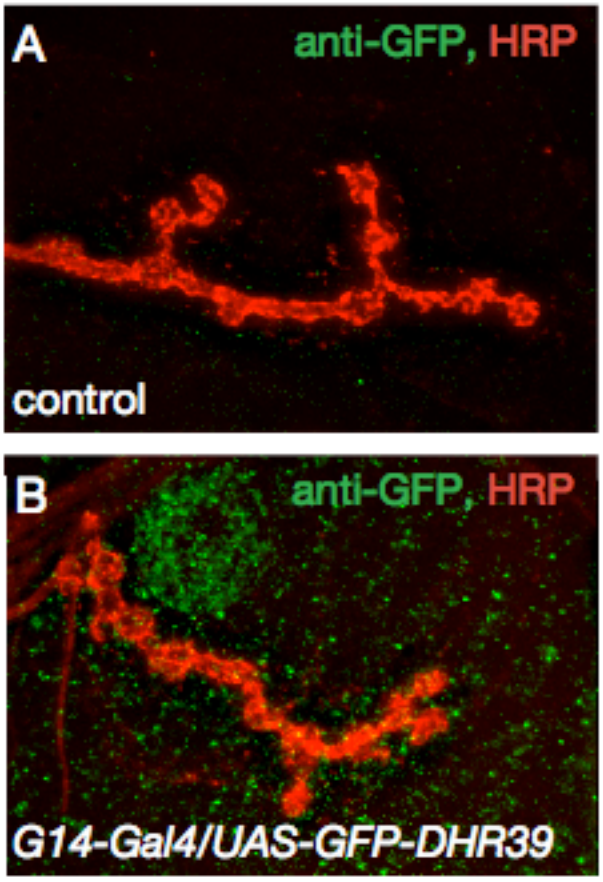

Figure 9. *k13215*, a double mutant in *DHR39* and *CG31626*, has normal synapses.

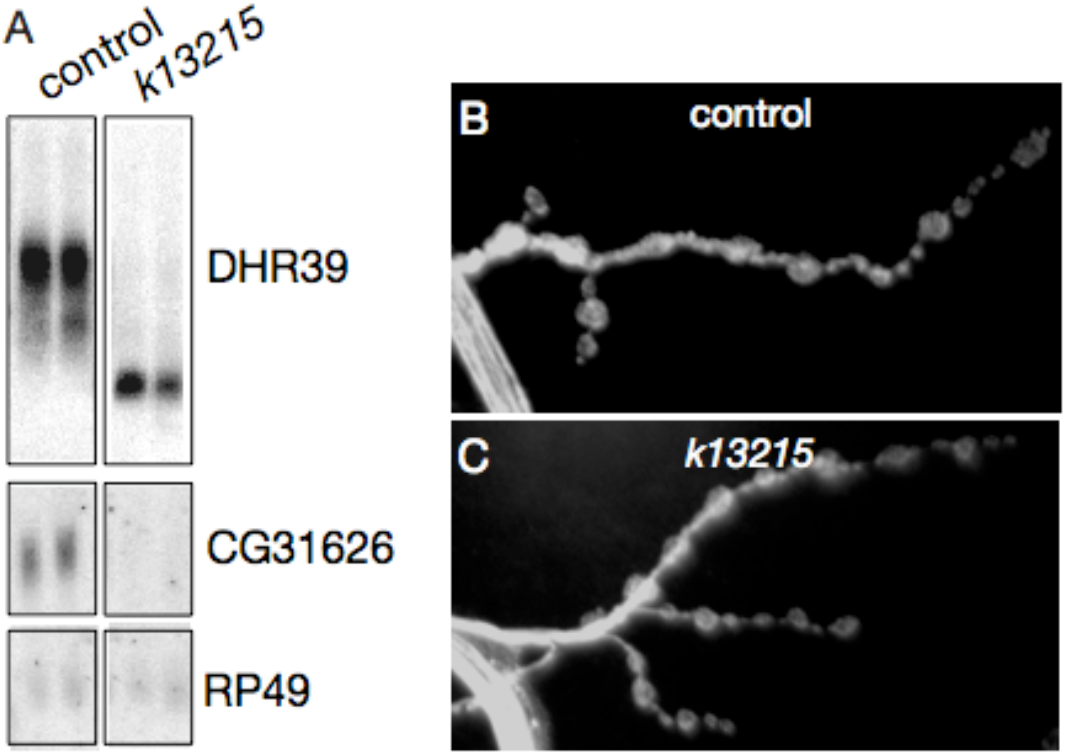

Figure 10. FTZ-F1 is required for synaptic growth.

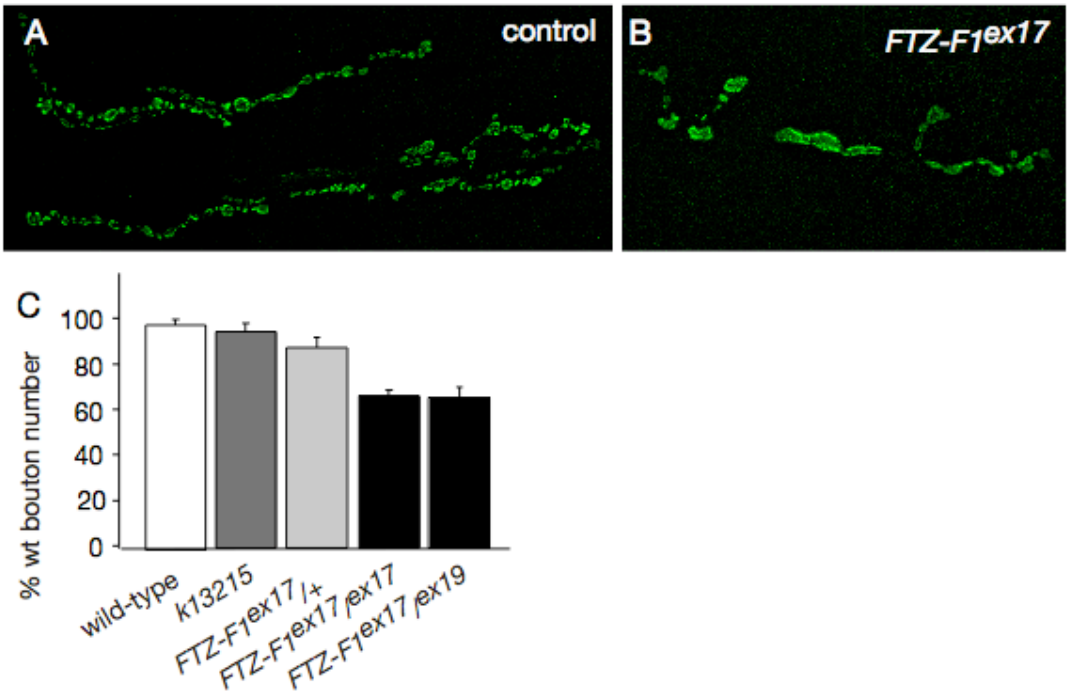

CHAPTER TWO

bad hair day perturbs synaptic morphology and encodes chromating-remodeling factor

Elizabeth S. Heckscher and Graeme W. Davis

SUMMARY

As neuronal synapses grow they take on characteristic morphologies that ultimately impact the fine-tuning of neuronal connectivity within complex neuronal circuits. Here we present a mutation called *bad hair day (bhd)*, which we characterized at the Drosophila neuromuscular junction. Mutations in *bhd* have a profound disruption of normal, orderly synaptic morphology due to increased growth of satellite boutons. *bhd* phenotypes are caused by mutations in a novel gene, *CG8677*. *CG8677* is orthologuos to the chromatin-remodeling factor, RSF-1/HBXAP. We propose that the protein encoded by *CG8677*, dRSF acts at the level of chromatin remodeling to suppress TGFβ signaling. In addition, we present a model in which increased neuronal growth unmatched by postsynaptic development leads to satellite bouton phenotypes.

INTRODUCTION

As neuronal synapses grow they take on distinctive shapes and branching patterns (Rollenhagen and Lubke, 2006) ultimately these characteristic morphologies will impact neuronal connectivity within complex neuronal circuits, and therefore are important for proper neuronal function within a larger network. Given the existence of these highly distinctive synapse morphologies, there must be regulatory mechanisms in place to sculpt the synapse. However, our understanding of these mechanisms is incomplete at best. The Drosophila neuromuscular junction (NMJ) is an experimentally amenable synapse that has relatively invariant morphology (Atwood et al., 1993, Johansen, et al., 1989, Keshishian et al., 1996). In wild type synaptic boutons grow into in a linear array, as if they are beads fitting onto a string (Figure 1A). Only occasionally do boutons project off the main axes of the synapse (Figure 1A arrow); these boutons are termed "satellite boutons" (Dickman et al., 2006, Torroja et al., 1999). By assaying this stereotyped synapse morphology in a variety of genetic backgrounds, researchers have identified a large collection of mutations that perturb normal synaptic morphogenesis. Specifically, many mutants have increased satellite bouton numbers, giving the synapses a bunches-of-grapes appearance. Mutations causing this phenotype can be grouped into different classes according to their molecular output. The largest of these classes, genes involved in endosomal trafficking, includes: *DAP-160*, *rab11, endophilin*, *synaptojanin*, *shibire*, *Iap/AP180*, and *synaptotagmin* (Dickman et al., 2006, Koh et al., 2004, Khodosh et al., 2006, Marie et al. 2004). The correlation between perturbed endosomal trafficking and satellite boutons in phenotypes, led to the hypothesis that satellite boutons arise as

secondary consequence to misregulation of unknown regulatory signals (Dickman et al., 2006). However, there are several other classes of genes, which give rise to satellite bouton phenotypes, that cannot easily be explained by this model. These mutations include, transmembrane proteins e.g. Integrin, β-Amyloid Precursor Protein Homolog (Beaumer et al. 1999, Rohrobough et al., 2000, Torroja et al. 1999), proteins that interact with cytoskeletal elements e.g encoded by *nwk*, *spastin* (Coyle et al. 2004, Sherwood et al., 2004), and signaling molecules e.g encoded by *shaggy*, *dad* (Franco et al., 2004, Sweeney and Davis 2002). To date there is no unifying model that can explain the large diversity of mutations leading to satellite bouton phenotypes.

Here we report the identification of another mutant, *bad hair day (bhd)*, with disrupted synaptic morphology due to an increase in satellite boutons. We show that the *bhd* phenotype is caused by loss *CG8677*. *CG8677*, an uncharacterized gene in the fly, is orthologous to human HBXAP/RSF-1 (Shamay et al. 2002). Because HBXAP/RSF-1 acts as a histone chaperone (Loyola et al., 2003), we suggest that *CG8677* encodes a protein termed Drosophila RSF (dRSF), which acts as part of a larger chromatin-remodeling complex. These findings, suggest that chromatin-remodeling is a critical step involved the mechanisms which regulate synapse morphology. In addition, I investigate how dRSF interacts with a signaling system known to regulate synaptic growth, TGFβ signaling, and present a model in which, at the level of chromatin remodeling, dRSF acts to repress TGFβ signaling.

Synaptic growth and morphology perturbed in *bad hair day* mutants

bad hair day (*bhd*) mutations disrupt normal synapse growth and morphology. In wild type, there is a stereotyped number of boutons in each third instar synapse (Schuster et al., 1996). In contrast, in two *bhd* alleles *KG2636*, and *KG766*, there is a significant increase in bouton number (wt 38 $\pm$ 1.7 n=38, *KG2636* 48 $\pm$ 2.4** n=27, *KG766* 47 $\pm$ 2.7** n=27, number of boutons on m4, **p<0.01). To better understand the nature of the overgrowth in *bhd*, I characterized the number of satellite and non-satellite boutons in wild type and mutant synapses. In comparison to wild type, *bhd* mutant synapses have a significant increase in satellite boutons, without an increase in non-staellite boutons (Figure 1). Thus, the increase in synaptic growth in *bhd* can be attributed to a specific increase in satellite boutons. The addition of these satellite boutons in *bhd*, results in an overall change in synapse morphology.

Are satellite boutons in *bhd* fundamentally different from non-satellite boutons? To answer this question I examined the subcellular organization boutons using a panel of pre- and postsynaptic markers. Presynaptically, I found that satellite and non-satellite boutons have a normal distribution of antibody staining with: anti-Horse Radish Peroxidase (HRP, neuronal membrane marker), anti-Synapsin (syn, synaptic vesicle protein), anti-Synaptotagmin (syt, exocytic protein), nc82 (active zone marker), anti-Fasiclin II (FasII, cell adhesion protein), anti-Dynamin Assoicated Protein-160 (DAP-160, periactive zone marker), and 22c10 (neuronal microtubule associated protein) (Figure 1 and data not shown). Similarly I found normal distribution postsynaptic of

antibody staining using: anti-Glutamate Receptor IIA (GluRIIA, glutamate receptor cluster marker), anti-Discs Large (Dlg, subsynaptic reticulum marker), and other postsynaptic proteins (Dliprin, Cactus, Dorsal) (Figure 1 and data not shown). The similarity of staining patterns between satellite and non-satellite boutons, suggests that these two types of boutons differ only in their position within the synapse.

Analysis with this panel of synaptic proteins revealed an interesting aspect of the *bhd* phenotype: the intensity of staining for many presynaptic antigens is reduced. Specifically, there is a decrease in the intensity of staining of synaptic vesicle trafficking proteins (syt, syn, DAP-160), and the presynaptic active zone maker, nc82 (Figure 1, wt 84.7 $\pm$ 2.5 n = 25, *KG2636*/+ 87.2 $\pm$ 4.9 n = 7, *KG2636*/*KG2636* 51.2 $\pm$ 2.0** n = 9, DAP-160 fluorescence in arbitrary units, $p<0.05$, data not shown). The reduction in fluorescence is limited to this subset of proteins, because the intensity of staining for other presynaptic and postsynaptic markers (e.g. Fas II, HRP, 22c10, GluRIIA, Dliprin, Dlg) antigens was unchanged in *bhd* mutants (Figure 1, data not shown). The reduced abundance of presynaptic trafficking proteins in *bhd* raised the possibility that this was the primary defect in *bhd* mutant synapses. To test this possibility, I examined the phenotype transheterozygous *bhd*, *DAP-160* larva, (*KG2636*/*Dap-160*^{Q24}). However, I see no difference in satellite bouton number or synapse morphology between this genotype and controls (data not shown). Thus, it is unlikely that upregulation of satellite boutons in *bhd* is due to a defect in protein trafficking within the neuron.

***Bad hair day* interacts with components of the TGFβ signaling pathway**

Next, I wondered whether the growth of satellite boutons was dependent on the same growth signals as normal synaptic boutons, or whether there was some specialized growth signal necessary for the formation of these structures. Thus, I asked whether satellite bouton growth in *bhd* was mediated in TGFβ-dependent manner, since TGFβ signaling through the Wishful Thinking (Wit) receptor is required for normal synaptic growth (Aberle et al., 2002, Marques et al., 2002). I constructed *bhd* animals lacking one copy of the *wit* gene, and find that in the *bhd* mutant background, heterozygous *wit* null mutations are sufficient to significantly reduce satellite bouton numbers (*KG2636/KG2636*; wit^{A12}/+, *KG2636/KG2636*; wit^{B11}/+) (Figure 2). In the same synapses the growth of normal boutons is not affected (Figure 2). These data suggest that satellite bouton growth is highly sensitive to the level of TGFβ signaling. Next, to determine whether this signaling was absolutely required for the growth of satellite boutons in *bhd,* I constructed a *bhd*; *wit* double mutant. Synapses in the double mutants are similar to *wit* mutant synapses alone (Figure 2), demonstrating that satellite boutons do not form in a system devoid of TGFβ signaling.

These data, together with data from a previously published report showing that mutation of a negative regulator of TGFβ signaling, *dad*, has satellite bouton phenotypes (Sweeney and Davis, 2002), raise the possibility that the cause of satellite bouton growth in *bhd* is inappropriate upregulation of the TGFβ pathway. To examine whether *dad* and *bhd* are in a linear pathway both suppressing TGFβ, I a constructed *bhd*; *dad* double mutant. To my surprise, I found that although both *dad* and *bhd* mutants are viable, *bhd; dad* double mutants are synthetically lethal (Figure 2). In addition, I find that when one

copy of *dad* is removed from a *bhd* synapse, the synaptic morphology is far more perturbed than in *bhd* synapses alone (data not shown). (As a side note this experiment should be repeated before publication, because there was a chromosomal balancer in the background when I did it). These data are consistent with a model in which *bhd* and *dad* represent two non-redundant negative regulators of TGFβ signaling (Figure 8). However, these data are also consistent with another model, in which *bhd* regulates a cellular process, which occurs subsequent to TGFβ-mediated synaptic growth.

bhd phenotype caused by reduction in *CG8677* transcript levels

To begin to understand the *bad hair day* phenotype on the molecular level, I did a molecular and genetic characterization of *KG2636*, the most severe *bhd* allele. First, I showed that the *KG2636* P-element is located within the first intron of a novel gene, *Candidate Gene Number 8677* (*CG8677)* (Figure 2A, B*)*. To map the phenotype to *KG2636*, I made use of two deficiency lines, one large (*Df(2L)TW1)* and one small ($K14029^{J1.1}$) neither of which contain *CG8677* coding sequence (Figure 3A). *KG2636* in trans to either deficiency is no worse than homozygous *KG2636* (Figure 1, data not shown for $K14029^{J1.1}$). Since KG elements contain Suppressor of Hairy Wing binding sites, which recruit silencing proteins, KG elements can efficiently repress transcription (Roseman et al., 1995). Thus, I determined the transcript levels of several genes near the insertion point of *KG2636*. By northern blotting of *KG2636*, I found normal transcript levels of *DHR39* and *CG31626*, the two genes, which lie closest to *CG8677* (Figure 3A). In contrast, I find less than 30% of wild type levels of *CG8677* remaining in homozygous *KG2636* larvae, making *KG2636* a hypomorphic mutation of *CG8677* (Figure 3C).

Next, I asked whether insertion of a large P-element in the first intron of *CG8677* was sufficient to cause the *bhd* phenotype. To do this I used a two-part strategy. First, I used P-element replacement to replace the KG element with a WeeP element, which contains a mini-white marker gene flanked with FRT sites followed by the coding sequence for GFP (Clyne et al., 2003). Animals with the WeeP element in place of the KG element have a *bhd* phenotype (*WeePW+,* Figure 1). Next, I used the internal FRT sites to convert the large *WeePW+* element into a smaller, non-mutagenic, 1.9kb element, which lacks the white gene (*WeePW-)* (Clyne et al., 2003). In this animal I see that the phenotype is reverted to wild type (Figure 1D). In addition, precise excision of the *KG2636* element gives similar results (Table 1, data not shown). Thus, three lines of evidence: deficiency mapping, measurement of transcript level in *KG2636* and phenotypic reversion using the WeeP element strategy, strongly suggests that the *bad hair day* phenotype results from loss of *CG8677*.

A second formal possibility exists, however. Specifically, *KG2636* may perturb a functional element not associated with *CG8677* (a microRNA, enhancer element for another gene, etc), and this perturbation rather than reduction in *CG8677* transcript levels may cause *bhd* phenotypes. To exclude this possibility, I performed RNAi to knock down *CG8677* transcripts independently of the *KG2636* P-element. Using several different RNAi constructs and two different delivery methods, I found that treatment with *CG8677* RNAi was sufficient to recapitulate the *bhd* phenotype (Figure 1). In addition, another P-element inserted into another location within the *CG8677* locus, *KG766* has similar phenotypes to *KG2636* (Figures 1, 3) and is allelic with *KG2636* (Figure 1).

Taken together these data show that reduction in *CG8677* levels cause *bad hair day* phenotypes.

Description of the *CG8677* locus

Since *CG8677* has not been previously studied, I did an extensive molecular characterization of this novel gene. *CG8677* is large gene spanning 13 kb on Chromosome 2R (Figures 3, 4). I sequenced a collection of ESTs to determine the intron/exon boundaries of *CG8677*. In addition to correcting errors found in BDGP (Figure 4), I discovered that *CG8677* encodes two splice variants. The short isoform of *CG8677* (*CG8677-s*) is 8,850 bp long and contains 8 exons (Figures 3 and 4). The long isoform of *CG8677* (*CG8677-l*) is at least 9,678 bp long. *CG8677-l* and *CG8677-s* share exons 1-7; *CG8677-l* only contains a portion of exon 8, before being spliced into exon 9 (Figure 3 and 4). Notably the *KG766* P-element inserts between exon 8 and exon 9, and thus is likely only to affect *CG8677-l*. These data suggests that perturbation of only the long isoform, *CG8677-l* is sufficient to yield the *bhd* phenotype.

The information I have for the 3' end of *CG8677-l* is incomplete. Because the EST containing Exon 9 of *CG8677* does not contain a polyA signal, and terminates in a stretch of As, it may be missing as many 1500 bp and perhaps another exon. To determine the extent of the 3' end of *CG8677*, I performed modified RACE experiments. I did RT-PCR reactions with primers just beyond each of five possible polyA sequences for *CG8677-l*, and then probed for the presence of *CG8677* cDNA using intron-spanning primers. Only in the most distally primed RT-PCR reaction did I find evidence of *CG8677-l* transcript. This finding suggests that the polyA tail of *CG8677-l* lies

approximately four kb beyond the known end of exon 9, just past the first exon of *DHR39* (Figures 3, 4). Another interesting feature of *CG8677-l* is that sequence within exon 9 is shared by another gene on the other DNA strand. In one orientation this DNA is part of exon 9 of *CG8677-1*; in the other orientation this sequence is part of exon 3 of *CG31626*.

CG8677 expression pattern

To begin to get an insight into the role of *CG8677*, I examined the expression of *CG8677* mRNA. First, I determined which *CG8677* mRNA isoform, *CG8677-s* or *CG8677-l* is present in third instar larva. Using RT-PCR in third larval instar extracts, I found expression of both *CG8677* isoforms (data not shown). Next, I determined the relative abundance of each isoform using northern blotting. Notably *CG8677-1* is easily detected by Northern blot, but *CG8677-s* is undetectable (Figure 3C). Thus, although both are present, only the long isoform (>9.5kb) is abundantly expressed in larval tissues. These observations are consistent with the idea that disruption of *CG8677-l* alone, by the *KG766* allele of *bhd*, is sufficient to perturb normal development of the Drosophila NMJ.

To determine the spatial expression of *CG8677* I turned to *in situ* hybridization. Although larval in situ analysis is particularly difficult in muscle, I was able to determine the embryonic expression pattern of *CG8677*. I find that *CG8677* is a maternally deposited RNA, expressed everywhere at early stages (Figure 5A). As the embryo develops *CG8677* expression becomes enriched in, but not restricted to the nervous system (Figure 5B, C, data not shown). At mid embryonic stages, *CG8677* is strongly expressed in the ventral neurogenic region, which gives rise to neuroblasts of the ventral

nerve cord (Figure 5B, data not shown). By the time the neuromuscular synapse is formed *CG8677* mRNA is detected in differentiated neuronal cell bodies, forming the latter like pattern of the ventral nerve cord (Figure 5C, data not shown). To confirm the specificity of the expression pattern, I used two different *in situ* probes, one from the 3' end and one from the 5' end of *CG8677*, and found the same expression pattern with both probes (Figure 2, data not shown). In addition a large-scale microarray analysis of genes enriched in different larval tissues identified *CG8677* as one of 400 genes uniquely enriched in the late larval CNS (Li and White, 2003). Finally, ESTs prepared from adult head extracts contain *CG8677-l* mRNA. Taken together these data suggest that *CG8677* is expressed in the nervous system.

CG8677 encodes the Drosophila orthologue of human RSF-1/HBXAP

CG8677 encodes a large, multi-domain containing protein. This protein contains several putative nuclear localization sequences (Figure 4), and two highly conserved domains (Figure 6A), both of which are thought to be involved in the regulation gene expression. First, the N-terminus contains an XCD (HBXAP Conserved Domain, Shamay et al., 2002), which is actually composed of two adjacent domains. The N-terminal region of XCD contains a DDT domain (DNA binding homeobox and Different Transcription factors) predicted to be a DNA binding domain (SMART SM00571); the C-terminal part of XCD is characterized by a particular structural classification, Superfamily: DNA repair protein MutS, domain II (SMART 53150). Second, the center of the protein encoded by *CG8677* contains a PHD-finger (Plant Homeodomain Finger, SMART SM00249). PHD-fingers bind two zinc ions, and are structurally related to

RING and FYVE fingers. Several reports suggest that PHD-fingers can function as protein-protein interaction domains, and it was recently demonstrated that they are involved in nucleosome binding *in vitro* (Aasland et al., 1995, Bienz 2006, Mellor, 2006).

The protein encoded by *CG8677* is evolutionarily conserved. Currently, its best-characterized orthologue is a Human protein, RSF-1/HBXAP (Remodeling and Spacing Factor-1/Hepatitus virus B protein X Associated Protein) (Shamay et al. 2002), (Figure 6A). The protein encoded by *CG8677,* henceforth called Drosophila Remodeling and Spacing Factor (dRSF) and RSF-1/HBXAP share high sequence similarity in both the XCD (41% identity) and the PHD-finger (62% identity). These two proteins also contain short stretches of highly conserved sequence in the region C-terminal to the PHD-finger (Shamay et al., 2002). Furthermore, dRSF and RSF-1/HBXAP both share several structural motifs of unknown function. These include several coiled-coiled domains, a glutamatic acid rich region (Prosite Profile 50313), and an arginine rich region (Prosite Profile 50323) (Figure 6A). It is interesting to note that the relative positions of these structural motifs within the proteins are conserved (Figure 6A).

The C-terminal approximately 300 amino acids of dRSF are unique to the fly protein. This region contains a motif of unknown function (PRINTS PRO1217), as well as a Proline-Rich domain (Prosite profile PS50099), which are found in structural, metal-binding and DNA-binding proteins. Although dRSF has two isoforms, they are almost identical. They differ only in the C-terminus, where *CG8677-s* encodes a unique 16 aa terminus and *CG8677-l* encodes a unique 22 aa terminus (Figure 4). Currently, the functional difference in this divergent C-terminus is unclear. Taken together there is compelling sequence and secondary-structural similarity to suggest that, with the addition

of a unique C-terminal tail, *CG8677* encodes a protein, dRSF that is orthologous to human RSF-1/HBXAP.

Human RSF-1/HBXAP is part of a chromatin-remodeling protein complex called Remodeling and Spacing Factor (RSF). RSF is composed of two proteins: SNF2H and RSF-1/HBXAP (Figure 6B) (Loyola et al., 2003). RSF-1/HBXAP acts as a histone chaperone, depositing histones onto DNA, and SNF2H has ATPase activity that provides energy to move histones along DNA (Loyola et al., 2003). The interaction between SNF2H and RSF-1/HBXAP is required for its chromatin-remodeling activity; and this interaction is likely mediated via the XCD of RSF-1/HBXAP (Loyola et al., 2003). By analogy a similar complex may exist in Drosophila, and dRSF may also participate in chromatin remodeling (Figure 6B).

X-Chromosome chromatin is normal in *bhd* mutants

The Drosophila homolog of the ATPase, SNF2H is Imitation of Switch (ISWI) (Figure 6B) (Lazzaro and Picketts, 2001). In *iswi* null mutants chromatin is perturbed. For example, in salivary gland polytene chromosome preparations the male X chromosome from *iswi* mutants are abnormal (Deuring et al., 2000). Instead of being elongated like the other chromosomes, the X-chromosome shorter and less densely packed. Because dRSF might interact in a complex with ISWI (Figure 6B), I examined the X chromosome of *bhd* mutants using salivary gland polytene chromosome preparations. In these preparations the X-chromosome, labeled with anti-MSL in green, appears in its normal elongated form (Figure 7). Thus, unlike *iswi* mutants, *bhd* mutants have normal X chromosomes. There are two explanations for this result. First, since

KG2636 is a hypomorphic allele, low levels of dRSF1 may be sufficient for normal X chromosome chromatin. Second, the ISWI ATPase is known to associate with a wide variety of proteins, for example Nurf301, and it is known that Nurf301 gives similar polytene chromosome phenotypes as *ISWI* (Figure 6B)(Xiao, et al. 2001). (As a side note I tried to look at the NMJ morphology of Nurf301 flies, and they do not survive to the third larval instar). Taken together these findings bring up the possibility that dRSF may impart some specificity to the ISWI, ATPase activity.

Neuronal over-expression of a dominant negative dRSF perturbs synapse morphology

To determine which cell types require dRSF1 for normal synaptic morphogenesis I turned to a dominant negative strategy. The UAS-containing, P-element, *EP838* (Rorth et al., 1998), which sits in the first intron of *CG8677* (Figure 3), should be able to drive a truncated dRSF protein (Figure 4). This protein is predicted to act as a dominant negative because it lacks an XCD, and in human cell lines over-expression of a such a truncated form of RSF-1/HBXAP interferes with the chromatin remodeling ability of the RSF complex (Loyola et al., 2003). By crossing *EP838* to variety of tissue specific Gal4 driver lines I over-expressed the truncated dRSF, either in the neuron or muscle. In synapses with neuronal over-expression, I found *bhd* phenotypes (*EP838* crossed to: *elaV3a4-Gal4* = 4.1 +/1 0.7, n= 8 *elaVc155-Gal4* 5.9 +/- 1.0, n=14, and *d42-Gal4* 8.7 +/- 1.3, n=6 satellite bouton number). In contrast, muscle over-expression (*EP838* crossed to: *MHC-Gal4* = 1.9 +/- 0.4, n=8 satellite bouton number) had no effect. These data

support the idea that *CG8677* activity is required presynaptically for proper synaptic morphogenesis.

DISCUSSION

We find an increase in satellite bouton number and perturbed synaptic morphology in *bad hair day* (*bhd*) mutant synapses. *bhd* phenotypes are caused by loss of function mutations in the novel gene, *CG8677*. Our data suggest that *CG8677* is expressed in neurons and normally functions there to repress satellite bouton formation. Further our data suggest that perturbation of one isoform of *CG8677*, *CG8677-l* is sufficient to generate *bhd* phenotypes. Below, I present two models: one model suggests a general mechanism for the genesis of satellite bouton phenotypes at the Drosophila NMJ; in the second model I propose a molecular function for *CG8677*.

Model for generation of satellite bouton phenotypes: unmatched neuronal growth

The synapse of the Drosophila neuromuscular junction (NMJ) is established by the end of embryogenesis, and during the next four days of larval development the synapse undergoes a dramatic increase in size to keep pace with an approximately 20-fold increase in muscle volume (Schuster et al., 1996). Like all synapses, the Drosophila NMJ is an asymmetric junction. The nerve terminal contains boutons, specialized structures that house neurotransmitter-filled vesicles and the machinery allowing for regulated neurotransmitter release. In contrast, the muscle side of the synapse is specialized for reception of neurotransmitter. In the most intensely studied synapses, type I, the nerve becomes entirely embedded within elaborate, specialized folds of the postsynaptic muscle, called the subsynaptic reticulum (Johansen et al., 1989). Thus, the normal addition of boutons to the synapse over this time period involves both neuronal

growth and large scale remodeling of postsynaptic structures to accommodate this new neuronal growth.

There is now a large collection of mutants with overgrown synapses and a majority of these mutants have satellite boutons that cause synapse to look like a bunch-of-grapes rather than beads-on-a-string. These mutations perturb: endosomal trafficking, cytoskeletal regulation, cell adhesion, signal transduction and now with the addition of *bad hair day (bhd)*, chromatin remodeling. The only unifying feature within this diverse group of mutations with satellite bouton phenotypes is that, where investigated, these molecules act presynaptically (Beaumer et al., 1999, Coyle et al., 2004, Dickman et al., 2006, Franco et al. 2004, Khodosh et al., 2006, Koh et al., 2004, Marie et al. 2004, Rohrbough, et al. 2000, Sherwood et al., 2004, Torroja et al. 1999). Thus, one model for satellite bouton formation is that the primary defect in these mutants is upregulation of neuronal growth, unmatched by postsynaptic growth. Thus as a secondary defect, boutons branch off the sides of prexising boutons, rather than adding to the terminus of a string of boutons, a process which requires remodeling of the complex architecture of the subsynaptic reticulum.

There are at least three lines of evidence supporting with such a model. First, there is a small collection of mutants with overgrown synapses, e.g. Spinster (Sweeney and Davis, 2002) and FasII (Schuster et al., 1996) that have normally sized boutons aligned into the stereotyped beads-on-a string morphology. These molecules act both in the neuron and muscle, potentially coordinately regulating presynaptic and postsynaptic growth. Second, such a model would predict that upregulation of presynaptic growth should be sufficient to generate satellite bouton phenotypes. TGFβ signaling is a potent

postitive regulator of neuronal growth at the NMJ (Keshisian and Kim, 2004, Sanyal et al., 2004), and previously published results show that mutation in a suppressor of TGFβ signaling, *dad* causes satellite bouton phenotypes (Sweeney and Davis, 2002). Finally, if such a model is correct, then impairment of presynaptic growth should be sufficient to suppress satellite bouton phenotypes. Here we demonstrate that just removing one copy *wit*, the TGFβ receptor is sufficient to significantly suppressed satellite bouton formation in *bhd* mutant synapses. Taken together these support the idea that neuronal growth without concomitant postsynaptic growth at the Drosophila NMJ, may lead to satellite bouton phenotypes.

Model: dRSF as a potential negative regulator of TGFβ signaling

bhd phenotypes are caused by loss of function mutations in *CG8677*. *CG8677* is a novel gene encoding the Drosophila orthologue of RSF-1/HBXAP, a human protein that acts as a part of a chromatin-remodeling complex. Due to this orthology we propose, first, to call the protein encoded by *CG8677*, Drosophila Remodeling and Spacing Factor, dRSF; and, second that dRSF likely acts as part of a chromatin-remodeling complex. In addition, we demonstrate that *bhd* alleles interact with TGFβ signaling components, *wit* and *dad*. These data are consistent with *bhd* acting to suppress TGFβ signaling in a manner that is not redundant with *dad*. Specifically we propose that while *dad* acts in the cytoplasm to attenuate TGFβ signaling (Inoue et al., 1998), *bhd* act in the nucleus to attenuate TGFβ signaling (Figure 8). Taken together our data are consistent with a model in which dRSF acts at the level of chromatin-remodeling to negatively regulate TGFβ signaling.

This molecular model for dRSF function (Figure 8) is attractive because it could explain the recently published role for RSF-1/HBXAP in human cancer. Specifically, recent work shows that RSF-1/HBXAP is an oncogene, upregulated in ovarian cancer cell lines (Davison et al., 2006, Hennessy et al., 2006, Mao et al., 2006, Shih et al., 2005). In contrast, although it has a complex role in cancer, TGFβ is a tumor suppressor (Reiss 1999). More specifically, normal expression of a TGFβ ligand, Inhibin-α blocks the proliferation of the ovarian surface epithelium (Nilson et al., 2002). The observations that RSF-1/HBXAP and Inbibin-α have opposing roles in ovarian cancer, parallel my observations at the NMJ where dRSF-1 and TGFβ have opposing roles in satellite bouton formation. These data, taken in light of the previous model (Figure 8), would suggest a molecular mechanism that could explain the oncogenic action of RSF-1/HBXAP in ovarian cancer: In a healthy ovary, TGFβ signals to repress proliferation of the ovarian surface epithelium. In a tumor, however, where chromosomal amplifications result in upregulation of RSF-1/HBXAP, TGFβ signaling would be inhibited; thus, leading to derepression of the ovarian surface epithelium and eventually excessive tissue proliferation.

Table 1. Genetic Reagents for Bad Hair Day

REAGENTS I ACQUIRED

P-elements	**Location and Molecular Details**	**In stocks/Source**
EY8336	5' of *CG8677*, potential UAS-*bhd* line, but no overexpression phenotypes	Yes/Bloomington
KG2403	5' of *CG8677*	Yes/Bloomington
KG4049	5' of *CG8677*	Yes/Bloomington
Sh778	Lethal, annotated as in first intron of *CG8677*, but is not actually located there.	Yes/Bloomington
KG1375	in first intron of *CG8677*	No/Bloomington
KG2636	in first intron of *CG8677*, 30% of *CG8677* transcript level	Yes/Bloomington
GS2202	in first intron of *CG8677*	Yes/Bloomington
EP(2)838	in first intron of *CG8677*	No/Szeged
KG7666	in exon 7 of *CG8677*, should disrupt only one splice form of *CG8677*	Yes/Bloomington
KG7664	3' of *CG8677*	Yes/Bloomington
KG6028	3' of *CG8677*	Yes/Bloomington
KG3325	3' of *CG8677*	Yes/Bloomington
HR39scim	3' of *CG8677*, extra band with *CG31626* probe on N. blot	Yes
EP2490	3' of *CG8677*, ("*nerve-wracked*"), extra band with *DHR39* probe on northern.	Yes/Bloomington
KG2908	3' of *CG8677*	Yes/Bloomington
KG7224	3' of *CG8677*	No/Bloomington
Lethals in the region		
l(2)k09410	5' of *CG8677*, lethality questionable	Yes/Bloomington
l(2)k11226	3' of *DHR39*	Yes/Bloomington
l(2)14505	3' of *DHR39*	Yes/Bloomington
Deficiencies		
K14029[J1.1]	male recombinant from *k14029*, uncovers *bur*, goes all the way to *k11226*	No/D. Huen
K7215[K11]	imprecise excision of *k7215* uncovers *bur* but not *clumsy*	No/D. Huen
Df(2L)TW1	large deficiency uncovers *DAP-160* and *CG8677* (38A7-B1 to 39C2-3)	No/Bloomington

Table 1. Genetic Reagents for Bad Hair Day

Df(2L)TW84	large deficiency uncovers *CG8677* (38A1 to 39D3-E1)	Yes/Bloomington
Df(2L)TW65	large deficiency uncovers *DAP-160* but NOT *CG8677* (38A1 to 39F1)	No/Bloominton
EP838[44A1]	uncovers *clumsy* but not *bur*, male recombo from *EP838* (not *bhd* allele)	Yes/D. Huen
EP838[7B1]	uncovers *clumsy* but not *bur*, male recobo from *EP838* (not *bhd* allele)	Yes/D. Huen
EP838[49e1]	uncovers acon but not k7215, male recobo from *EP838* (not *bhd* allele)	Yes/D. Huen
EP838[5C1]	doesn't uncover clumsy, male recobo from *EP838*, lethal (not *bhd* allele)	No/D. Huen
REAGENTS I MADE		
Male recombination		
KG2636 [Q513]	lethal (not a mutant)	yes
KG2636 [T421]	lethal (not a mutant)	yes
KG2636 [K511]	lethal (not a mutant)	yes
P-element replacement		
KG2636 [34.5.1]	w+, GFP (has WeeP with *white* not KG)	yes
KG2636 [34.8.3]	w+, GFP (has WeeP with *white* not KG)	yes
KG2636 [31.1.1]	w-, GFP+ (has WeeP with *white* flipped out)	yes
KG2636 [34.8.5]	w-, GFP+ (has WeeP with *white* flipped out)	yes
P-element hopping		
KG2636 (2-6)	homozygose lethal (viable over DF)	yes
KG2636 [4-17]	26bp deletion of the sequence flanking the 3' end of *KG2636* (14 bp of P remain)	yes
KG2636 [4-25]	precise exicsion	yes
KG2636 [5-5]	precise excision	yes
KG2636 [9-6]	small insert (not a mutant)	yes
KG2626 [12-10]	3'end gone, small insertion, 5'end gone	yes
KG2626 [14-10]	precise (orange eyes) (don't USE!)	yes
KG2636 [15-12]	lethal (viable over DF)	yes

Figure 1. Satellite boutons in *bad hair day* mutants

A-C) Synapses are colabeled with a synaptic vesicle marker, synapsin (syn) and a neuronal membrane marker (HRP). In wild type (A) boutons are aligned in a beads-on-a-string configuration. Note the arrow pointing to a satellite bouton. Whereas in *bad hair day* mutants, *KG2636* (B) and *KG766* (C), many smaller, satellite boutons project off the main axes of the synapse. **D-F)** Synapsin staining of the synapses shown in (A-C) are psuedocolored for easy visualization of the difference in staining intensity. Syn is high in wild type (D), but much lower in *bhd* synapses (E, F). **G)** Quantification of satellite bouton phenotype in different mutant backgrounds (*wt* 3.5 $\pm$ 0.4, n=78, *KG2636*/+ 8.6 $\pm$ 0.7 n=17**, *KG2636*/*KG2636* 17.8 $\pm$ 1.3 n=46**, *KG2636*/*Df(2L)TW1* 15 $\pm$1.3 n=29**, *KG766*/*KG766* 12.1 $\pm$ 0.8 n=27**, *KG2636*/*KG766* 12.3 $\pm$ 0.9 n=22**, *KG2636 WeePW*+ 11.5 $\pm$ 1.0 n=23**, *KG2636WeePW*- 3.7 $\pm$ 0.5 n=61, number of satellite boutons on m4, ** $p<0.01$). Significance determined by Student's Ttest. **H)** Although *bhd* synapses have an increase in satellite boutons, the number of non-satellite boutons in no different than wild type. (*wt* 34.3 $\pm$ 1.9 n=38, *KG2636* 30 $\pm$ 1.9 n=27, *KG766* 34.7 $\pm$ 2.7 n=27, non satellite boutons). **I-J)** Double stranded *GFP* RNA (I) or double stranded *CG8677* RNA (J) was injected into wild type embryos. ds*CG8677* injection, but not ds*GFP* injection, results in the *bhd* phenotype. **K-N)** Satellite and non-satellite boutons in wild type and *bhd* have normal pre and postsynaptic markers. wild type (K, L) and *bhd* (M, N) synapses were costained with the synaptic vesicle protein, synaptotagmin (syt) (K, M), and a post synaptic glutamate receptor subunit (GluRIIA) (L, N). Note the reduced staining of syt, but not GluRIIA in *bhd* synapses.

Figure 2. TGFβ -mediated synaptic growth is required to generate satellite bouton phenotype in *bhd*.

A-C) Synapses were costained with a synaptic vesicle marker, (syn) and a presynaptic membrane marker, (HRP). *bhd* mutant synapses (A) have a large number of satellite boutons. Where as *bhd* synapses lacking the TGFβ receptor, *wishful thinking* (*wit*) (B), or lacking one copy of the receptor (C) have significantly fewer satellite boutons. **D)** Sattelite bouton numbers in mutant combinations are quantified (*KG2636/KG2636* 17.8 ± 1.3, n=46, *KG2636/KG2636*; wit^{A12}/+ 9.1 ± 1.5 n=28**, *KG2636/KG2636*; wit^{B11}/+ 8.3 ± 1.1 n=22**, *KG2636/KG2636*; wit^{A12}/ wit^{B11} 0.5 ± 0.2 n=65** satellite boutons, ** p<0.01). **E)** Non-satellite bouton numbers in mutant combinations are quantified (*KG2636/KG2636* 30.3 ± 1.9 n=27, *KG2636/KG2636*; wit^{B11}/+ 26.7 ± 1.6 n=18, *KG2636/KG2636*; wit^{A12}/ wiB^{b11} 11.8 ± 1.4 n=20 non satellite boutons). Note that *bhd; wit* double mutants are significantly undergrown (B, E). *bhd* mutants lacking only one copy of *wit* have normal synaptic growth, but a significant suppression of satellite boutons (C, D, E). **F)** Synthetic lethality between TGFβ inhibitor, *dad*, and *bhd*. (*KG2636* 0.4% n=677, *dad* 15% n=77, *KG2636/KG2636, dad/dad* 100% n=267 % larval lethality).

Figure 3. Molecular characterization of *bad hair day* mutants

A) A schematic diagram of a gene rich region on the second chromosome in which *CG8677* sits. *CG8677* is uncovered by a small deficieny, $k14029^{J1.1}$, which removes only ten genes. *CG8677* is also uncovered by a large deficiency, *Df(2L)TW1*. **B)** A more detailed diagram of the genomic region containing *CG8677* shows that *KG2636* and *KG766*, two *bhd* alleles, sit in intronic regions of *CG8677*. *CG8677* has two splice forms, one of which overlaps with the coding region for another gene, *CG31626*. In

addition, this longer *CG8677* splice form most likely terminates in *DHR39* intronic sequence (yellow bar). *EP838*, a UAS-containing element sits in the first intron of *CG8677*. **C)** A northern blot of wandering third instar larvae shows expression of the longer isoform of *CG8677* in wild type. This expression is greatly diminished in *KG2636* mutant larvae. Rp49 is a housekeeping gene, shown as a loading control.

Figure 4. *bad hair day* gene and protein sequence

The first 8158 common nucleotides of *bhd* gene sequence are shown, and the alternative 3' ends are shown individually. Intron/exon boundaries marked by an astrix (*); the start codon is boxed; the stop codons are boxed; the polyA signal for *CG8677-short* is shown in bold. The *bhd* protein sequence is shown beneath each codon. Amino acids highlighted by gray represent the highly conserved regions of *CG8677* such as XCD and PHD-fingers; underlined amino acids are coiled-coils; nuclear localization sequences are boxed and highlighted in gray; the boxed M is the predicted start of a truncated protein produced by driving *CG8677* using the *EP838* P-element.

Figure 5. Embryonic mRNA expression pattern for *CG8677*

A-C) *in situ* hybrization was performed with a *CG8677* probe. (A) Cellular blastoderm stage embryo, shows *CG8677* is a maternally contributed protein. (B) Gastrula stage embryo shows *CG8677* expressed in regions of the embryo including the ventral neurogenic region. (C) Late stage embryo shows expression of *CG8677* in regions including the ventral nerve chord.

Figure 6. The protein encoded by *CG8677,* dRSF is orthologous to the histone chaperone RSF-1/HBXAP.

A) The proteins encoded by *CG8677*, dRSF and RSF-1/HBXAP are similar. They share two domains: the X Conserved Domain (XCD, 41% identity) and the Plant Homeodomain Finger (PHD-Finger, 62% idenity). In addition, both proteins have coiled-coil domains flanking the XCD and PHD-Fingers (shown as black boxes), and contain stretches of glutamine rich regions (E-Rich) and arginine rich regions (R-Rich). dRSF has other putative domains in the C-terminus not found in RSF-1/HBXAP. **B)** RSF-1/HBXAP is a histone chaperone, which together with the SNF2H ATPase make up a chromatin remodeling complex called Remodeling and Spacing Factor (RSF). A similar complex may exist in Drosophila, and would contain the dRSF and the ISWI ATPase (SNF2H homolog). In Drosophila ISWI can associate with other proteins, e.g. NURFp301, to make up other biochemical complexes such as Nucleosome Remodeling Factor (NURF).

Figure 7. Male X-chromosome chromatin is normal in *bhd* mutants.

Polytene chromosome preparations from bhd mutants shows normal male X-chromosome chromatin. DAPI in purple highlights all chromosomes, and anti-MSL in green, highlights the X. Note the X-chromosome does not look different from other chromosomes.

Figure 1. Satellite boutons in *bad hair day* mutants

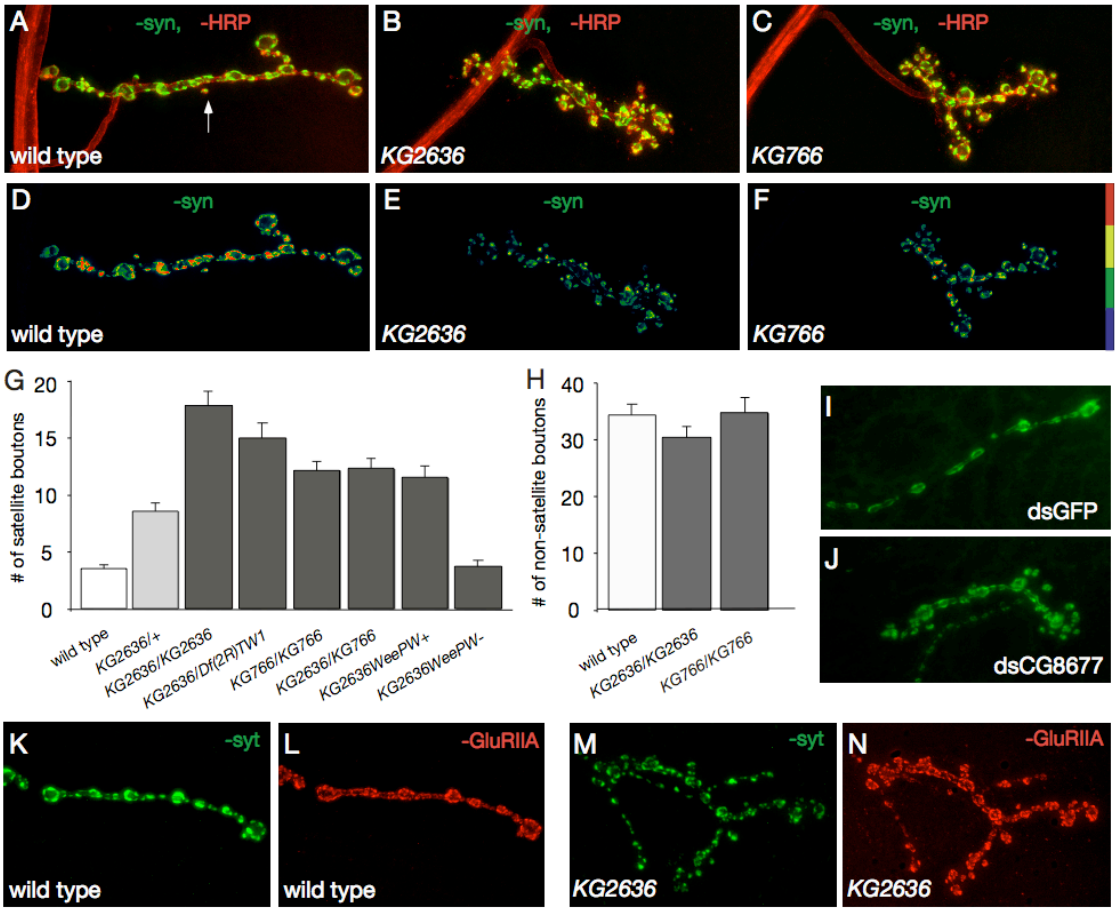

Figure 2. TGFβ -mediated synaptic growth is required to generate satellite bouton phenotype in *bhd*.

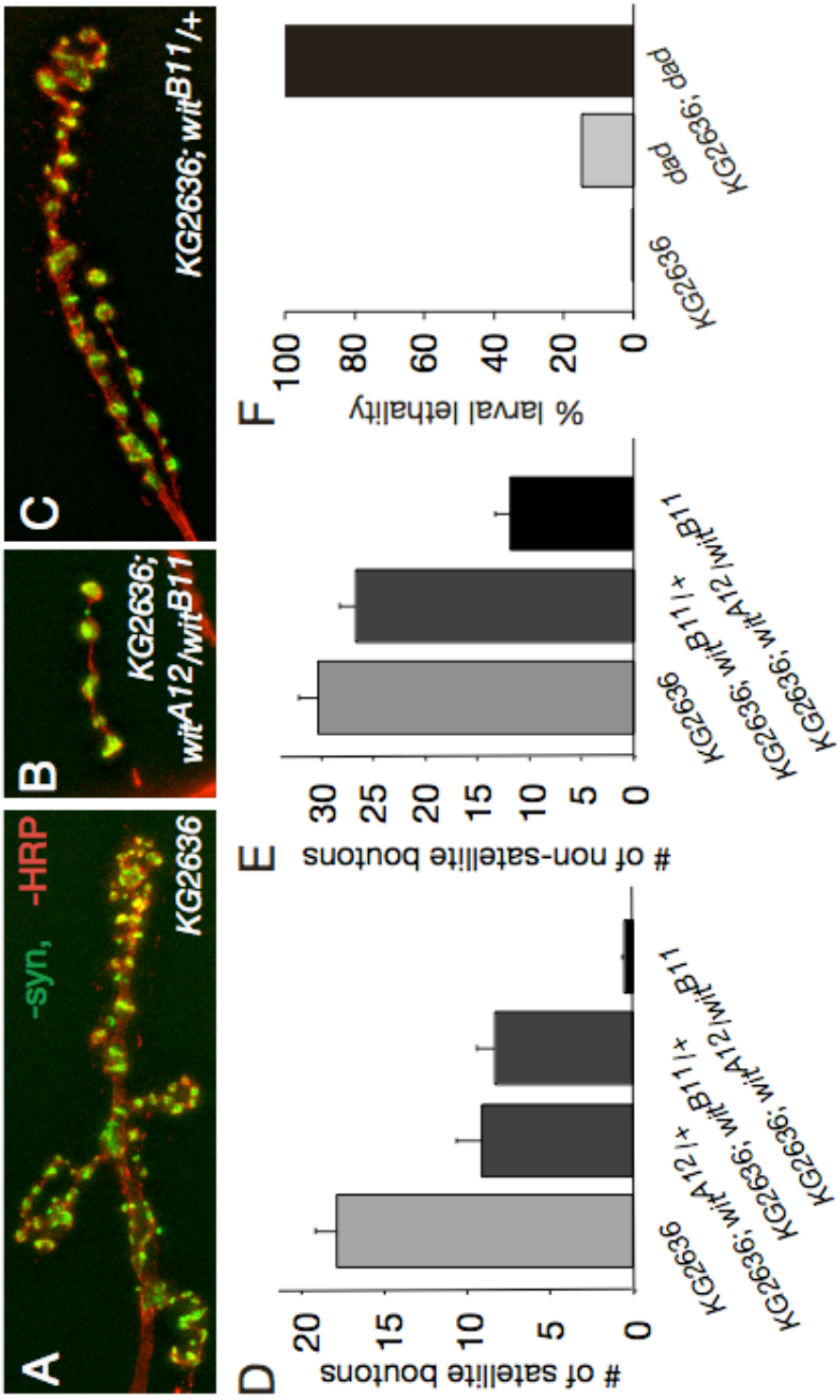

Figure 3. Molecular characterization of *bad hair day* mutants

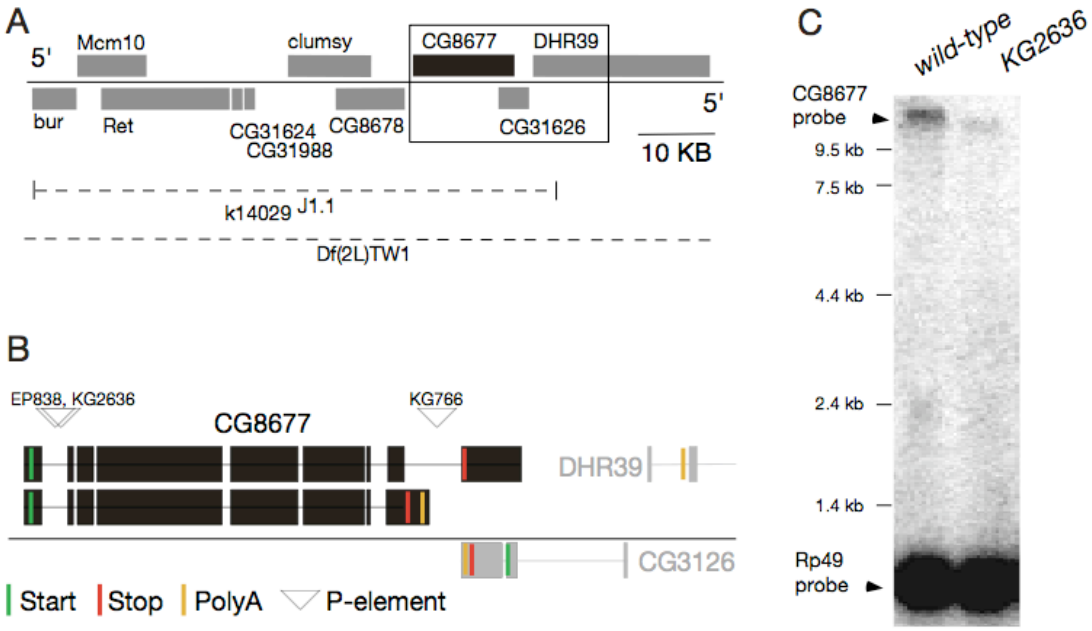

Figure 4. *bad hair day* gene and protein sequence

```
ATA AAG CAT TTT CGC TTG CTT TAA AAT AGG ATT TTA TCC CGT ACA AGA GCT GTC TCG CGG 60
CAA GAA ATA TGC ACC CTC GAA GTC TCG CAG TGC CGT GCG ACC AGA GAA CTT GAT CCT TGG 120
ACA AAT GAC TCG TGT TTG CAG TGC CCG TTT TGA GGT TTT GCC AGA GTA GTA TAC AAC ACC 180
CGA AAA TTT TCG CTG GTT CTC GGG GAC GCA TGA AAA ATG GCG GCG TCC TCA GCT GCG GCT 240
                                               M   A   A   S   S   A   A   A
GCG GCG CCC ACC AAT CCG ATC CCG CTT CCG ACG GAC TCC ATA TCG GAG GAG TGC AAG GAC 300
 A   A   P   T   N   P   I   P   L   P   T   D   S   I   S   E   E   C   K   D
GAC GAC GCC CTC ACC TCC ACG CTG CAC ACA TGC GCC AAT GAT CCG GAC TTT GCG GTC ATT 360
 D   D   A   L   T   S   T   L   H   T   C   A   N   D   P   D   F   A   V   I
TGC GCC TTC CTG CAA AAA TTC GGC AAG GAC CTG GGT CTT AAC CTG CCC AAC TTC AAG CAT 420
 C   A   F   L   Q   K   F   G   K   D   L   G   L   N   L   P   N   F   K   H
CTG CAG GAG TGG TTG ACA AAC AAC AAC GAT*GTT CCT GAG CTA AGG GAC TTG CAC ATA AAG 480
 L   Q   E   W   L   T   N   N   N   D   V   P   E   L   R   D   L   H   I   K
CTG CTC CGT AAG ACC CGT AAG ACG GTT CAC GAA AAG AGT TGG GAG TCC GCC CTC AGC AAA 540
 L   L   R   K   T   R   K   T   V   H   E   K   S   W   E   S   A   L   S   K
TTC TGC TTC GGC TAC TCG GTG CAA GAT GCC TGG GAA ATC GAA CGT TTC GGT TAT AGG AAT 600
 F   C   F   G   Y   S   V   Q   D   A   W   E   I   E   R   F   G   Y   R   N
TCC AGC TTG AAG GTT AAG CTG CGA ATA TTT CGG*GAA CTT CTC GAA AGT CAG TTT GAA CGC 660
 S   S   L   K   V   K   L   R   I   F   R   E   L   L   E   S   Q   F   E   R
AAT GCC AAG TTT CGG GCC CAC ATC CTC ACC TTG AAT GCC GAT ACT TTA CGC TCT GAG CCA 720
 N   A   K   F   R   A   H   I   L   T   L   N   A   D   T   L   R   S   E   P
ATT GGA AGG GAC CGG TTG GGA CAT GCC TAC TGG CTG ACT CAG GAT GCC CAC TGT AAT CTG 780
 I   G   R   D   R   L   G   H   A   Y   W   L   T   Q   D   A   H   C   N   L
CGG ATC TAC CAG GAG CAT CTA GAC GAG GAA ATT TGG CAG GTG GTT GCC ACG AAC AGG GAC 840
 R   I   Y   Q   E   H   L   D   E   E   I   W   Q   V   V   A   T   N   R   D
GAG TTT GTA AAT CTC ATT TCA AGG CTG CGC GGA AAT GAG GTG GTA CTT CCT TCG AAG GAC 900
 E   F   V   N   L   I   S   R   L   R   G   N   E   V   V   L   P   S   K   D
ATT GGT GAG GCC GAT GAG GAC ACC AGC AGC AGC AAC AGT TGT CAT CCC AAA CCA CCG CCC 960
 I   G   E   A   D   E   D   T   S   S   S   N   S   C   H   P   K   P   P   P
CCC GAA CAG AAA GAA GAA GAG GAC GAT GAG GAA GTT GGA GAT GAG CCC GAA AAA ACT GTA 1020
 P   E   Q   K   E   E   E   D   D   E   E   V   G   D   E   P   E   K   T   V
CCC AAT CTA AAG ATT AAA CTC CGC TCT CCC GAG CAA GAG GAT CAA AAG TCT AAA AAG GTT 1080
 P   N   L   K   I   K   L   R   S   P   E   Q   E   D   Q   K   S   K   K   V
AAG CCA CTG CTC ATT AGC CAG GCC AAA CTT TCG AGT AGC GCA TCG CCG GCC CCA ACC AAA 1140
 K   P   L   L   I   S   Q   A   K   L   S   S   S   A   S   P   A   P   T   K
AAA CGT TCT ATC GAA GAC GTA GAC AGC AGC CCC ACA GCC TCC CAG GAG GAA CAG CAG AAG 1200
 K   R   S   I   E   D   V   D   S   S   P   T   A   S   Q   E   E   Q   Q   K
AAG CAC CGT CCC ACA CTG CTT GAT ACA AAG CGA ATC AAA AAG CCA AGT CGC TAC GAA AGC 1260
 K   H   R   P   T   L   L   D   T   K   R   I   K   K   P   S   R   Y   E   S
ACT AAG GAT GAA ATC GAA GAA GAG TCC GGA GAA GAG GAT GAG GAA GAA GAG GAC GAG GAG 1320
 T   K   D   E   I   E   E   E   S   G   E   E   D   E   E   E   E   D   E   E
GAT TCT GAA TTG GAT GAG GGT GAG GAA GAG GAA GAT GTC GAT AGT GCG GCG GCG GAT ATC 1380
 D   S   E   L   D   E   G   E   E   E   E   D   V   D   S   A   A   A   D   I
GAG GAA GAT GAC GAT GAG GAA GAT ACT GGA GAG CCT ATA GAG GAT CCA ACG ATA GTG GTG 1440
 E   E   D   D   D   E   E   D   T   G   E   P   I   E   D   P   T   I   V   V
CAG GGC CAA GGA TCA GGA CTT GAC TGT GAA GCC ATC CCT TAT AAT TTA ATT GGC AAC TTT 1500
 Q   G   Q   G   S   G   L   D   C   E   A   I   P   Y   N   L   I   G   N   F
GAT TAT GAG GAT GAC TTG GAG ATC GGG GAA GCC ATT GCA GAT CCA ATG CTC CAT GTG ATT 1560
 D   Y   E   D   D   L   E   I   G   E   A   I   A   D   P   M   L   H   V   I
GGT CAA GGG TGG GGG ACC GAC TGT CTC GTG GGG AAT GGT AAA AAC GAA GCT TCC GTG GAG 1620
 G   Q   G   W   G   T   D   C   L   V   G   N   G   K   N   E   A   S   V   E
GAA ACG TCA ACG CGC ACA TCG GAA CCA AAA GCG ACG TTC TTT TTT GGC GAG CCC GGA TGT 1680
 E   T   S   T   R   T   S   E   P   K   A   T   F   F   F   G   E   P   G   C
CTC AAG CTA AGT CCC ATG AAG CAA ACA TCA AAA CCA GAG GCA AAA CGG GGC ATT TTT GAC 1740
 L   K   L   S   P   M   K   Q   T   S   K   P   E   A   K   R   G   I   F   D
AGC TTG AGC GAG GAG AAA ACA AAT GGT GAA AGC GAA AAG TGT ATA GTG AAC ACA CCG CCC 1800
 S   L   S   E   E   K   T   N   G   E   S   E   K   C   I   V   N   T   P   P
CGA AAT GGA AGC GAA CTC ACA AAA ACT CTG GGA GAT AGT GAA GAA ACA GCA TCT GCG AGT 1860
 R   N   G   S   E   L   T   K   T   L   G   D   S   E   E   T   A   S   A   S
GCA GCT ACA TTA GAA GAG ACT AAC ATA TGC CAA GAA GCT AAC GTA AAT AAA ATC TCA GAT 1920
 A   A   T   L   E   E   T   N   I   C   Q   E   A   N   V   N   K   I   S   D
GAT CAA ATA AAA AAA AAG GAA TCC GTA CCA GTG GCT AAA AGG AAT ATA CAG GAT AGT ACA 1980
 D   Q   I   K   K   K   E   S   V   P   V   A   K   R   N   I   Q   D   S   T
ATA AGC GTG ATC GAA AAG AAT GAG GAA ATC TCT AAA GGT CGT ACC GAA AGT GAG GCA ATT 2040
 I   S   V   I   E   K   N   E   E   I   S   K   G   R   T   E   S   E   A   I
GAA GAA GGA GTG AGG AAT AGG ACA GAA GTT TCA GTC TTA CAA AAT AAT TCA AAT GAA AGT 2100
 E   E   G   V   R   N   R   T   E   V   S   V   L   Q   N   N   S   N   E   S
GAT AAC TCC TCT ATT CAG ACT CAG GAT CAG CAT AAA GTT CCA GCT GAT CTG AAC AAT ACA 2160
 D   N   S   S   I   Q   T   Q   D   Q   H   K   V   P   A   D   L   N   N   T
```

```
AAG AAA CCA GTA ACA GAA AAA TGC GTC CTG GAA AGC GGT ACA GTT GAG GAT AAA CTG GTA 2220
 K   K   P   V   T   E   K   C   V   L   E   S   G   T   V   E   D   K   L   V
ATA AAT CAT CAG CAA ATT TCG ACA AAT GCC TTG GAC ACT GCA TGT GAT GAG AAA CTT TCG 2280
 I   N   H   Q   Q   I   S   T   N   A   L   D   T   A   C   D   E   K   L   S
TGT GAA ACA GAA AGC CCT GTA CCT AAC CAA CAT GAT TCC AAA ATG AAA TCA GAA CAG GAA 2340
 C   E   T   E   S   P   V   P   N   Q   H   D   S   K   M   K   S   E   Q   E
ACG GCA ACG AGC GCT AAG GAA TCA GTA TCT GAA TCT TCT CCA ACG GAT GGG GAA GAT GAA 2400
 T   A   T   S   A   K   E   S   V   S   E   S   S   P   T   D   G   E   D   E
ACA GCA AAA TCG AAA TGT TTG ATT GAC CCT TAT GCA GGA AAA ACC AAT GAT AAA GGT ATT 2460
 T   A   K   S   K   C   L   I   D   P   Y   A   G   K   T   N   D   K   G   I
ATT ATA AAT AAA ATT GAT AAG GCA GAA GGG GTT ATT AAA ACC TTG CTT CAA GAT GAT CCA 2520
 I   I   N   K   I   D   K   A   E   G   V   I   K   T   L   L   Q   D   D   P
CCT AAA GAT ATT TCA AAA AGC GAA ACG AAT ACA ACA TGT CTT GAA ATC AAT ATT TCG CCA 2580
 P   K   D   I   S   K   S   E   T   N   T   T   C   L   E   I   N   I   S   P
TCT GCA GAA CAT AGG ATT TCG GAA AAA GTT CAA ACC ATA GAA CCA AGT ACA TCC CAA AAC 2640
 S   A   E   H   R   I   S   E   K   V   Q   T   I   E   P   S   T   S   Q   N
TTA CTT TTC GAA GAC AAT GGA AAA TCC GGA GAG GTT GAC GGT AAG TCA AGG ACG AGT GGT 2700
 L   L   F   E   D   N   G   K   S   G   E   V   D   G   K   S   R   T   S   G
GCT GTT GAA GAA ATA TCT AAG ACA TCT ACG TTA TTA AAT CGC AAG CGG CGT CTT AAT GAC 2760
 A   V   E   E   I   S   K   T   S   T   L   L   N   R   K   R   R   L   N   D
TCT CAG TCC GCT CTA CGA AAC TCC ACC TCC GAA AGC GAA GTG CAC GAA GAG GAA CCG CAA 2820
 S   Q   S   A   L   R   N   S   T   S   E   S   E   V   H   E   E   E   P   Q
GAT GAC GAT CCT ACC CTG GAC GAT CTA GAT GTG GGC GGC AAG CGC ATT AAA ATG AGA CCG 2880
 D   D   D   P   T   L   D   D   L   D   V   G   G   K   R   I   K   M   R   P
AAG ACC ACT AAC GCG GAG TCC AGG CGA AAG GTG GAG GCT CAA AAA ACG CAG ATA GAA GAA 2940
 K   T   T   N   A   E   S   R   R   K   V   E   A   Q   K   T   Q   I   E   E
ACT ACT TCG TCC AGC GGA GAA GAC GAT GCG CGT ATT CGC CGC AAG TGT ATA GCT CCT CAC 3000
 T   T   S   S   S   G   E   D   D   A   R   I   R   R   K   C   I   A   P   H
ACT AAA ACC AAG CCC ACT CTG GAG GAA ATT ATT GAA AGA AAG TTA AAG AAA AGT ATA GAG 3060
 T   K   T   K   P   T   L   E   E   I   I   E   R   K   L   K   K   S   I   E
ATG GAT TTG CCG GAA AAG ACA ACT GAA AAA GTA ATG GAG ATG CCA ACG CAA CTG ATG CAG 3120
 M   D   L   P   E   K   T   T   E   K   V   M   E   M   P   T   Q   L   M   Q
AAA ACT AGA GAA GCT ACA CCG CCC ATC ATC TCC TTA AGT CCG CAA AAA AAA ACA CCG ATA 3180
 K   T   R   E   A   T   P   P   I   I   S   L   S   P   Q   K   K   T   P   I
ACC AAG CCC CTA AAG AAA AAT CTC CTG ACA CAA CTA CGA CAG GAG GAG AGT GAA GAA GAG 3240
 T   K   P   L   K   K   N   L   L   T   Q   L   R   Q   E   E   S   E   E   E
ACC ATA CCA AGA AAA CGA ACA AAC AGT GAG ACC CTC GTG CCT GCA ATT CCA GCA TCT AAT 3300
 T   I   P   R   K   R   T   N   S   E   T   L   V   P   A   I   P   A   S   N
GTA CTT TGT CAA CCG GAC GAG CGT CAT CGC AAG CGT CGT AGC AGT GAG GAT GCA AAT GAG 3360
 V   L   C   Q   P   D   E   R   H   R   K   R   R   S   S   E   D   A   N   E
GCG TTT TCG AAG GAA TCC TCC CCT ACT GAA GTG CCT CCG TCA GCC GTA AGC GAG AAG TTG 3420
 A   F   S   K   E   S   S   P   T   E   V   P   P   S   A   V   S   E   K   L
AAG CGC AAT AAC GAG CAG GAC ATA CAG GAG GAA GTC GAG GAC CCA CTT GCA ATG TCT GTC 3480
 K   R   N   N   E   Q   D   I   Q   E   E   V   E   D   P   L   A   M   S   V
AAG GAT TCA TTA CGT TCA GCT AAA GAC CAA TCG CCT GTA CCG GAG GGA TCT GCC CGT CGT 3540
 K   D   S   L   R   S   A   K   D   Q   S   P   V   P   E   G   S   A   R   R
TCT GGT CGC AGA GGT GGA CCT GCT GTC ATT CAC TCT GAG CTT CCT CAG CCA AAA AGG ACT 3600
 S   G   R   R   G   G   P   A   V   I   H   S   E   L   P   Q   P   K   R   T
CGA GGT GGG GCC AGG GAT AAA ATG CAG CCA GAG GTC AAT GCT GAG CTG AAG CAG GAA TCC 3660
 R   G   G   A   R   D   K   M   Q   P   E   V   N   A   E   L   K   Q   E   S
GAA GAT GAT GAG AAA ATT TCA ACC AAA ATA AAA TCT GAA GCT AAA GAC GAT CCA GCC CCA 3720
 E   D   D   E   K   I   S   T   K   I   K   S   E   A   K   D   D   P   A   P
GAA AGC CCA GAA AAT AGA AAG AAA CCT GAG GAG AAA CCC ATC AAG GAA GAG CCC AAC GAG 3780
 E   S   P   E   N   R   K   K   P   E   E   K   P   I   K   E   E   P   N   E
GAG CCA AAG CCA AAG GTG GGT CGT GGA CGT GGG CCG AGA AAG AAG CGT GAG GTG GAT ACT 3840
 E   P   K   P   K   V   G   R   G   R   G   P   R   K   K   R   E   V   D   T
ACC AAT ATC ATT GAG ACC AAC GAC TCG GAG ACA CCT GTG CGC CAA TCT AGG CGC ATT GCC 3900
 T   N   I   I   E   T   N   D   S   E   T   P   V   R   Q   S   R   R   I   A
CAG CAG AAG ATC AAA GAG GAA GCT GAA AGG CGA AAG CAA GAG GAG GTT GCT CTA CGT ACC 3960
 Q   Q   K   I   K   E   E   A   E   R   R   K   Q   E   E   V   A   L   R   T
ATG AAA CAG GAG CTT AAG AAA AAG AAA AAA GCC GAG AAG GAA GCA GAT CCT ACT GTG CTA 4020
 M   K   Q   E   L   K   K   K   K   K   A   E   K   E   A   D   P   T   V   L
GAA CCA TCA GGA GAA GAA TCA GAA TCC GAG GCC AGC GAG GCG GAG GAG GAG GCA CGT AAT 4080
 E   P   S   G   E   E   S   E   S   E   A   S   E   A   E   E   E   A   R   N
AAG AAG AAA AAA AAG TGT CCT GGC AAG GAT GGC TGG TCT TCC GAT TCA GAA GAA CAG CCA 4140
 K   K   K   K   K   C   P   G   K   D   G   W   S   S   D   S   E   E   Q   P
GAA AGT GAG GAG GAG GAG GAG CCA CCG CAC TAT GAA ACG GAT CCT GGT TCG CCA CTC 4200
 E   S   E   E   E   E   E   E   P   P   H   Y   E   T   D   P   G   S   P   L
TTC CGG TCC GAT CAC GAA TTT TCA CCA GAA TCG GAG CTT GAA GAT GAG TCT CAA GTG GTG 4260
 F   R   S   D   H   E   F   S   P   E   S   E   L   E   D   E   S   Q   V   V
CCA ATG AAA AGG GCG CGC ACC GTA CGG AAG GAG AAC GCC GAT GAC CTA GAG*GAG GAG GAT 4320
 P   M   K   R   A   R   T   V   R   K   E   N   A   D   D   L   E   E   E   D
```

```
GCG GAG GAA GCT TGT CAG AAA TGC GGC AAG TCT GAC CAT CCG GAG TGG ATT TTG CTC TGC 4380
 A   E   E   A   C   Q   K   C   G   K   S   D   H   P   E   W   I   L   L   C
GAC ACG CCT ACC TGT AAC AAA GGA TAC CAC TGC TCC TGC CTT TCA CCA GTG CTC TTC TAC 4440
 D   T   P   T   C   N   K   G   Y   H   C   S   C   L   S   P   V   L   F   Y
ATT CCT GAG GGC GAT TGG CAC TGC CCT CCT TGT CAG CAG GAG CAG CTC ATA GCT GCC CTG 4500
 I   P   E   G   D   W   H   C   P   P   C   Q   Q   E   Q   L   I   A   A   L
GAG AGA CAG CTG GAG CAA TAC GAC ACA TTG GTA GCT CAA AAG CAA CAG GAG CGG ATC TTG 4560
 E   R   Q   L   E   Q   Y   D   T   L   V   A   Q   K   Q   Q   E   R   I   L
GCT GAA GAG CAA GCC GAG CGA GAG CGT CAG GAG CTA GAG GCG GCC ACG CTG GCG GCG AAG 4620
 A   E   E   Q   A   E   R   E   R   Q   E   L   E   A   A   T   L   A   A   K
GAC GAA AAC TTC AAG AGC GAA AAG GAA GAG GAC GAA GAC GAT AGG GAT GAT ATG GCA GTC 4680
 D   E   N   F   K   S   E   K   E   E   D   E   D   D   R   D   D   M   A   V
GGC AAG GCT GAA AAG GTA AAG CGG CGT CGC GGA GAT GGA CGC ATT AAT AGG AGA GCT GCC 4740
 G   K   A   E   K   V   K   R   R   R   G   D   G   R   I   N   R   R   A   A
AAG CGA GGC ACC AGG CGC CGT CGT GGA AAC GAA TCT GAC TCC AGC CAC CGC AAA TCC TTA 4800
 K   R   G   T   R   R   R   R   G   N   E   S   D   S   S   H   R   K   S   L
GGC AGT GGC TCT AGA TCC GGA TCT GGA TCT GAC TCA AGT AGC GAC AAT AGC ACT AGC TTT 4860
 G   S   G   S   R   S   G   S   G   S   D   S   S   S   D   N   S   T   S   F
TCT GAC TCG GAT GAT GAA CCC ATA TAC AAG TTG CGC AAG CGG CGG CAA ATC AAC GTG AGC 4920
 S   D   S   D   D   E   P   I   Y   K   L   R   K   R   R   Q   I   N   V   S
TAT CGG CTT AAC GAG TAT GAC GAC CTT ATC AAT TCT GCT TTA AAA AAG GAG ATG GAT GAG 4980
 Y   R   L   N   E   Y   D   D   L   I   N   S   A   L   K   K   E   M   D   E
GTT GCC GGA GCA GGA AAT CTG GGC CGC GGC AAA GAC ATA TCC ACC ATT ATT GAG GCG GAT 5040
 V   A   G   A   G   N   L   G   R   G   K   D   I   S   T   I   I   E   A   D
AAG GAA AAG GCA CGA CGT GAT GAT CTG CCT ACG GAG GAT GAA GTG GGG AAT AAG GAA GAC 5100
 K   E   K   A   R   R   D   D   L   P   T   E   D   E   V   G   N   K   E   D
GGT GAG AAG GAT AAA CAA AAG TCA AAA TCT AGC GGC AGT AGT CCG TCG TCG TCA GAA GAC 5160
 G   E   K   D   K   Q   K   S   K   S   S   G   S   S   P   S   S   S   E   D
GAA GTA CCT CTC AAA CGT AGT AAC AAG TTT AAA CAA CCT CCT GCC AAA AAG AAG GCT CGA 5220
 E   V   P   L   K   R   S   N   K   F   K   Q   P   P   A   K   K   K   A   R
AAA CTG ACC ACC CTG GAC GTT AGC AGC GAA GAA GAT CAT GGA AGC GAT GAG GAC TTT AAA 5280
 K   L   T   T   L   D   V   S   S   E   E   D   H   G   S   D   E   D   F   K
ACG TCC AGT TAC TCG GAT GAA GAT ACT TCA CAG TCC GCA TCC GGA GAC TCA GAC TCA AGC 5340
 T   S   S   Y   S   D   E   D   T   S   Q   S   A   S   G   D   S   D   S   S
TTG GAG GCA TAC AGG CGA CCC GGT CGA GGA AAA AAG CAA AGA AAG GCA GCC AGG AGA GCG 5400
 L   E   A   Y   R   R   P   G   R   G   K   K   Q   R   K   A   A   R   R   A
GCA CGT GAA AGG CGC AAG GAT AGA AAG TTT GTG GTT GAA GAG AGT GAC GAA AGC GAA GAT 5460
 A   R   E   R   R   K   D   R   K   F   V   V   E   E   S   D   E   S   E   D
GAA GAT CAG AAG AGA CGG ACT ACA AAG TCA AAA AAG AAG AAA GAC GAT TCT GAC TAT ACA 5520
 E   D   Q   K   R   R   T   T   K   S   K   K   K   D   D   S   D   Y   T
GAA ACG GAA ACG GAA GAT GAC GAT GAT AAT GAG TTG TCC GAT AAC GTG GAC AGC GCC GAT 5580
 E   T   E   T   E   D   D   D   D   N   E   L   S   D   N   V   D   S   A   D
TTG TGT GAC GAC ACC ACT TCT GAG AGC GAG GAT GGT GCC TGG AAT CCT TCT TCC AAA AAG 5640
 L   C   D   D   T   T   S   E   S   E   D   G   A   W   N   P   S   S   K   K
AAA AAG ACG GTG GCC GCA AAG AAG TCG AAT TCG TCG GGT GGC ATC GCC AGA AAA TCA CCT 5700
 K   K   T   V   A   A   K   K   S   N   S   S   G   G   I   A   R   K   S   P
AAG CTA AAG AAG CTA GCC ACC CAG GCT GAG AAA AAG GTC AAG CGC TTG GAG TAC TCT GAC 5760
 K   L   K   K   L   A   T   Q   A   E   K   K   V   K   R   L   E   Y   S   D
GAC GAC ATA AGC GAG AGC GAT TTG GAA GAG GAT GAT GAC GAT GAC GAG GAA GAT GAA GAG 5820
 D   D   I   S   E   S   D   L   E   E   D   D   D   D   D   E   E   D   E   E
GGT GTA CCA TTG TCG GGC AAA GGT TCA GGC AAA CAA CCT CGC TCC CAG CCT CTT AAG CCG 5880
 G   V   P   L   S   G   K   G   S   G   K   Q   P   R   S   Q   P   L   K   P
ACC GCA TCT TCA ACC CTA ACA GGC AAG GGG AAA GGA AAA GGC AAG GCC AAA AAG AAA AAA 5940
 T   A   S   S   T   L   T   G   K   G   K   G   K   G   K   A   K   K   K   K
CAG GTG TCC TCT GAA GAA GAG GAC GGC GCC GCT TCC GAC GAT CGC ACT CGC ACC CGT GGT 6000
 Q   V   S   S   E   E   E   D   G   A   A   S   D   D   R   T   R   T   R   G
CGC CGA TAC GCC TAC ATT GAG GACG*AC GAC GAC AGC TCT GAC GGC GGC ATT AAA CCT GGC 6060
 R   R   Y   A   Y   I   E   D   D   D   D   S   S   D   G   G   I   K   P   G
GTG CAT CGG CCG GAT ACG CCA CCT GAG GAG CGT CAA AAA TTC ATC CAG CGG CAG GAG GAG 6120
 V   H   R   P   D   T   P   P   E   E   R   Q   K   F   I   Q   R   Q   E   E
ATA AAG CGT ATG CTC GCA GAG AAA AAT GCA GAG GGT GCG AAG ATT GCT GCT ACA CCA CGT 6180
 I   K   R   M   L   A   E   K   N   A   E   G   A   K   I   A   A   T   P   R
CTC ACG CCC CTT AAA TCT GGT GTC ACT GCA TCG GAG AAG CGC ACA CCT GGC AAG GCA GCA 6240
 L   T   P   L   K   S   G   V   T   A   S   E   K   R   T   P   G   K   A   A
AGC GGT GAT TCG CTT TCC ACG GTG CCC CTC TCG GTG ATT CGA CAG GCC AAG GTG CTG GAC 6300
 S   G   D   S   L   S   T   V   P   L   S   V   I   R   Q   A   K   V   L   D
ATC GAT TAC CTG CAA CGC AAA GGA GAG ACC ATT GGA GAT CTA GAT GAT GTG GAC GAG TCG 6360
 I   D   Y   L   Q   R   K   G   E   T   I   G   D   L   D   D   V   D   E   S
GAG CTA GAC GAC GCT GAG CTG CCC GAC GAC TTG CCC GAG GAC ATG GAG GAC GCG ATT GCT 6420
 E   L   D   D   A   E   L   P   D   D   L   P   E   D   M   E   D   A   I   A
CGA ATG GTG GAG GAG GAA GAA CAG TTC AGC GCG GAA GTG GCA GCT CGT GAG CTA CCT GGA 6480
 R   M   V   E   E   E   E   Q   F   S   A   E   V   A   A   R   E   L   P   G
```

```
GCA GAG GAG GTT CTG CGC ACT ACG CCT TCC AAG TCC AAG CAA ACT AGC AGG GTG ATG CCT 6540
 A   E   E   V   L   R   T   T   P   S   K   S   K   Q   T   S   R   V   M   P
GAG AGT CCA GCT CAA AAC TCC GCG CCC AGT ACA TCT GGC TTG CAG GAA CCA CAC CGA AAG 6600
 E   S   P   A   Q   N   S   A   P   S   T   S   G   L   Q   E   P   H   R   K
CGC CTT CCC ATG CCC ACG ATG CAT CCG CCG CTT CTG CGC CAC CAG TTC CCA ATC TCT GCC 6660
 R   L   P   M   P   T   M   H   P   P   L   L   R   H   Q   F   P   I   S   A
GGC CCG TCA CAT TCT CCT GCA TCT CTG GTT CCT CCT CAT GCA GCT CAG GGT ATG CAT CCC 6720
 G   P   S   H   S   P   A   S   L   V   P   P   H   A   A   Q   G   M   H   P
ATG CTC CAA AGA CAC CTT TCG CAG ACT GTC CCC CCA CCA CAG GCT ATG CAT CTC CTG CAA 6780
 M   L   Q   R   H   L   S   Q   T   V   P   P   P   Q   A   M   H   L   L   Q
AAT GCC CTA TCC GCT CCT CTT GGT CAG CCG CTC GGA TGT GGT AAT TAC GGA TCC GGC CCA 6840
 N   A   L   S   A   P   L   G   Q   P   L   G   C   G   N   Y   G   S   G   P
AAT TCT GCC CAA CAT CTG CCT CTG GTC ATG TCT ATG CCT TCG GCT GCG GCG GCG GCT GCC 6900
 N   S   A   Q   H   L   P   L   V   M   S   M   P   S   A   A   A   A   A   A
CAT CTT ATG CAA TCG GCG GTC GCT TCT GCT ACA GCG CGT CCA GTT GAG ACA GCA TCG GGT 6960
 H   L   M   Q   S   A   V   A   S   A   T   A   R   P   V   E   T   A   S   G
AAC CCA GCT TCT GAT CCG AAA CCA AGG GGT AGA CGA AAA AAG GTT ACA CCC CTT AGG GAT 7020
 N   P   A   S   D   P   K   P   R   G   R   R   K   K   V   T   P   L   R   D
CAG TTG CAG AAG CAA CAA ACG GCG GCC GCT GTT ACG GCT GCC ACT TCT TCA ACT ACA CCG 7080
 Q   L   Q   K   Q   Q   T   A   A   A   V   T   A   A   T   S   S   T   T   P
GGA TCA GCC CCC TCG GAA AAG GTG AAG GCC CAA CCG CTC TTT AAG CCG CAC GAG GAT GCT 7140
 G   S   A   P   S   E   K   V   K   A   Q   P   L   F   K   P   H   E   D   A
GCC CCT AGC GCT CCT GCT TCC CAA GCC TCT GTG ATT ACC CGG ATG CCG TCG CTC CTT CCT 7200
 A   P   S   A   P   A   S   Q   A   S   V   I   T   R   M   P   S   L   L   P
CCG GCC CAT GGA CGA AAT CAT GGA CCG CCC AGT GGT TTA TAT CCA AGC AGT GCG GAT TTG 7260
 P   A   H   G   R   N   H   G   P   P   S   G   L   Y   P   S   S   A   D   L
GCC CGA TTC TAT GGC CAA GTA GCT AAC CAG CAA CCC ATT CCC GCT GTC CCA GGC TCT CGT 7320
 A   R   F   Y   G   Q   V   A   N   Q   Q   P   I   P   A   V   P   G   S   R
TCT CCT TCT TCG ACG TCA GGA CCT CCT AGA CAC CTT TTG CGA CCG CAA ATG CCA CCT GGA 7380
 S   P   S   S   T   S   G   P   P   R   H   L   L   R   P   Q   M   P   P   G
TTG CCT CCG CCT CAC GCA TCC CTA CGA CCC ACC TAC GGA CCA CCG CCG CCA CTT CGC GGA 7440
 L   P   P   P   H   A   S   L   R   P   T   Y   G   P   P   P   P   L   R   G
TCT GGC CCA CCA ACT TCT ACG CCC AGT ACT ACG ACC AAT TCC AGG CCG GCT TAC CTT CAC 7500
 S   G   P   P   T   S   T   P   S   T   T   T   N   S   R   P   A   Y   L   H
GGA GCC GAG CAT CAC GGT GGA CCC TCT GGG CCC CCA ATG GGA GGA GTC TTT AGT TCC GGG 7560
 G   A   E   H   H   G   G   P   S   G   P   P   M   G   G   V   F   S   S   G
CCG CCA CCA GCG CGA CAT GCA ACT CCC CAC TTG AAT CCC TAC AGAG*CG CCG CCC ATT TAT 7620
 P   P   P   A   R   H   A   T   P   H   L   N   P   Y   R   A   P   P   I   Y
GGC AAT CCA AAC TAT TCC CCT CGT CTT GGT GGA GCT CCC GGA ACT GGA AGT ATG CGC CCT 7680
 G   N   P   N   Y   S   P   R   L   G   G   A   P   G   T   G   S   M   R   P
GGA GCT GTG GAC TAC GTT GCT GGA CCAC*GT GGA TAT TCC CCA TAT GGC TAT TAT CCC CCG 7740
 G   A   V   D   Y   V   A   G   P   R   G   Y   S   P   Y   G   Y   Y   P   P
CCC CCG CCG CTG TCC ACA CCA TCT GCC CAC GCA GCG ACA AGT TCT GTG ATC GTA AGT GCT 7800
 P   P   P   L   S   T   P   S   A   H   A   A   T   S   S   V   I   V   S   A
CCG CAC ACC CTG ACG CCA ACG AAT CAC TCG GTT CCC ACT TTG ACG CAT GGA AAG ACT CCT 7860
 P   H   T   L   T   P   T   N   H   S   V   P   T   L   T   H   G   K   T   P
CCT CAA CAA ACT CCG ACA CAG TCT TCA GGT CCA CCA CCC GCT GCA GCC CCG CCA CCC ACA 7920
 P   Q   Q   T   P   T   Q   S   S   G   P   P   P   A   A   A   P   P   P   T
ATA ACC AGC GAA ACC AGC AGC CAC AAG CCA CCA CTG GCT TCT GTG ATA ACC AGC AAA AAG 7980
 I   T   S   E   T   S   S   H   K   P   P   L   A   S   V   I   T   S   K   K
CTA ACT ACT CTA GAG GCG TAT CCC ATC AGG AAG TCC CCG ATT GCA GTA GTG GCC GAT GTA 8040
 L   T   T   L   E   A   Y   P   I   R   K   S   P   I   A   V   V   A   D   V
TCG GGT CCG GCA GAA CCT ACT AGG TCA CCG GCA CCT ATA GCC GAG GAA GAC TCA GGA TCA 8100
 S   G   P   A   E   P   T   R   S   P   A   P   I   A   E   E   D   S   G   S
GCT CAT GAC ACG AGA GCT CCG TCA TCC GCA ACA GGA ACA GCA GTC GTG GGA GAG TTC A   8158
 A   H   D   T   R   A   P   S   S   A   T   G   T   A   V   V   G   E   F
```

CG8677-short:

```
aGT GGG TTG GTA AGC TAC TTT AGC TCG CAA CAG GAT GAT TAT GAC ACA TAA CAA ACG CCG
 S   G   L   V   S   Y   F   S   S   Q   Q   D   D   Y   D   T
       GCG GGA GCA TTA TTT AAA TTT GTA TAT ATC GAT CTG CTT GTA AAG TTA AAA AAC AAT TTT
       ACT TTA GGG CTA GAA ATC AAT CTT GGC AAT ACT TTA CCA ATA TAA GCT TTG TGT TTA AAC
       TAT AAT AAA ACA TAC ACA CAC CAA ACT GAT CCG AAT TCT TTA AAA AGA TTT CCA AAG ATT
       CTT TTA AAT TCG GTT TTG GCG ATC AGT TAA TGT TTT ATA GAA ATT TTA TGT TTG ATT GCT
       TTG TAA CGT CAC TCC CAT CGG CTT TCT ATG TTG TAT TTA ACT TAG TTC CCT TTA TGT GCT
       GTT ACA GTT TAG CTA AAT CAA GCA TCA ACT ACT TTT AGT ATT TTA ATT TAG CTC TAT ATG
       ATT TGA GCC CTA ACG CAA TAA AAG TAA GTT ATT AAT TAT ACA TAC CAT TAT AAT TAT ACG
       AAT ATA AGA TAA ACT TAT GAT CAT AAA TAT ATA TAG TCA ATA AAT ATA TAG ATT GAG TTA
       ATT ACA AAA TTA TGT AAG TAA ACC AGT TAT GCA GTG CAT ACT TAA AAA GAT TGA CTT GCG
       TAT CCA TTA TAA CGT TAA GAA GAT GGT ACT AAA TCA AAA AAG GGC GAA AAC ATA ATG TTC
       AC A ATA AAA CTA TTT ATT ATT AGT GGA AAG TA           8849 bp
```

CG8677-long:

```
aCT AAA ATC TCA ACG GGA ACT TTG CGT AAC AAC AAA TAT TCA ACA ACA ATG GGC GAC GGC
 T   K   I   S   T   G   T   L   R   N   N   K   Y   S   T   T   M   G   D   G
ACT TGT TAA TTT AAC AAG CTG TCA CCA CTC AAA TGG CTG CGG AAC TCT TTG GAA TCC ACC
 T   C
TGA TGT CCA TTT AGA AGC GGA AAC GCT TGG CAG GCA CAT TGT ACT GGT AGC CCG ACT CCA
       CGG GAG CTG GGG CAG AGT AAA CTG GAG CTG GAG CAG GAG CAG AGT AAA CTG GAG CGG GAG
       CAG GAG CCG AGT AAA CTG GAG CTG GAG CTG GAG CAG GAG CAG AGT AAA CTG GAG CGG GCG
       CAG GAG CGG GAA GGT CCT GGA CGG GAG GTA AAT ACT CGG GAG CTG GCG CAG GAG CAG AGT
       AAA CTG GAG CTG GGG CAG GAG CAG AGT ATA CCG GAG CTG GCG CAG GAG CAG AAT ACA CTG
       GGG CGG GAG CAG GGA TGT CTT GAA CAG GAG GCA GAT ACT CCG AAA CGG GTG CTG GTG CGG
       GAG CAG AGT AGA CTG GAG CTG GGG CTG GAG CGG AGT AAA CAG GAG CAG GTG CAG GAG CGG
       AGT AAA CGG GAG CTG GAG CCG GAG CTG GAA TGT CCT GGA CGG GAG GCA AGT ACT CAG GAG
       CTG GCG CAG GAG CAG AGT AAA CTG GAG CTG GGG CAG GAG CAG AGT AAA CTG GAG CTG GAG
       CAG GAG CAG AAT AAA CAG GAG CTG GAG CTG GGA TGT CTT GAA CAG GAG GCA GGT ACT CCG
       AAA CAG GTG CTG GTG CCG GAG CGG AGT AGA CTG GGG CTG GGG CTG GAG CGG AGT AAA CAG
       GAG CAG GCG CAG GAG CAG AGT ACA CAG GAG CTG GAG CCG GCG CAG ATA TCA CCT CCT GAA
       CGG GTG GCA GAT AAG CTG GAG CTG GAG CCG AGG GGA TGT TGA AGG TCG GCG TGG GCT TGT
       TGT AGC TAT AAC CAC TGC CCA GGT TAA GGT GGG AAA CAT CGG CGG AGG CCA AGG CGA TGG
       CGC ACA CAG CGA AGA CGA AGA GTT TCT AAA ATA AGC GGA AAT TTA AGG GTC AAG TGA GCG
       ATC GGG ATC CCC GAC ATC TTG ACG GTT GGC CAA GGC GAG CGG TTG AGC AAG GCC AAC GGC
       TTT CTT GAT CGA AGT TGT GAC CAG TGG ACA GTT TAC TCA CCA TTG TTA TTG ATT TGT TGG
       TCG GGC TTT TAA AGT TCG TTG GAT TTG CTT TGG CAA GCT CTT GTC GCA AGA CGC TCA AGC
       TGA ATG ATG TCG AAC TGC AGA TGG GCC CGC ACT TTT ATA CCA AAA GCC ATG CTT AAC TTG
       GTC TGG CCC ATT ATT ATT GCT GGA TAT CCG TCT TCG CGT CTT CGG TGT GGG CCT GGC GCT
       TCT TCT AGT CGA AGA AAA GGT AGA CAG TTA AGA AGA GAG CGG AGC AGT GAT CAT TAA CCC
       AGA GGC GGC TGT TGG GCG ATC AAA ACG AAA CAA AGA TAT ATT TAT TTT ATT TTT CCC TTT
       GAT CTT ACG TAT TAA CAT TAA GAA ACG TTA ATT TTC AAG TTT TGA ATA TGG TTT AGG GAG
       AAT TAA AAA AAA AAA AAC TAT           9678 bp
```

Figure 5. Embryonic mRNA expression pattern for *CG8677*

Figure 6. The protein encoded by *CG8677*, dRSF is orthologous to the histone chaperone RSF-1/HBXAP.

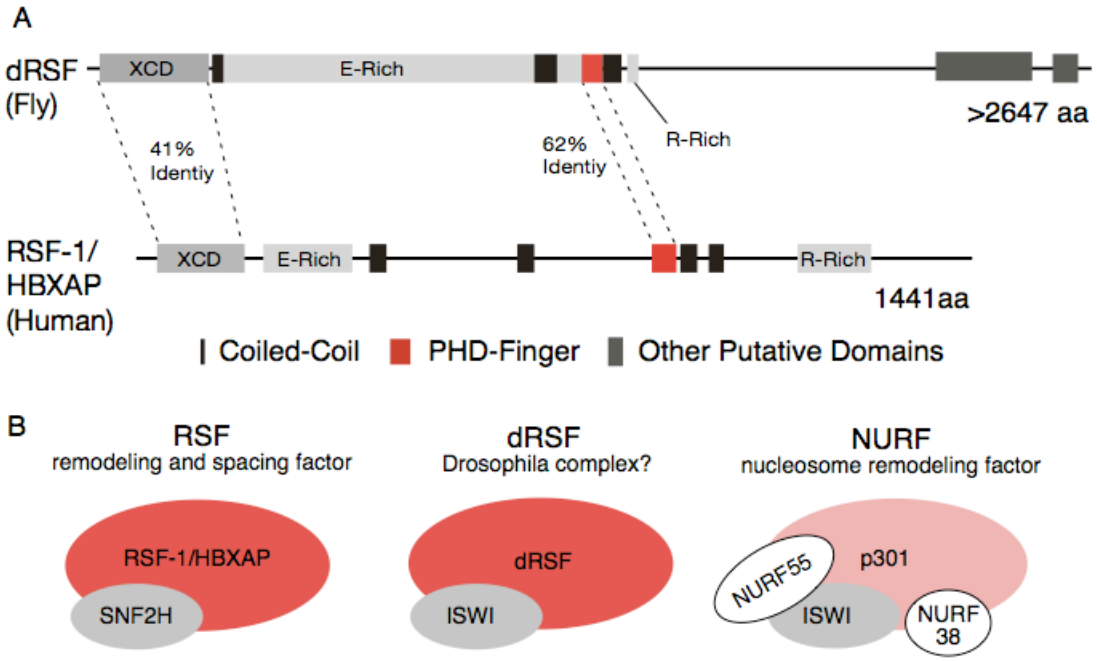

Figure 7. Male X-chromosome chromatin is normal in *bhd* mutants.

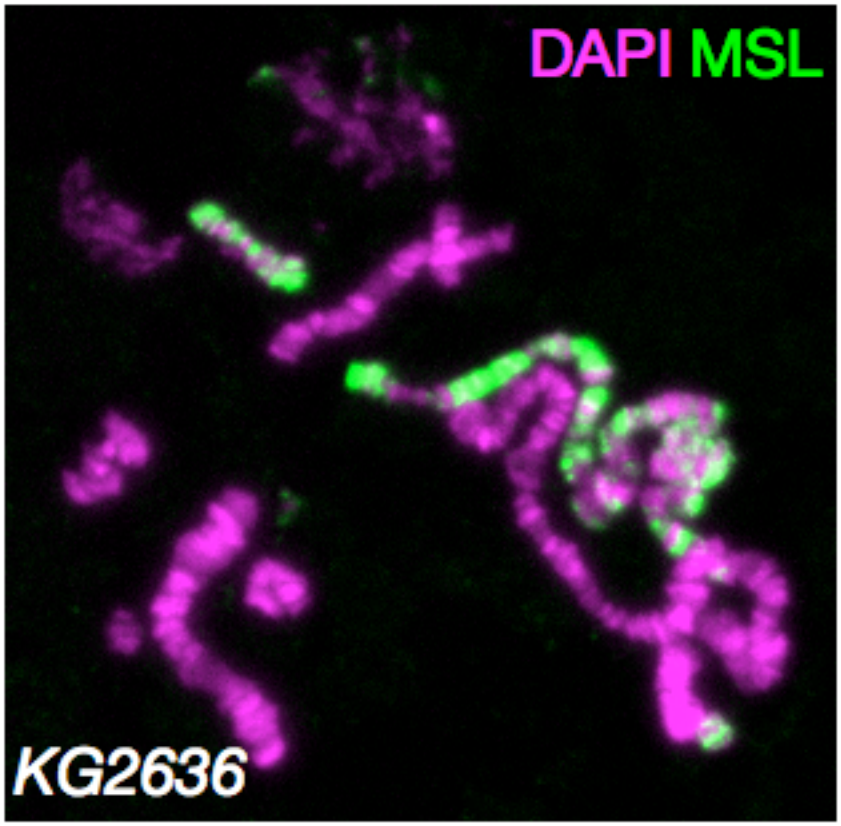

CHAPTER THREE

Cytoplasmic NF-κB, I-κB and IRAK Control Glutamate Receptor Density at the Drosophila NMJ

Elizabeth S. Heckscher, Richard D. Fetter, Kurt W. Marek, Stephanie D. Albin and Graeme W. Davis*

* to whom correspondence should be addressed

Department of Biochemistry and Biophysics

Programs in Neuroscience and Cell Biology

University of California, San Francisco

1550 4th Street

San Francisco, CA 94158-2822

SUMMARY

The NF-kB signaling system has been implicated in neurodegenerative disease, epilepsy, and neuronal plasticity. However, the cellular and molecular activity of NF-kB signaling within the nervous system remains to be clearly defined. Here we show that the NF-kB and IkB homologues Dorsal and Cactus surround postsynaptic glutamate receptor (GluR) clusters at the Drosophila NMJ. We then show that mutations in *dorsal*, *cactus* and *IRAK/pelle* kinase specifically impair GluR levels, assayed immunohistochemically and electrophysiologically, without affecting synaptic growth, active zone size or homeostatic plasticity. Additional genetic experiments support the conclusion that *cactus*, *dorsal* and *pelle* function together in this process. Finally, we provide several lines of evidence that Dorsal and Cactus act post-transcriptionally, outside the nucleus, to control GluR density at the NMJ. Taken together, our data support a model in which Dorsal, Cactus and Pelle function as a postsynaptic signaling complex that locally specifies GluR density.

INTRODUCTION

NF-kB is the founding member of a highly conserved family of Rel-homology domain containing transcription factors that have been ascribed diverse functions ranging from immunity and host defense to apoptosis, embryonic patterning and neural plasticity (Baldwin, 1996; Ghosh et al., 1998; Hacker and Karin, 2006; Meffert and Baltimore, 2005; Sen and Baltimore, 1986). The NF-kB transcription factor is embedded within an elaborate signaling cascade that conveys receptor signaling at the cell surface to NF-kB-dependent gene regulation in the cell nucleus. At the heart of the NF-kB signaling system is a core group of proteins that control NF-kB activity including the IkB/Cactus family of inhibitory molecules and the IRAK/Pelle protein kinase. The basic organization of NF-kB signaling is conserved from fly to human (Ghosh et al., 1998). Signaling is induced by ligand binding to cell surface receptors such as the Toll-like receptors involved in the recognition of microbes, antigen receptors (B-cell and T-cell receptors) and cytokine receptors such as the TNF-a super family receptors (Baker and Reddy, 1998). In general, receptor activation initiates receptor-associated intracellular signaling, including the activation of IRAK/Pelle kinase, followed by the phosphorylation and subsequent degradation of IkB/Cactus (Haker and Karin, 2006). In the absence of signaling, IkB/Cactus binds and sequesters cytoplasmic NF-kB. In response to signaling activation, the degradation of IkB/Cactus releases NF-kB/Dorsal into the cytoplasm allowing it to translocate into the cell nucleus where it functions as a transcriptional regulator capable of increasing or decreasing target gene transcription.

Although NF-kB has been studied intensively in the context of immunity, inflammation and cancer, far less is understood about the function of NF-kB in the nervous system. NF-kB is highly expressed in both the vertebrate and invertebrate central and peripheral nervous systems. The function of NF-kB in the vertebrate central nervous system can be divided into two categories. In the first category, NF-kB is thought to regulate processes related to disease and injury. For example, NF-kB has been implicated in the cellular response to brain injury, seizure and neurodegenerative diseases such as Alzheimer's and Parkinson's (Denk et al., 2000; Mattson and Camandola, 2001; Mattson et al., 2000a). Additional related functions could include the regulation of cellular anti-oxidation and neuronal apoptosis (Mattson and Camandola, 2001). In the second category, NF-kB has been suggested to function during neural development and synaptic plasticity (Bakalkin et al., 1993; Meffert and Baltimore, 2005; Meffert et al., 2003; Schmidt-Ullrich et al., 1996). For example, NF-kB knock-out mice have behavioral learning deficits (Meffert et al., 2003) and NF-kB has been suggested to play a role in the mechanisms of long-term synaptic plasticity (Albensi and Mattson, 2000; Mattson and Camandola, 2001; O'Mahony et al., 2006; O'Riordan et al., 2006). NF-kB is also highly expressed in muscle at the vertebrate and invertebrate neuromuscular junction (Baghdiguian et al., 1999; Cantera et al., 1999a). At the vertebrate NMJ, activation of NF-kB has been implicated in the mechanisms of muscle wasting associated with disease (dystrophies and cachexia) and denervation (Cai et al., 2004; Fraser, 2006; Guttridge et al., 2000). In these studies, enhanced NF-kB signaling has been shown to be deleterious. However, in both the central and peripheral nervous systems, the function of endogenous NF-kB is not well understood.

To date, studies of NF-kB signaling in the nervous system have highlighted a transcriptional function for NF-kB signaling that is consistent with the known activity of this signaling pathway in other systems. Core components of the NF-kB signaling system are present both pre- and postsynaptically and it is hypothesized that NF-kB/Dorsal can translocate from the synapse to the neuronal nucleus to control gene expression (Albensi et al., 2000; Albensi and Mattson, 2000; Furukawa and Mattson, 1998; Meberg et al., 1996; Meffert and Baltimore, 2005; Meffert et al., 2003). It has been speculated that NF-kB could also function locally at the synapse (Meffert and Baltimore, 2005). However, despite being an attractive hypothesis, direct experimental evidence in favor of a local synaptic function for NF-kB has yet to be defined.

We have performed a genetic analysis of NF-kB signaling at the Drosophila NMJ by examining mutations in several core components of the NF-kB signaling system including *NF-kB*/*dorsal*, *IkB*/*cactus* and *IRAK*/*pelle*. To our knowledge, this analysis includes the first description of the effects of *IRAK*/*pelle* mutations in the nervous system of any organism. We have assayed synapse morphology, synaptic efficacy, synaptic ultrastructure, glutamate receptor (GluR) density and the homeostatic modulation of presynaptic release. Our analysis provides evidence that NF-kB/Dorsal, IkB/Cactus and IRAK/Pelle are necessary to control glutamate receptor density at the postsynaptic muscle membrane. Remarkably, we find no evidence for a nuclear function of NF-kB/Dorsal. Rather, our data support a model in which NF-kB/Dorsal, IkB/Cactus and IRAK/Pelle function locally, at the postsynaptic NMJ to specify GluR density. These data define a cytoplasmic function for the core components of the NF-kB signaling system that may be directly relevant for the observed changes in synaptic plasticity and learning

related behavior observed in mammalian systems following disruption of NF-kB signaling. Our data may also have relevance to the neuronal response to injury or infection that has been shown to potentiate NF-kB signaling in the vertebrate central and peripheral nervous systems.

Dorsal and Cactus surround postsynaptic GluR clusters

It was previously shown that NF-kB/Dorsal and IkB/Cactus are present postsynaptically at the Drosophila NMJ (Cantera et al., 1999a). We have confirmed and extended this finding. First, we demonstrate the specificity of the Cactus and Dorsal antibodies (Gillespie and Wasserman, 1994; Reach et al., 1996) that we use in our analyses at the NMJ. We show that anti-Dorsal immunoreactivity at the NMJ is eliminated in a *dorsal* null mutant (Supplemental Figure 1A-D). Similarly, anti-Cactus synaptic immunoreactivity is eliminated in the *cactus* null mutant (Supplemental Figure 1E-H).

Given the specificity of the Dorsal and Cactus antibodies, we went on to characterize the sub-synaptic localization of these proteins in greater detail. First, we show that Dorsal immunoreactivity surrounds presynaptic markers that delineate the neuronal membrane (anti-HRP) and define the presynaptic vesicle pool (anti-synapsin) (Figure 1A-F). In addition, Dorsal staining is absent from presynaptic axons just prior to entry into the muscle field, indicating that Dorsal protein is absent from the presynaptic motor axon (Figure 1D-F arrow). These data are consistent with the proposed postsynaptic localization of Dorsal at the NMJ (Cantera et al., 1999a). In addition, consistent with other reports (Cantera et al., 1999b), we find no evidence for expression of either Dif or Relish, two additional Rel homology domain transcription factors, at the Drosophila NMJ (data not shown).

A similar analysis demonstrates that Cactus, like Dorsal, is localized postsynaptically and is absent from the presynaptic axon prior to muscle innervation (Supplemental Figure 1 arrow, and data not shown). Interestingly, 3D confocal imaging of synaptic boutons at the third instar NMJ demonstrates that Cactus immunoreactivity surrounds postsynaptic GluR clusters within the muscle (Figure 1G-I). Again, Dorsal immunoreactivity shows a similar distribution (data not shown). Ultimately, we were prevented from directly testing Cactus/Dorsal co-localization because the available antibodies were raised in the same species. However, we went on to confirm that Cactus and Dorsal both precisely co-localize with an independent postsynaptic marker Discs-Large (Dlg) (data not shown). Based on these data, and data from previously published reports (Cantera et al., 1999a), we conclude that Dorsal and Cactus co-localize postsynaptically in a region surrounding the GluR clusters. This is in contrast to the general cytoplasmic localization of these proteins in other cell types.

Dorsal controls GluR abundance at the NMJ

To study the function of Dorsal at the NMJ we have taken advantage of a series of mutations that have been previously shown to disrupt the *dorsal* gene during embryonic patterning and innate immunity (Table 1). Importantly, homozygous *dorsal* mutants derived from heterozygous females have sufficient quantities of maternally supplied Dorsal protein to allow for normal embryonic development. This allows us to analyze the function of *dorsal* mutations during larval development.

We first demonstrate that Dorsal is not required for synaptic growth or synapse morphology. All *dorsal* mutations analyzed in this study, including null mutant

combinations, survive as healthy, normally sized third instar animals. We quantified bouton numbers at the NMJ of muscles 6 and 7 as done previously (Eaton and Davis, 2005). Bouton numbers are normal in a *dorsal* trans-heterozygous zygotic null mutant combination ($dorsal^{1}/dorsal^{H}$) and in a second trans-heterozygous mutant combination ($dorsal^{2}/doral^{H}$) compared to wild type controls (*wild-type* = 100±7.8, n=19; dl^{1}/dl^{H} = 109 ± 6.3, n=28; dl^{2}/dl^{H} = 98 ± 6.7, n=17; data represent % wild-type bouton number on muscles 6/7).

In the vertebrate nervous system, NF-kB signaling has been implicated in forms of neuronal plasticity that are typically associated with changes in the abundance of postsynaptic GluRs (Furukawa and Mattson, 1998; Meffert and Baltimore, 2005; Meffert et al., 2003; O'Mahony et al., 2006). Therefore, we assayed GluR abundance at the NMJ of *dorsal* mutant animals. To do so, we quantified the fluorescence intensity of GluRs at the NMJ using previously published methodology (Albin and Davis, 2004). We find that GluR levels are significantly decreased in *dorsal* null mutant animals (dl^{1}/dl^{H}) compared to wild type and heterozygous controls (Figure 2). A similar decrease in GluRIIA levels is also observed in a second strong loss-of-function *dorsal* mutant, dl^{PZ}/dl^{PZ} (Figure 2; Table 1; Isoda et al., 1992; Norris and Manley, 1992). Finally, over-expression of *dorsal* in muscle did not change GluR levels compared to wild type indicating that increased Dorsal protein levels are not sufficient to enhance GluR abundance beyond that observed in wild type (Figure 2D). In all experiments, the level of a control antigen, anti-HRP, did not consistently differ between genotypes (Figure 2E) and a small, but statistically significant, change in Dlg was observed (*wild-type* = 100+/-0.9, n=19; dl^{1}/dl^{H} = 93+/- 0.9, n=18, $p<0.05$). The change in synaptic Dlg is far less than that observed in other

mutations that control postsynaptic morphology (Albin and Davis, 2004). Thus, we conclude that Dorsal is necessary for normal postsynaptic GluR abundance.

We next took advantage of existing mutations to examine the domain requirements of Dorsal/NF-kB for the regulation of GluR abundance. All NF-kB family members contain a highly conserved Rel Homology Domain (RHD). The RHD of Dorsal mediates signal-dependent phosphorylation, homodimerization, DNA binding, nuclear localization as well as interaction with other NF-kB signaling proteins such as Cactus and Pelle (Ghosh et al., 1998; Govind, 1999; Isoda et al., 1992). The *dorsal*^{2} allele (*dl*^{2}) harbors a point mutation that specifically disrupts the RHD (Figure 3E, Table 1). Mutant Dorsal protein in the *dl*^{2} background remains concentrated at the NMJ (Figure 3F). Quantification of GluRIIA fluorescent intensity demonstrates that GluRIIA levels are strongly reduced in the *dl*^{2} mutant (Figure 2B, D; $p<0.001$ compared to wt). Surprisingly, we also observe a significant decrease in GluRIIA levels in the *dl*^{2}/+ heterozygous animal (Figure 2D). Since the heterozygous null mutations show normal GluRIIA levels (*dl*^{H}/+; Figure 2D), our data demonstrate that the *dl*^{2} mutation acts in a dominant-negative manner to impair GluR abundance. This would be consistent with Dorsal functioning as part of a protein complex that controls GluR levels.

Dorsal also contains a transactivation domain (Figure 3E) that mediates the interaction between Dorsal and nuclear co-factors that are required for Dorsal-dependent transcriptional regulation (Flores-Saaib et al., 2001; Isoda et al., 1992; Shirokawa and Courey, 1997). The *dl*^{U5} mutation truncates the transactivation domain and disrupts Dorsal-dependent transcriptional regulation (Isoda et al., 1992). First, we demonstrate that mutant protein remains at the NMJ in *dl*^{U5} animals (Figure 3C,F). However, unlike

the dl^2 mutants, GluRIIA levels are not decreased in dl^{U5} mutants (indeed there is a statistically significant increase in abundance compared to wild type, $p<0.05$; Figure 3A-D, G). These data are surprising since both the RHD and transactivation domains are necessary for Dorsal-mediated transcriptional activity (Govind et al., 1999). For example, both the dl^2 and dl^{U5} mutations cause mutant phenotypes in embryonic patterning consistent with disrupted Dorsal-mediated transcription (Isoda et al., 1992). At a minimum, our data demonstrate that mutation of the protein domains necessary for Dorsal-dependent transcription does not always correlate with decreased GluR abundance.

Mutations in *dorsal* Alter Synaptic Function

To determine whether the observed changes in receptor abundance correlate with altered synaptic efficacy, we performed an electrophysiological analysis of synaptic function in *dorsal* mutants. We find a significant reduction in the average amplitude of spontaneous miniature excitatory postsynaptic amplitudes (mEPSP) in the *dorsal* null mutation (dl^1/dl^1) compared to wild type (Figure 4A, B, G). Importantly, there was no change in the average resting membrane potential or the average muscle input resistance (Figure 4C, D). Similar observations were made for a separate allele (dl^{PZ}/dl^{PZ}; data not shown). Thus, the observed decrease in GluR abundance assayed by fluorescence microscopy is correlated with a change in GluR sensitivity assayed electrophysiologically. Since a genetic reduction in GluRIIA abundance is sufficient to reduce mEPSP amplitude at the Drosophila NMJ (Petersen et al., 1997), we suspect that reduction in GluR abundance in *dorsal* is the cause of the decrease in mEPSP amplitude.

At least five different genes can contribute to the composition of multimeric GluR complexes at the Drosophila NMJ (Featherstone et al., 2005; Marrus et al., 2004; Petersen et al., 1997; Qin et al., 2005). To investigate whether Dorsal specifically controls the levels of the GluRIIA subunit, we examined *GluRIIA-dorsal* double mutant animals. We find that that mEPSP amplitudes in the *GluRIIA-dorsal* double mutant animals are decreased beyond that observed in the *GluRIIA* mutant alone (Figure 4A, B, G). This observation suggests that Dorsal may influence the abundance of GluR subunits in addition to the GluRIIA subunit. Consistent with this possibility, we find a statistically significant decrease in the levels of the GluRIIC subunit in the *dorsal* mutant background (Figure 2F). In conclusion, our genetic analysis demonstrates that Dorsal is required to establish or maintain normal GluR abundance at the Drosophila NMJ.

At the NMJ, pharmacological or genetic manipulations that decrease mEPSP amplitude initiate a homeostatic, compensatory signaling system that increases presynaptic transmitter release and restores normal muscle excitation (Davis, 2006; Davis et al., 1998; Petersen et al., 1997). Therefore, we asked whether NF-kB signaling participates in the homeostatic regulation of presynaptic transmitter release. Excitatory postsynaptic potential (EPSP) amplitudes are normal in the *dorsal* mutant despite decreased mEPSP amplitudes (Figure 4E). Furthermore, in the *GluRIIA-dorsal* double mutant we observe a further decrease in mEPSP amplitude compared to *GluRIIA* alone, and a further increase in quantal content (Figure 4). Taken together, we conclude that loss of Dorsal impairs GluR abundance but does not interfere with the signaling systems that mediate a homeostatic increase in presynaptic release at the Drosophila NMJ.

Pelle is Necessary for Normal GluR Abundance and Synaptic Function

In canonical NF-kB signaling, Pelle kinase (IRAK homologue) acts upstream of Dorsal to convey signaling from activated receptors to the Cactus/Dorsal complex (Edwards et al., 1997; Hecht and Anderson, 1993). Therefore, mutations in *pelle* are predicted to phenocopy the effects of the *dorsal* mutants on GluR abundance. We were able to use several *pelle* mutations to examine Pelle function at the NMJ. The alleles we analyzed included null mutations (pll^{25} and pll^{RM8} and *Df(3R)D605*) and a mutation that specifically impairs the kinase domain (pll^{078}) (Table 1). The mutant combinations that we examine here survive as normally-sized, third instar larvae with normal bouton numbers (*wild-type* = 100±7.8 and pll^{078}/pll^{078} = 100 ± 8.6, n=19; data represent % wild type bouton numbers).

In *pelle* mutant animals we find a significant decrease in GluRIIA fluorescence intensity demonstrating that Pelle is necessary for normal GluRIIA abundance (Figure 5 A-C). There is no change in a control antigen (anti-HRP; Figure 5D) and no change in the levels of postsynaptic Dlg (*wild-type* = 100+/-0.9, n=19; pll^{078}/pll^{078} = 94 +/- 6.0, n=24; data represent % *wild-type* synaptic anti-DLG fluorescence). Importantly, the kinase dead mutation (pll^{078}/pll^{078}) causes a decrease in GluRIIA levels that is as severe as observed in the null mutant conditions (pll^{RM8}/pll^{RM8} or pll^{25}/*Df(3R)D605*). Thus, Pelle kinase activity is required for the regulation of GluR abundance. We also observe a significant reduction in GluRIIA levels in the heterozygous null (pll^{RM8}/+) and heterozygous kinase dead (pll^{078}/+) animals (Figure 5C). It has been previously shown that the kinase activity of Pelle is sensitive to Pelle protein levels (Shen and Manley, 1998; Shen and Manley, 2002). Thus, our data also suggest that GluRIIA abundance is

sensitive to the levels of postsynaptic Pelle kinase activity at the NMJ. Finally, we demonstrate that muscle specific expression of a *UAS-GFP-Pelle* transgene restores GluRIIA fluorescence intensity to wild type levels in a *pelle* mutant supporting the conclusion that Pelle functions postsynaptically to specify normal GluR abundance (Figure 5C). We find that Pelle-GFP is present throughout the muscle, surrounds muscle nuclei and can traffic to the postsynaptic membranes where Dorsal and Cactus reside (data not shown). Together, our data indicate that Pelle kinase activity is required postsynaptically to control GluR levels.

We next performed an electrophysiological analysis of synaptic function in the *pelle* mutant background. As in the *dorsal* mutants we find a significant decrease in mEPSP amplitude in *pelle* mutants that correlates with the observed decrease in GluRIIA levels (Figure 5F-I). Again, there is no significant change in the average muscle input resistance or resting membrane potential that could account for this change (Figure 5G, H). In addition, we demonstrate that the muscle specific expression of *UAS-pelle* restores mEPSP amplitude to wild type levels (Figure 5F-I).

Finally, to formally test whether Pelle and Dorsal function in the same postsynaptic signaling cascade at the NMJ, we examined GluRIIA levels in a *pelle*; *dorsal* double null mutant animal (dl^1/dl^1; $pll^{25}/Df(3R)D605$). In these animals the decrease in GluRIIA levels is no greater than that observed in the *pelle* or *dorsal* mutants alone (Figure 5E). These genetic data indicate that *pelle* and *dorsal* function together in the same postsynaptic signaling pathway to control GluR abundance at the NMJ. These data are consistent with the known organization of NF-kB signaling in other systems.

Mutations in *cactus* Impair GluR Abundance

In canonical NF-kB signaling IkB/Cactus binds to and sequesters NF-kB/Dorsal protein in the cytoplasm (Edwards et al., 1997; Isoda and Nusslein-Volhard, 1994). As such, IkB/Cactus acts to inhibit NF-kB/Dorsal-dependent transcription until IkB/Cactus is degraded in a signal-dependent manner (Belvin et al., 1995; Bergmann et al., 1996; Reach et al., 1996). Consistent with Cactus acting to inhibit Dorsal in Drosophila, mutations in *cactus* and *dorsal* result in opposing phenotypes during both embryonic patterning and innate immunity (Govind, 1999). Therefore, we predicted that mutations in *dorsal* and *cactus* would also result in opposing GluR phenotypes. Instead, we find that *cactus* mutations phenocopy the *dorsal* and *pelle* mutations.

We analyzed severe loss of function mutations in *cactus* including $cactus^{E10RN}$ and $cactus^{A2}$ and observe decreased Cactus protein and decreased GluRIIA levels at the NMJ (data now shown). However, analysis of these mutations is complicated by the fact that these mutants are mid-larval lethal and have melanotic tumors associated with an essential function of Cactus in the larval hematopoietic cell lineage (Govind, 1996; Qiu et al., 1998). To circumvent mid-larval lethality, we analyzed two independent, temperature sensitive *cactus* alleles ($cactus^{RN}$ and $cactus^{HE}$, Table 1; Roth et al., 1991). Both alleles cause defects in embryonic patterning similar to, but less severe than, *cactus* null mutations indicating that $cactus^{RN}$ and $cactus^{HE}$ are loss-of-function mutations (Schupbach et al., 1989; Schupbach et al., 1991). When we raise $cactus^{RN}$ and $cactus^{HE}$ mutants at the non-permissive temperature (29ºC), these animals survive as healthy, normally sized third instar animals. This allows us to assay the function of Cactus at the mature, third instar NMJ.

We defined the molecular nature of the *cactus*^{RN} and *cactus*^{HE} mutations by sequence analysis and immunostaining (Table 1). The *cactus*^{RN} mutation is an A196Y mutation near the signal dependent domain of the Cactus protein. This domain is important for the signaling-dependent degradation of the Cactus protein (Bergmann et al., 1996; Govind, 1999; Reach et al., 1996). The *cactus*^{HE} mutation is a C315Y mutation within the third ankyrin repeat of Cactus. Ankyrin repeats in Cactus mediate protein-protein interactions, including the interaction between Cactus and Dorsal (Govind, 1999; Kidd, 1992). Both *cactus*^{RN} and *cactus*^{HE} have near normal levels of Cactus protein at the synapse, (*cactus*^{RN}/*cactus*^{RN} has 93±1.1% normal Cactus protein; *cactus*^{HE}/*cactus*^{HE} has 88±3.7% normal Cactus protein, $p<0.01$; n=8), indicating that these mutations do not strongly disrupt the synaptic localization of Cactus protein.

We tested whether *cactus* mutations affect synaptic growth and morphology. We quantified bouton numbers in *cactus*^{RN}/*cactus*^{RN} and *cactus*^{HE}/*cactus*^{HE} animals and compared these data to control animals raised under identical conditions. We find bouton numbers in both *cactus* alleles are not significantly different from wild type (*wild-type* = 100 +/- 7.8, n=19; *cact*^{RN}/*cact*^{RN} = 98+/- 10.2, n=9; *cact*^{HE}/*cact*^{HE} = 83+/- 8.8, n=14; data represent % wild-type bouton number at m6/7). In addition, using anti-HRP to visualize synaptic boutons, we find that synapse morphology is qualitatively normal in these *cactus* mutant backgrounds (data not shown).

We analyzed GluR levels in homozygous *cactus*^{RN} and *cactus*^{HE} mutant animals as well as trans-heterozygous allelic combinations in which these temperature sensitive alleles were placed in trans to the *cact*^{D13} null allele. We find that GluRIIA levels are significantly decreased in all four *cactus* mutant combinations compared to wild type

(Figure 6A-C). The levels of a control antigen are unchanged (anti-HRP; Figure 6D), and there is no change in postsynaptic Dlg (*wild-type* = 100+/-0.9, n=19; $cact^{RN}/cact^{D13}$ = 98 +/- 0.98, n=23; $cact^{HE}/cact^{D13}$ = 99 +/- 0.97, n=24; data represent % wild-type Dlg levels). Interestingly, the $cact^{RN}$ mutation acts as a dominant mutation for decreased GluRIIA levels (compare wild type, $cact^{RN}/+$ and $cact^{RN}/cact^{D13}$, Figure 6C). Finally, as observed in the *dorsal* alleles, GluRIIC staining is also slightly, but significantly ($p<0.05$) reduced in these *cactus* mutant backgrounds indicating that multiple GluR subunits are affected (*wild-type* = 100+/- 1.6, n=30; $cact^{RN}/cact^{D13}$ = 85+/-1.9, n=31; $cact^{HE}/cact^{D13}$ = 89+/-1.6, n=32; data represent % *wild-type* synaptic GluRIIC levels).

To further explore the possibility that *cactus* and *dorsal* act together to control GluR levels (rather than Cactus acting to oppose Dorsal signaling) we examined GluRIIA levels in a trans-heterozygous *dorsal* and *cactus* null mutant combination. Heterozygous null alleles of either *cactus* or *dorsal* alone have normal GluRIIA levels (Figures 2D, 6C). However, when we place the null alleles for *cactus* and *dorsal* in *trans* ($cactus^{D13}/dorsal^{H}$) we find a significant decrease in GluRIIA levels ($cact^{D13}/dl^{H}$ = 74 +/- 6.0, n=10; data represent % wild-type synaptic GluRIIA levels, $p<0.01$). These genetic data are consistent with *dorsal* and *cactus* functioning together in the same genetic pathway to control GluR levels.

An electrophysiological analysis confirms that the observed decrease in GluRIIA immunostaining correlates with a decreased mEPSP amplitude in $cactus^{RN}$ (Figure 6E). Since there is no change in the muscle input resistance or resting membrane potential we conclude that the change in mEPSP amplitude is likely caused by the observed decrease in GluR abundance at the NMJ (Figure 6G, H). Finally, we assayed whether *cactus*

mutations affect evoked neurotransmission. We find that EPSP amplitudes are unchanged comparing *cactus*^{RN} to wild type ($p>0.3$; n=15, Figure 6F) demonstrating that a homeostatic increase in presynaptic release compensates for the decreased mEPSP amplitude in the *cactus*^{RN} background. Thus, neither Cactus nor Dorsal appear to be involved in the mechanisms of synaptic homeostasis.

Mutations in *cactus* alter GluR density not active zone size

During larval development both GluR abundance and active zone size increase. GluRIIA antibody staining intensity at the postsynaptic membrane increases by ~350% when we compare the first instar NMJ to the third instar NMJ (Figure 7A-B). These data are consistent with the insertion of new GluRIIA receptors into pre-existing GluR clusters during synapse maturation (Rasse et al., 2005). We also observe a parallel increase in the size of individual active zones. We quantified active zone diameters using serial section EM at three stages of NMJ development including the nascent embryonic NMJ (18 hours after egg laying), the newly formed first instar synapse (~30 hours after egg laying) and the third instar NMJ (~ 4 days after egg laying). Active zone size increases significantly during the first ~12 hours of synapse development and increases dramatically by the third instar (Figure 7C-E). Thus, it appears that developmental mechanisms are in place to control both GluR abundance and active zone size during this period of rapid synaptic growth.

We next addressed whether postsynaptic Cactus controls active zone size with secondary effects on GluR abundance, or whether it specifically controls GluR density within otherwise normally sized postsynaptic densities (PSD). To do so, we compared

active zone sizes measured in wild type and *cactus*^{RN} mutants. Despite a ~50% decrease in GluR abundance, there is no change in active zone size in the *cactus*^{RN} mutant (Figure 7E). We also analyzed GluR cluster size at the light level and find no significant difference comparing *cactus*^{RN} or *pelle*^{078} to wild type (data not shown). Finally, we find no change in the extent of the SSR in the *cactus* mutant background at the ultrastructural level (wt SSR cross-sectional thickness: 429 nm +/- 40.3 n=16, *cact*^{RN} SSR: 525 nm +/- 75.0, n=12). Since GluR abundance decreases without a change in active zone size, our data demonstrate that *cactus* is required, specifically, for the control of GluR density.

Dorsal functions in the cytoplasm to control GluR levels

Our data raise the possibility that Dorsal and Cactus function together as a regulated postsynaptic protein complex to control GluR density. This model predicts that Dorsal acts cytoplasmically to control GluR levels rather than functioning as a transcription factor in the cell nucleus. Consistent with this possibility, we find that mutations that render Dorsal transcriptionally incompetent do not always correlate with decreased GluR levels (Figure 3). Furthermore, we and others do not observe Dorsal protein in the muscle nucleus of wild type larvae (Figure 8C-F; Cantera et al., 1999a). Therefore, we set out to examine in greater detail whether or not Dorsal functions in the muscle nucleus to control GluR density.

First, we tested whether nuclear translocation of Dorsal occurs in temperature sensitive *cactus* mutations that cause decreased synaptic GluR levels. We stained for Dorsal protein in the *cactus* mutants and assayed for the loss of synaptic Dorsal and the accumulation of Dorsal in the muscle nucleus. We find that synaptic Dorsal protein levels

are unaltered in the *cactus*^{RN} and *cactus*^{HE} mutant backgrounds (*wild-type* = 100 +/- 4.6, n=19; *cact*^{RN}/+ = 91 +/- 6.5, n=20; *cact*^{RN}/*cact*^{RN} = 99 +/- 3.6, n=14; *cact*^{HE}/*cact*^{HE} = 101 +/- 4.4, n=15; data represent % *wild-type* Dorsal fluorescence intensity). Indeed, we find no evidence of Dorsal protein in the muscle nuclei, either in wild type or in any of the *cactus* mutants that we tested (Figure 8E-H), consistent with prior studies using other *cactus* alleles (Beramendi et al,. 2005). Next, since it is formally possible that small amounts of Dorsal protein in the nucleus escape our detection, we tested whether over-expression of Dorsal could generate increased Dorsal in muscle nuclei. We were able to generate a significant increase in synaptic and non-synaptic Dorsal protein, but still did not see any Dorsal immunoreactivity within the muscle nuclei (Figure 8C, D). Finally, it remains possible that we are unable to detect small but transcriptionally relevant changes in nuclear Dorsal protein. Therefore, we used a series of Dorsal transcriptional reporters (Table 2) to monitor Dorsal mediated transcription in the muscle nucleus. Since Dorsal can both activate and repress transcription, we assayed these reporters in a *wild-type* background, a *dorsal* null mutant background (*dl*^{1}/*dl*^{H}) and in animals over-expressing Dorsal using a heat shock activated *dorsal* transgene (*HSP70-dl*). We did not find any evidence of Dorsal activity in the muscle nuclei using four separate Dorsal transcriptional reporters, despite seeing robust reporter activity in other control tissues where we observe the expected changes in reporter activity (Table 2). Taken together, these data suggest that Dorsal functions in the cytosol to regulate GluR levels.

Post-transcriptional regulation of GluRIIA abundance by Dorsal and Cactus

The next question that we addressed was how NF-kB signaling influences the density of postsynaptic GluRs. We first performed real-time PCR to assay whether there is a decrease in GluRIIA transcript levels in *dorsal* and *cactus* compared to wild type. Although there was a trend toward reduced levels of GluRIIA transcript in *dorsal* and *cactus* mutants compared to *wild-type*, these differences are not statistically significant (*wild-type* = 1.0 +/- 0.2; dl^2/dl^2 = 0.8 +/- 0.2; $cact^{HE}/cact^{HE}$ = 0.7+/- 0.2; $GluRIIA^{sp16}/GluRIIA^{sp16}$ = 0.0+/- 0.02). However, it remains possible that even a small change in GluR transcription could result in a significant change in GluR levels over a period of several days. Therefore, we asked whether expression of a GluRIIA cDNA, driven from a heterologous, muscle-specific promoter, could restore normal GluR levels to the *cactus* or *dorsal* mutant NMJ.

In this experiment, we expressed a myc tagged *GluRIIA* transgene using the myosin heavy chain promoter (*MHC:GluRIIA-myc*) in wild-type as well as both *dorsal* and *cactus* mutations. It is important to note that *MHC:GluRIIA-myc* is able to rescue the *GluRIIA* null mutation (Petersen et al., 1997). We assayed the levels of myc tagged receptor that reached the muscle surface by staining with an anti-myc antibody in un-permeabilized tissue. We find that significantly less *GluRIIA-myc* reaches the synaptic surface in *dorsal* and *cactus* mutants compared to wild type controls (Figure 8I-M). This experiment was then repeated with quantitatively similar results using animals harboring two copies of the *GluRIIA-myc* transgene in a *cactusRN* mutant (data not shown). These data provide further evidence that GluR levels are not controlled by Dorsal-dependent GluRIIA transcription. In combination with the observations that Dorsal protein does not

enter the muscle nucleus (Figure 8), that the Dorsal transactivation domain is dispensable for GluR regulation (Figure 3) and that Dorsal reporters fail to show nuclear activity in muscle (Table 2), our data suggest that Dorsal does not function in the muscle nucleus to control GluR abundance. Since our genetic data indicate that *dorsal*, *cactus* and *pelle* function in the same genetic pathway to control GluR abundance, our data support a model in which a Cactus/Dorsal protein complex functions locally, at the NMJ, to specify normal GluR density during synapse development.

NF-kB signaling has been implicated in the mechanisms of neural plasticity, learning, epilepsy, neurodegeneration and the adaptive response to neuronal injury (Mattson and Camandola, 2001; Mattson et al., 2000b; Mattson and Meffert, 2006; Meffert and Baltimore, 2005). The data presented here advance our understanding of neuronal NF-kB signaling in two ways. First, we present multiple lines of evidence that NF-kB/Dorsal signaling is required for the control of GluR density at the postsynaptic density (PSD). These data provide a synaptic function for NF-kB signaling that may be directly relevant to the diverse activities ascribed to NF-kB in the nervous system. Second, we provide molecular and genetic evidence that Dorsal, Cactus and Pelle form a regulated postsynaptic signaling complex that acts locally, at the postsynaptic membrane, to specify GluR density during postembryonic development.

GluR density is specified by synaptic NF-kB signaling

Several independent lines of experimentation suggest that Cactus, Dorsal and Pelle function together at the PSD to specify GluR density. First, we provide evidence that Cactus and Dorsal co-localize at the PSD, consistent with a well-established physical association of these proteins. Next, we show that over-expression of a GFP-tagged Pelle protein that is sufficient to rescue a *pelle* mutation, can traffic to the PSD where Cactus and Dorsal reside. In addition, it is well established that Pelle can bind to Dorsal, and here we show that mutations in the domain of Dorsal that mediates Pelle binding (dl^2 ;

Govind, 1999) cause a reduction in synaptic GluR density. Together, these data suggest the existence of a postsynaptic complex that includes Pelle, Dorsal and Cactus.

We next present genetic evidence that *cactus, dorsal* and *pelle* function together, in the same genetic pathway to control GluR density. Mutations in each gene show similar mutant phenotypes including decreased GluR density without a change in NMJ growth, muscle development, or synaptic homeostasis. In addition, muscle specific expression of *UAS-GFP-pelle* rescues the decrease in GluR levels in the *pelle* mutant background. Finally, genetic epistasis experiments indicate that all three genes function together in the same genetic pathway, most likely in postsynaptic muscle.

It is particularly surprising that mutations in *cactus* behave similarly to *dorsal* and *pelle*. In other systems (embryonic patterning and immunity), Cactus inhibits Dorsal-mediated transcription by binding and sequestering cytoplasmic Dorsal protein. As a result, in these other systems, *cactus* mutations cause phenotypes that are opposite to that observed in *dorsal* mutations. Here we have used the same *cactus* and *dorsal* mutations that previously have been observed to generate the predicted opposing phenotypes during embryonic patterning (Govind, 1999) and yet we observe that *cactus* phenocopies the *dorsal* mutations. Thus, at the NMJ, Cactus functions in concert with, rather than in opposition to, Dorsal. One explanation for this observation could be that Dorsal does not function as a nuclear transcription factor at the NMJ. In support of this idea we demonstrate that: 1) Dorsal protein is not found in the nucleus, 2) reporters of Dorsal-dependent transcription fail to show activity in muscle nuclei, and 3) mutation of the Dorsal transactivation domain, dl^{U5} does not impair GluR abundance even though this same mutation has been shown to impair transcription-dependent patterning during

embryogenesis. Finally, since Dorsal, Pelle and Cactus localize at the PSD, and since these genes are required for normal GluR density, we favor a model in which Dorsal, Cactus and Pelle form a postsynaptic protein complex that functions to control GluR density during neuromuscular development.

Post-transcriptional control of GluR density by NF-kB

If our model is correct and Dorsal is not functioning as a nuclear transcription factor at the NMJ, then we predict that NF-kB does not control GluR density through transcriptional regulation. This prediction is supported by two experimental observations. First, GluR transcript levels (assessed by QT PCR) are not statistically different from wild type in *dorsal* and *cactus* mutations that cause a ~50% decrease in GluR abundance. Second, we demonstrate that over-expression of a myc-tagged GluRIIA cDNA using a heterologous, muscle-specific promoter is not able to restore synaptic GluRIIA levels in either the *cactus* or *dorsal* mutant backgrounds. We demonstrate that the GluRIIA cDNA is expressed, translated and the GluR-myc protein is inserted into the synaptic membrane by showing surface labeling of synaptic receptors with an anti-myc antibody. However, GluRIIA levels remain significantly lower in *dorsal* and *cactus* mutants compared to wild type animals over-expressing the identical GluRIIA transgene. These data demonstrate that Dorsal and Cactus act post-transcriptionally to control GluR density at the NMJ.

There are two general mechanisms by which GluR levels could be controlled post-transcriptionally: 1) altered receptor delivery to the NMJ or 2) altered receptor internalization/degradation. If receptor internalization/degradation were enhanced in the

cactus, *dorsal* or *pelle* mutant backgrounds, one might expect GluRIIA-myc overexpression to overcome this change and restore normal receptor levels. This is not what we observed. Therefore, we favor the hypothesis that a putative Cactus/Dorsal/Pelle signaling complex is involved in the regulated delivery of receptors to the NMJ.

Intercellular signaling, NF-kB activation and the control of GluR density

It remains unknown how NF-kB signaling is activated at the Drosophila NMJ. In Drosophila embryonic patterning and innate immunity, NF-kB signaling is initiated through activation of Toll or Toll-like receptors. There are nine Toll and Toll-like receptors encoded in the Drosophila genome. However, none of these receptors appear to be present in Drosophila larval muscle. The Toll receptor is expressed in a subset of embryonic muscle fibers (Halfon et al., 1995; Halfon and Keshishian, 1998), but is absent from larval muscle (Nose et al., 1992). None of the Toll-like receptors are expressed in Drosophila embryonic muscle (Kambris et al., 2002) and none appear to be expressed in larval muscle either (data not shown). An alternative possibility is that TNF-a receptors activate NF-kB in Drosophila muscle as has been observed in vertebrate skeletal muscle (Jackman and Kandarian, 2004; Ladner et al., 2003). Indeed, a TNF-a receptor homolog has been identified, and it is expressed in Drosophila skeletal muscle (Kauppila et al., 2003). The possibility that TNF-a signaling is mediated via NF-kB is intriguing given the recent demonstration that TNF-a regulates GluR abundance in the vertebrate central nervous system (Stellwagen et al., 2005; Stellwagen and Malenka, 2006). In both cultured neurons and hippocampal slices glial-derived TNF-a signaling is required for the

increase in postsynaptic AMPA receptor abundance observed following chronic activity blockade (Stellwagen et al., 2005; Stellwagen and Malenka, 2006). Thus, our data raise the possibility that a conserved TNFa / NF-kB signaling system controls GluR abundance at both neuromuscular and central synapses during development and in response to chronic activity blockade.

Finally, the demonstration that cytoplasmic NF-kB can influence GluR density does not rule out the possibility that NF-kB may also translocate to the muscle nucleus at the Drosophila NMJ under the right stimulus conditions. Indeed, in both the vertebrate central and peripheral nervous systems NF-kB is found within neuronal and muscle nuclei, and nuclear translocation can be stimulated by neuronal activity, glutamate, injury and disease (Mattson and Commandola, 2001). The possibility that NF-kB signals both locally at the synapse and globally via the nucleus is not unique to this signaling pathway. A similar organization has been documented for wingless/wnt signaling where non-canonical cytoplasmic signaling can impact cytoskeletal organization while canonical signaling involves the nuclear translocation of downstream beta-catenin and TCF-dependent gene transcription (Moon et al., 2002). Likewise, synaptic BMP signaling appears to modulate synapse stability through local LIM Kinase signaling while downstream Smad mediated signaling influences gene transcription in the neuronal nucleus necessary for neuronal growth (Eaton and Davis, 2005).

It is interesting to speculate that the ability of NF-kB to generate local synaptic change and modulate cell-wide gene transcription could link the mechanisms of learning-related synaptic plasticity and homeostatic receptor scaling (Meffert et al., 2003; Stellwagon and Malenka, 2006). For example, the restricted activation of NF-kB

signaling could locally modulate GluR levels without initiating a nuclear response, thereby participating in learning-related synaptic plasticity. However, if NF-kB were activated at a sufficient number of synapses, either simultaneously or over some period of time, then nuclear NF-kB signaling could be induced to generate a cell-wide response related to homeostatic receptor scaling. In this manner, NF-kB could be centrally involved in the mechanisms of both learning-related plasticity and homeostatic receptor scaling. Indeed, NF-kB could be important for the transition between these two fundamental forms of neural plasticity.

Table 1 Molecular characterization of *dorsal*, *pelle*, and *cactus* alleles

Allele	Description	Molecular Lesion	References
Dorsal			
dl^{H}	Protein null	X-ray rearrangement	Roth et al., 1989
dl^{1}	Protein null	unsequenced EMS allele	Roth et al., 1989
dl^{Pz}	Unstable protein	R310H, altered PKA consensus site	Isoda et al., 1992
dl^{2}	Point mutation	G68Q, altered Rel Homology Domain	Isoda et al., 1992
dl^{U5}	Truncated protein	Q488Stop, in Transactivation Domain	Isoda et al., 1992
Pelle			
Df(3R)D605	Protein null	Large deficiency	Hecht and Anderson, 1993
pll^{25}	Protein null	Q93Stop in Death Domain	Towb et al., 2001
pll^{RM8}	Protein null	Q422Stop in Kinase Domain	Towb et al., 2001
pll^{078}	Kinase dead	G225E in Kinase Domain	Towb et al., 2001
Cactus			
$cact^{D13}$	Protein null	V188Stop	Bergmann et al., 1996
$cact^{255}$	Protein null	P-element in first intron	Bergmann et al., 1996, Nicolas et al., 1998
$cact^{RN}$	Point mutation	A196Y, near Signal-Dependent Domain	Schupbach et al., 1991, this study
$cact^{HE}$	Point mutation	C315Y, altered Ankyrin Repeat	Schupbach et al., 1989, this study

Table 2. Dorsal-dependent transcription not detected in muscle

Reporter name, reporter description	Genotype	Activity in muscle	Activity in other larval tissues
-920twi/lacZ, 0.9kb of *twist* promoter driving *lacZ*[1]	Dl over-expression	none	trachea
	wild-type	none	trachea
	dl^{1}/dl^{H1}	none	trachea
DD1, promoters of *Dpt* driving *lacZ* and *Drs* driving *GFP*[2]	Dl over-expression	none	trachea
	wild-type	none	trachea
D4/hsp70, 4 Dorsal binding sites + TATA box driving *lacZ*[3]	Dl over-expression	none	hemocytes
	wild-type	none	hemocytes
	dl^{1}/dl^{H1}	none	hemocytes
***cactus*^{255}**, *cactus* enhancer trap driving *lacZ*[4]	$cactus^{255}/cact^{D13}$	none	none
	$cactus^{255}/+$	none	none

[1] Pan, et al., Genes and Development 1991
[2] Manfruelli, et al., EMBO 1999
[3] Pan, et al., EMBO 1992
[4] Nicolas, et al., JBC 1998

Figure 1. Dorsal and Cactus surround postsynaptic GluR clusters at the NMJ.

A-F) The NMJ is triple-labeled with anti-Dorsal (A, D), anti-Synapsin (B), and anti-HRP (E). Dorsal protein is absent from the axon prior to the NMJ (arrow in D-F). **G-I)** High magnification of a synaptic bouton co-labeled with anti-Cactus (G) and anti-GluRIIA (H). A three-dimensional reconstruction shows that Cactus surrounds GluRIIA. The large panel in (I) is a single optical section of the synapse. The smaller panels on top (Za) and on left (Zb) show the Z dimension reflected along the thin vertical and horizontal lines.

Figure 2. Decreased GluRIIA abundance in *dorsal* mutants.

A-C) Pseudocolor images of GluRIIA staining in *wild-type*, dl^2/dl^2, and dl^1/dl^H (bar at left indicates color scale). **D)** Quantification of GluRIIA staining at the NMJ shows that GluRIIA is reduced in all *dorsal* alleles. Values represent % of average wt synaptic anti-GluRIIA fluorescence levels. Values for each genotype are as follows: *wt* 102 ± 2.0 n=170; dl^2/dl^2 41 ± 2.8 n=22; dl^2/dl^H 56 ± 2.4 n=22; dl^{PZ}/dl^{PZ} 76 ± 6.2 n=10; dl^1/dl^H 77 ± 3.4 n=40; dl^2/+ 70 ± 6.7 n=10; dl^{PZ}/+ 93 ± 4.2 n=18; dl^H/+ 91 ± 6.2 n=12; dl^{UY2278}/+; *MHC-Gal4*/+ 103 ± 3.1 n=20). **E)** Synaptic HRP levels are not decreased in the same *dorsal* mutant synapses compared to wild type, except in dl^2/dl^2. **F)** Synaptic GluRIIC fluorescence level in *dorsal* alleles is significantly reduced (*wt* = 100 ± 1.8 n=44, dl^{PZ}/dl^{PZ} = 86 ± 5.5 n=16, dl^1/dl^H = 86 ± 3.5 n=21. Data represent % of average wt synaptic GluRIIC fluorescence levels). In all figures data are presented as the mean value (± standard error of the mean). Significance is shown according to **p<0.01.

Figure 3. Disruption of the Dorsal transactivation domain does not impair GluRIIA abundance at the NMJ.

A-D) NMJ co-stained for Dorsal and GluRIIA are shown for *wild-type* (A, B) and dl^{U5}/dl^{U5} mutants (C, D). **E)** Schematic of the Dorsal protein showing that dl^{2} is a point mutation in the Rel Homology Domain (RHD), and dl^{U5} is a truncation of the Transactivation Domain. **F)** Both dl^{2} and dl^{U5} leave Dorsal protein at the synapse (*wt* = 100 ± 2.5 n=51; dl^{2}/dl^{2} = 82 ± 2.7 n=17; dl^{U5}/dl^{U5} = 110 ± 3.5 n=15; values show % wt synaptic Dorsal fluorescence level, **p<0.01). **G)** Disruption of the RHD causes a decrease in synaptic GluRIIA levels (*wt* = 102 ± 2.0 n=170, dl^{2}/dl^{2} 41 ± 2.8 n=22). Disruption of the transactivation domain results in a significant increase in GluRIIA (dl^{U5}/dl^{U5} 120 ± 5.5 n=17 % wt synaptic GluRIIA fluorescence level, ** p<0.01).

Figure 4. Decreased mEPSP amplitude correlates with decreased GluR abundance.

A) There is a significant decrease in the average mEPSP amplitude in the dl^{1} mutant compared to wild type (p<0.01). There is a significant decrease in mEPSP amplitude in the dl^{1}, *GluRIIA* double mutation compared to *GluRIIA* mutant alone (p<0.01). **B)** Cumulative frequency distributions show that the entire mEPSP distribution is shifted toward smaller values in mutant backgrounds that include the dl^{1} mutation. **C)** There is no difference in average resting membrane potential across genotypes. **D)** There is no difference in muscle input resistance comparing *wild-type* with dl^{1} or when comparing the dl^{1}, *GluRIIA* double mutation to *GluRIIA* alone. **E)** There is no difference in EPSP amplitude comparing *wild-type* with dl^{1} or when comparing the dl^{1}, *GluRIIA* double mutation to *GluRIIA* alone. **F)** Quantal content is increased in dl^{1} compared to wild type and in dl^{1}, *GluRIIA* double mutation compared to *GluRIIA* alone. **G)** Representative traces showing mEPSP events in each indicated genotype. Significance is shown according to * p<0.05; **p<0.01.

Figure 5. Pelle kinase regulates GluRIIA abundance at the NMJ.

A, B) Pseudocolored images reveal that GluRIIA levels are reduced in *pelle* mutant synapses compared to wild type. **C)** Synaptic GluRIIA fluorescence intensity is reduced in all *pelle* alleles examined. This reduction can be rescued by muscle-specific expression of a *UAS-GFP-pelle* transgene (*wt* = 100 ± 2.1 n=104; pll^{078}/pll^{078} = 56 ± 3.4 n=24; pll^{RM8}/pll^{RM8} = 68 ± 4.0 n=24; pll^{25}*/Df(3R)D605* = 72 ± 2.6 n=45; pll^{078}/+ = 80 ± 4.4 n=38; pll^{RM8}/+ = 68 ± 2.0 n=24; *UAS-Pelle/+;* pll^{RM8}*/24B-Gal4* = 94 ± 1.6 n=22; *UAS-Pelle/+; 24B-Gal4/+* = 96 ± 1.4 n=21). Values represent % wt synaptic GluRIIA fluorescence level. **D)** HRP fluorescence intensity is unaltered at the same *pelle* synapses. **E)** *pll* and *dl* null mutations are not additive (*wt* = 100 ± 2.7 n=42, dl^1/dl^1 = 83 ± 2.9 n=38, pll^{25}*/Df(3R)D605* = 72 ± 2.6 n=45, dl^1/dl^1*;* pll^{25}*/Df(3R)D605* = 75 ± 3.5 n=20). **F)** A significant decrease in average mEPSP amplitude in pll^{078}/pll^{078} and pll^{RM8}/+ correlates with decreased GluRIIA in these mutant backgrounds. Decreased mEPSP amplitudes are restored to wild type levels by muscle-specific expression of *UAS-pelle-GFP* (red). **G)** The decrease in mEPSP amplitude is not correlated with a decrease in muscle input resistance. **H)** There is no difference in resting membrane potential of the muscle across genotypes. **I)** Representative recordings show the rescue of mEPSP amplitudes comparing a *pelle* mutant (top) to the *pelle* mutant expressing *UAS-pelle-GFP* postsynaptically (bottom, "rescue"). Significance is shown according to * $p<0.05$; ** $p<0.01$.

Figure 6. GluRIIA abundance is decreased in *cactus* mutants.

A-B) The intensity of anti-GluRIIA fluorescence is reduced in *cactus* mutant synapses. **C)** Quantification of the decrease in GluRIIA levels observed in *cactus* mutants (*wt* = 101

± 1.9 n= 186; $cact^{RN}/cact^{RN}$ = 74 ± 6.7 n=18; $cact^{RN}/cact^{D13}$ = 59 ± 2.3 n=16; $cact^{HE}/cact^{HE}$ = 60 ± 6.1 n=16; $cact^{HE}/cact^{D13}$ = 55 ± 4.8 n=17; $cact^{RN}/+$ = 63 ± 3.3 n=22; $cact^{HE}/+$ = 86 ± 4.9 n=22; $cact^{D13}/+$ = 94 ± 7.0 n=17). **D)** Synaptic HRP levels are not reduced in *cactus* alleles. **E)** Average mEPSP amplitude is decreased in $cact^{RN}$ compared to wild type. **F)** EPSP amplitudes are not different comparing $cact^{RN}$ and wild type. **G)** Muscle input resistance is not different comparing $cact^{RN}$ and wild type. **H)** Resting muscle membrane potential is not different comparing $cact^{RN}$ and wild type. Significance is shown according to *p<0.05; **p<0.01.

Figure 7. Cactus mutations impair GluRIIA abundance without affecting active zone size.

A, B) NMJ from a first instar animal (A) and third instar animal (B) are shown stained for GluRIIA and imaged under identical conditions. There is a large increase in GluRIIA staining intensity per GluR cluster. **C, D)** Representative electron micrographs of a stage 17 embryonic synaptic bouton (C; arrows delineate an active zone) and a third instar synaptic bouton (arrows delineate an active zone). The area of the presynaptic terminal is shaded pale yellow to discriminate presynaptic terminal from postsynaptic muscle membrane. Scale is 200nm. **E)** Quantification of active zone diameter demonstrates a significant increase in active zone size during development in wild type. There is no difference in active zone diameter comparing wild type and *cactus* third instar NMJ.

Figure 8. Dorsal and Cactus control GluRIIA levels post-transcriptionally.

A, B) The Dorsal antibody is able to recognize nuclear Dorsal staining during embryogenesis. Stage 4 embryos, co-labeled with anti-Dorsal (A) and DAPI (B). Dorsal enters nuclei on the ventral side (bottom) of the embryo; nuclear Dorsal appears white

because of co-localization with purple DAPI. **C, D)** Overexpression of Dorsal is not sufficient for Dorsal nuclear entry at the NMJ. Animals harboring an heat-shock-inducible *dorsal* transgene (*HSP70-dl*) were raised at room temperature, (-heat shock, C) or treated with multiple heat shocks (+heat shock, D). Synapses are co-labeled with anti-Dorsal (green) and DAPI (purple). Inset in (D) highlights anti-Dorsal accumulating around, rather than within muscle nuclei. **E-H)** Dorsal does not enter the nucleus in *wild-type* (E, F) or *cactus* mutants (G, H). The nucleus is indicated by a dashed line (E, G) or highlighted by purple DAPI stain (F, H). **I-L)** NMJ were co-labeled with anti-myc (I, K) and the synaptic membrane marker, anti-HRP (J, L) in wild type and *cactus* mutant animals. A myc-tagged GluRIIA transgene, driven under the control of the MHC promoter, localizes to the NMJ in wild type (I). Less myc-tagged GluRIIA reaches the synaptic surface in $cact^{RN}$/+ animals (K). **M)** There is a significant reduction in the amount of anti-myc staining in the $cact^{RN}$/+ and $dorsal^{2}$/+ mutations ($cact^{RN}$/+ = 64 ± 6.7%, n=14; $dorsal^{2}$/+ = 73 ± 4.4%, n=34) in comparison to *wt* (wild type = 100 ± 4.4%, n=29; ** $p<0.01$).

Figure 1. Dorsal and Cactus surround postsynaptic GluR clusters at the NMJ.

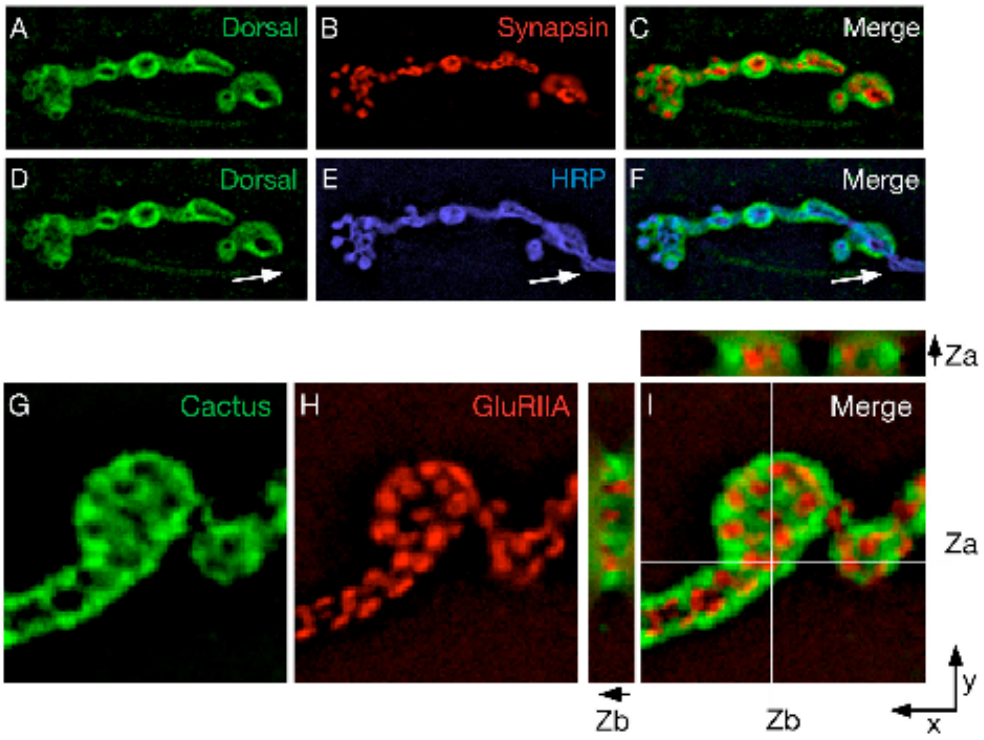

Figure 2. Decreased GluRIIA abundance in *dorsal* mutants.

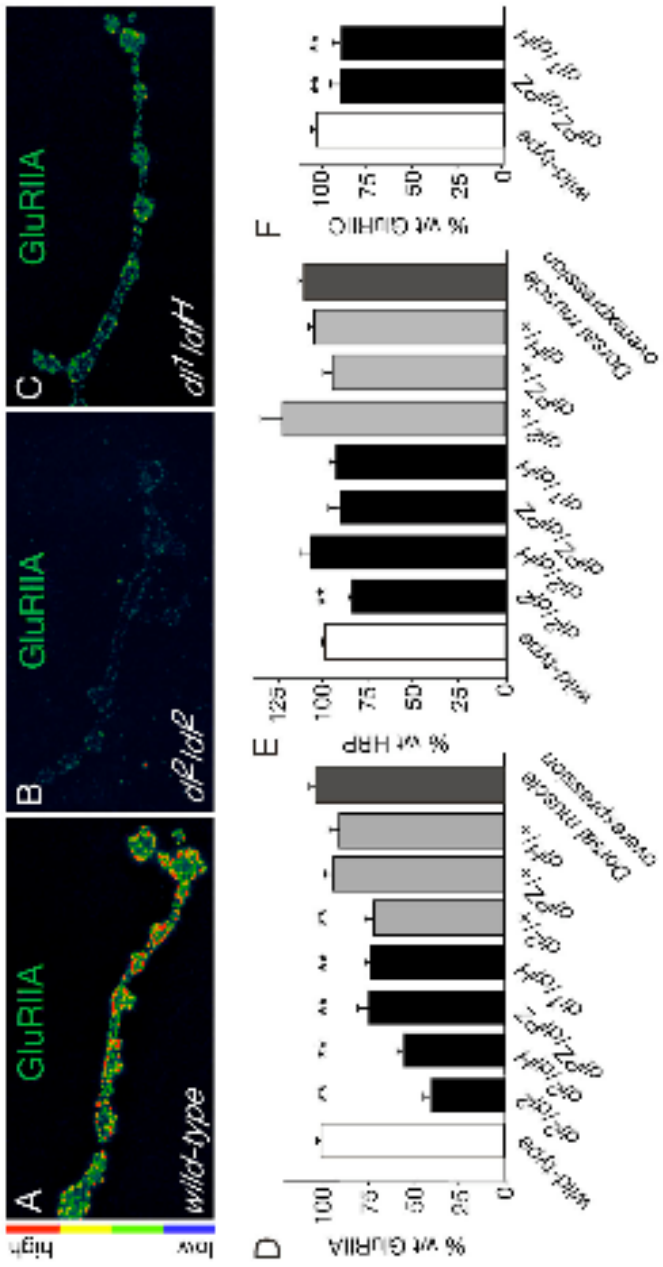

Figure 3. Disruption of the Dorsal transactivation domain does not impair GluRIIA abundance at the NMJ.

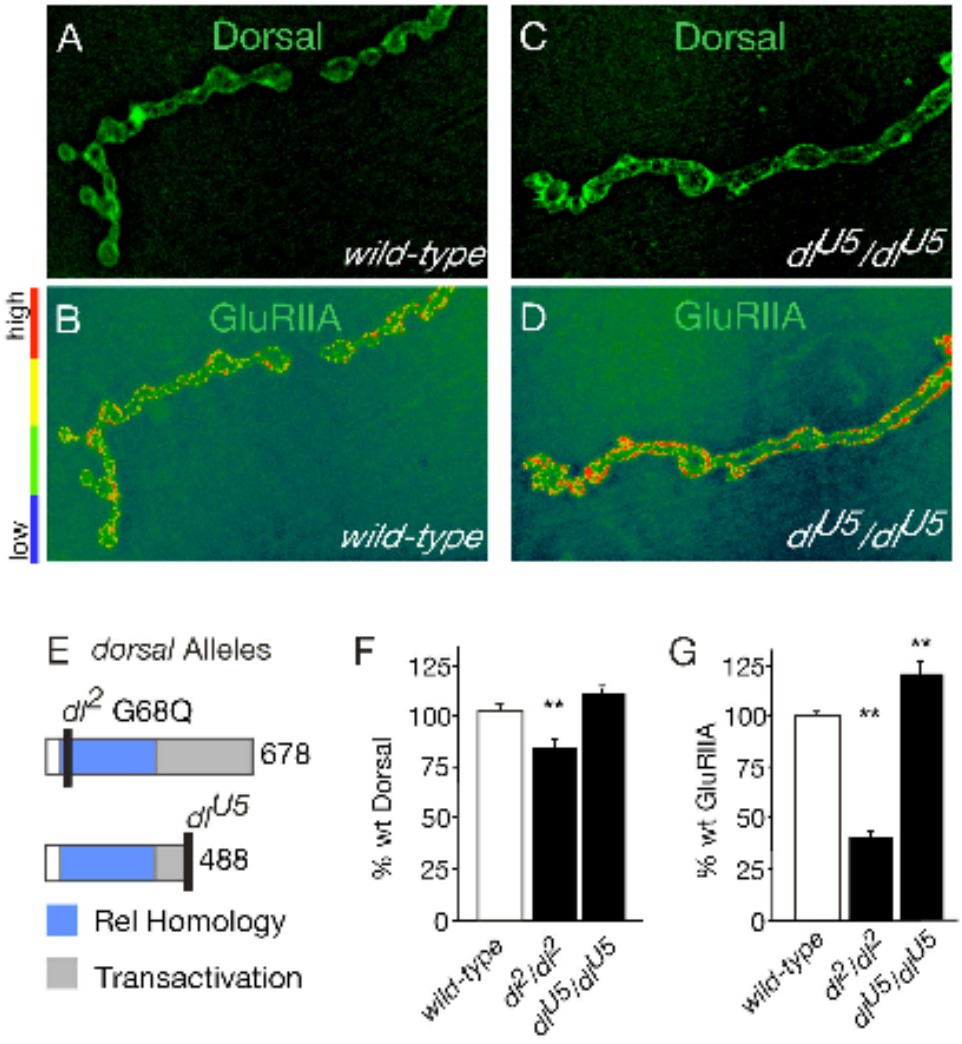

Figure 4. Decreased mEPSP amplitude correlates with decreased GluR abundance.

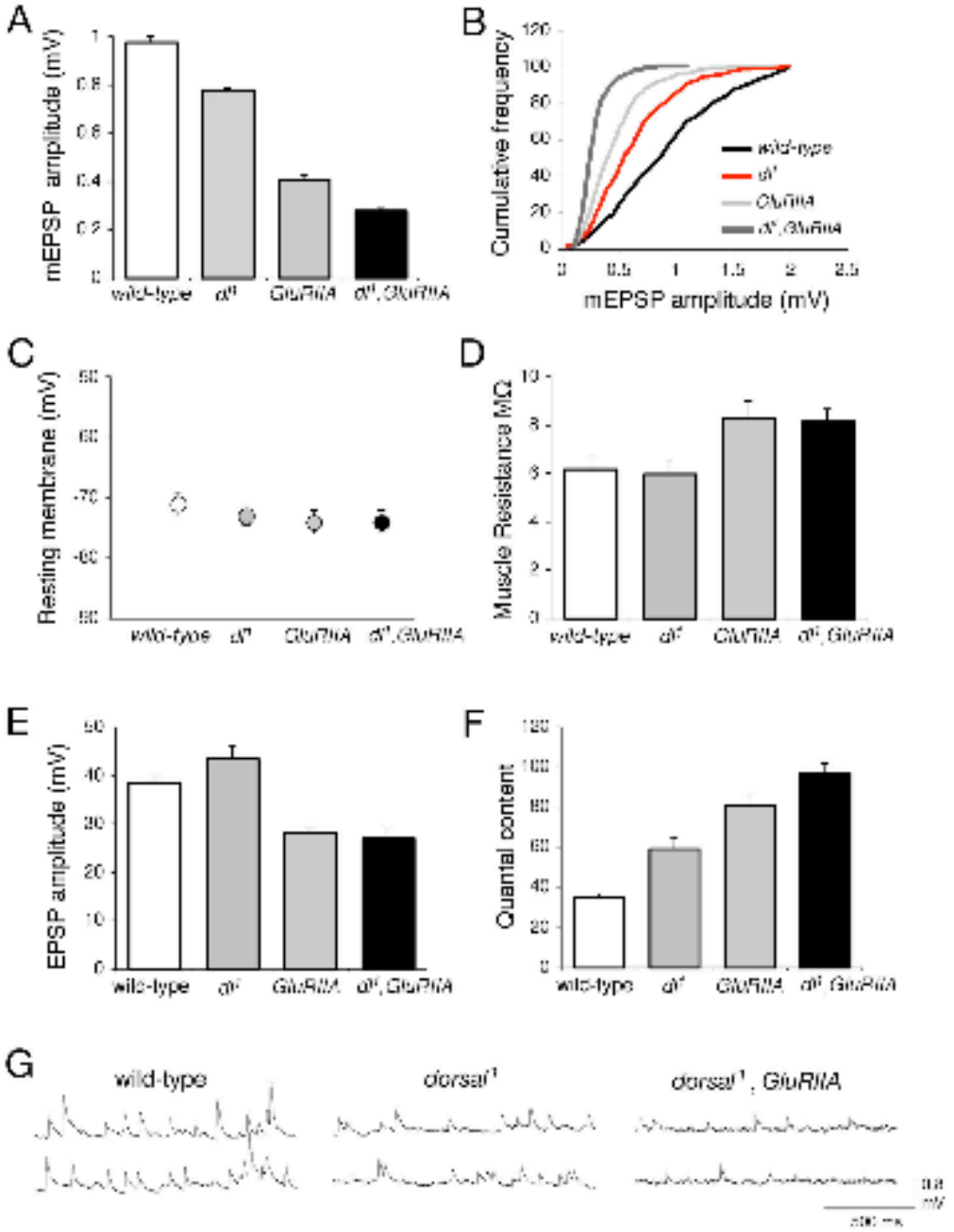

Figure 5. Pelle kinase regulates GluRIIA abundance at the NMJ.

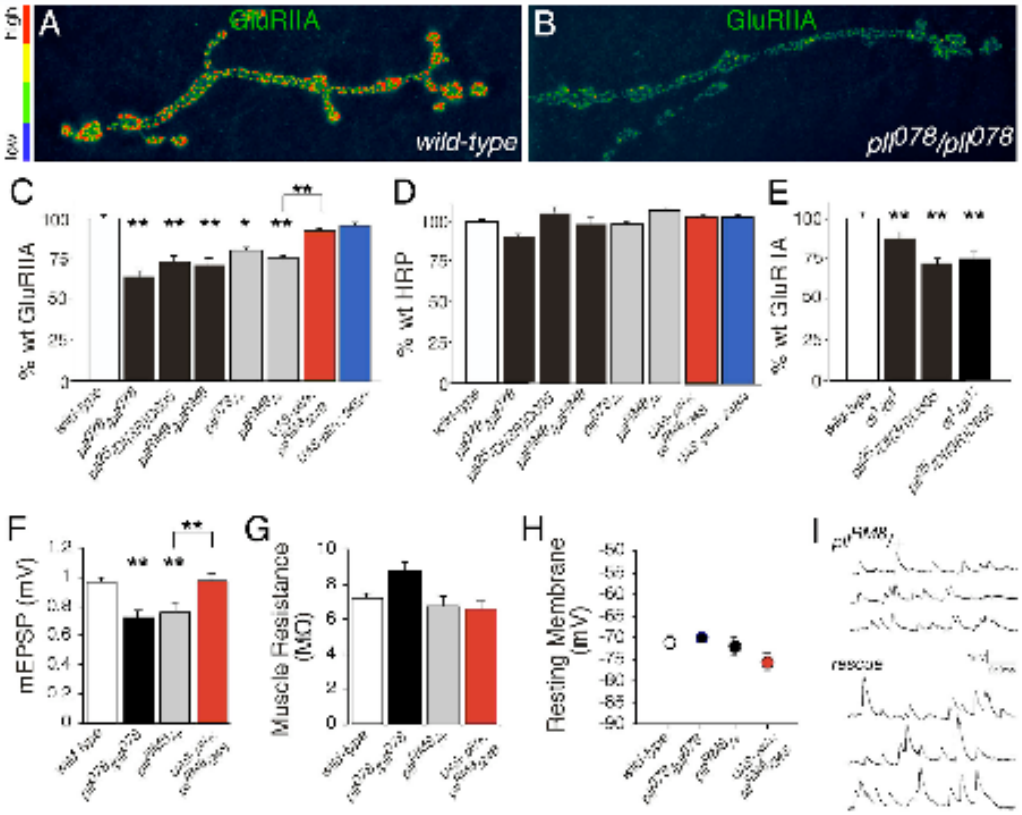

Figure 6. GluRIIA abundance is decreased in *cactus* mutants.

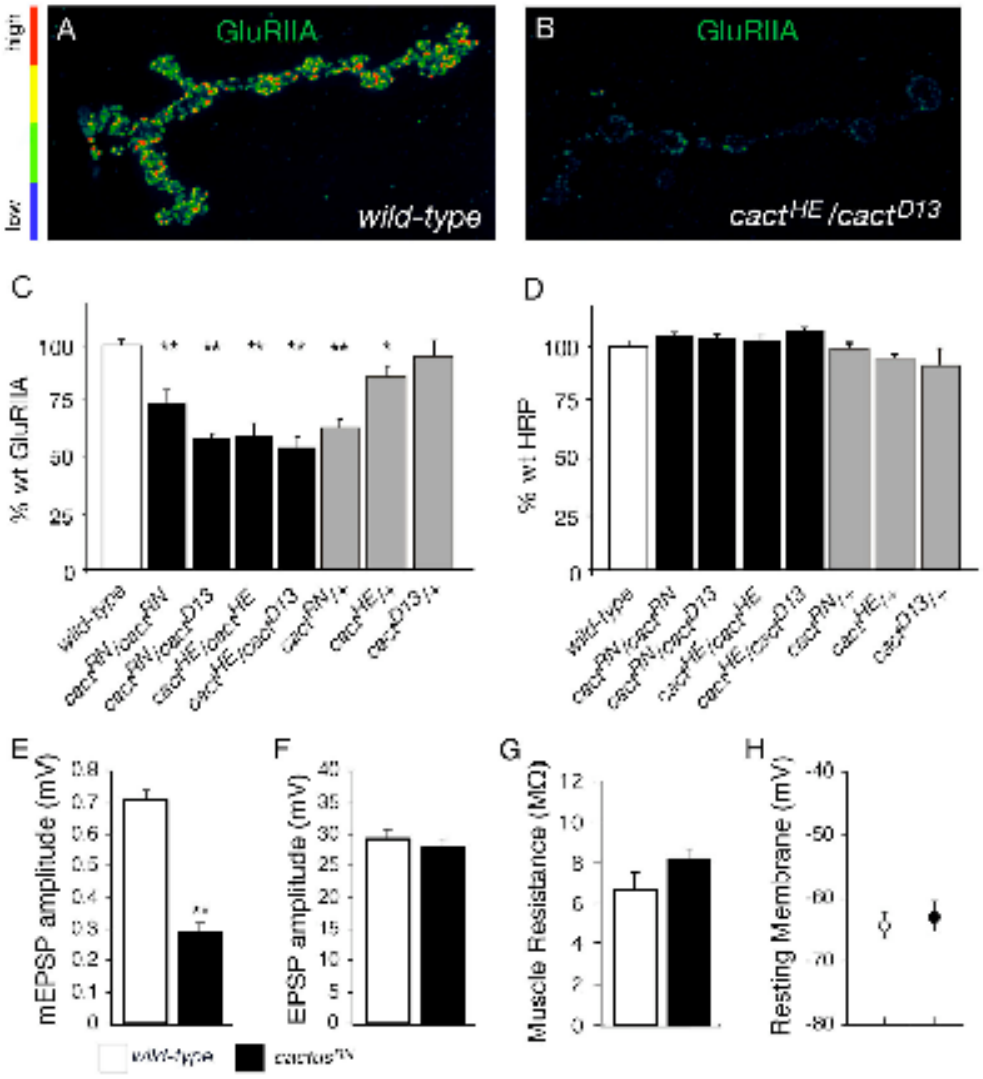

Figure 7. Cactus mutations impair GluRIIA abundance without affecting active zone size.

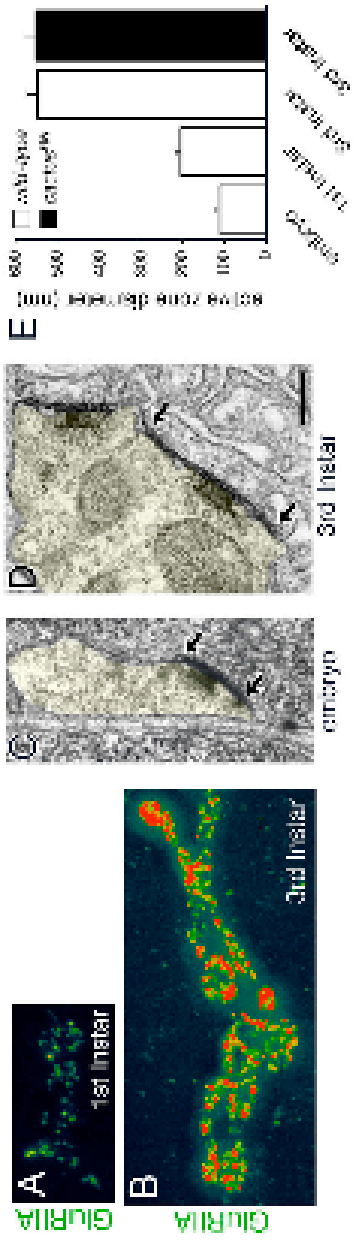

Figure 8. Dorsal and Cactus control GluRIIA levels post-transcriptionally.

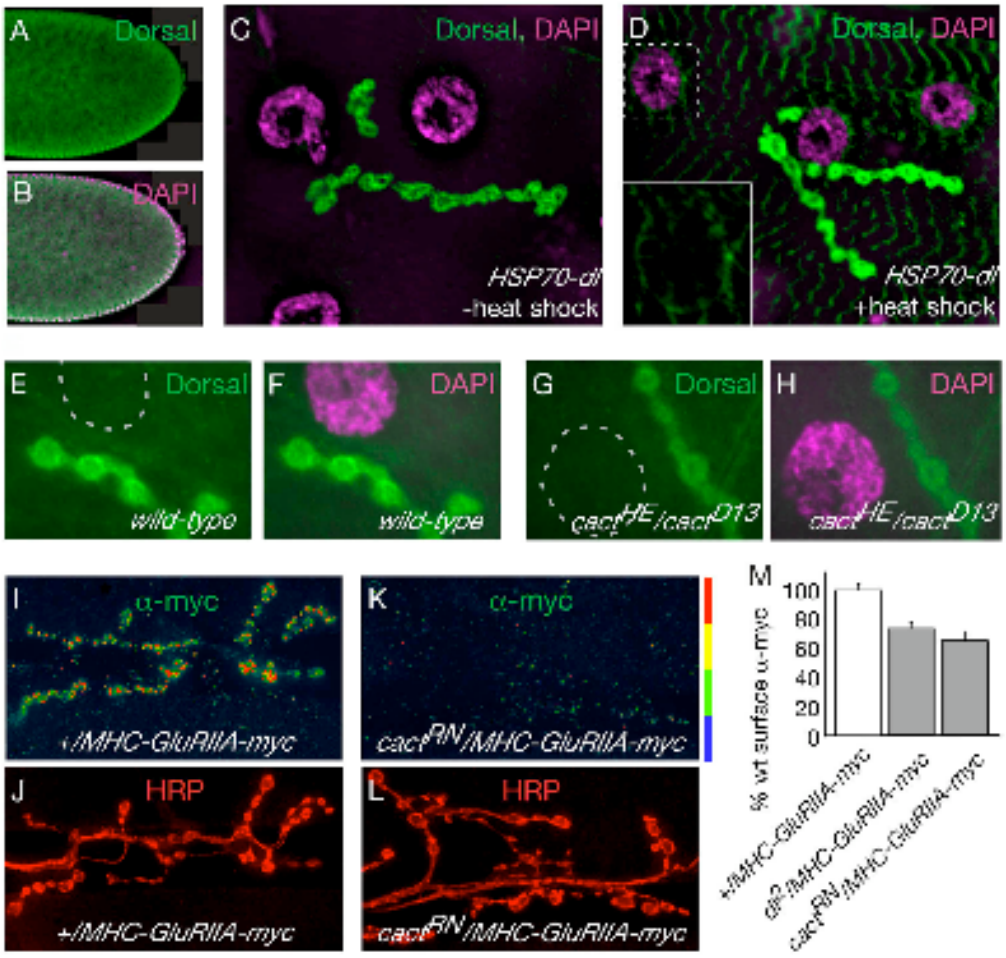

SUPLEMENTAL FIGURES AND LEGENDS

Suplemental Figure 1. Cactus and Dorsal antibodies are highly specific.

A-D) A NMJ from third instar larva is co-stained with anti-HRP to visualize the neuronal membrane and anti-Dorsal in both wild type (A, C) and the *dorsal* null (dl^1/dl^H). Dorsal immunoreactivity is absent from *dorsal* null synapses. **E-H)** A NMJ from a second instar animal is co-stained with anti-HRP and anti-Cactus in wild type (E, G) and *cactus* null mutants (F, H). Cactus is absent from the *cactus* null synapse. Note that synaptic morphology is grossly normal in both the *dorsal* null and *cactus* null animals compared to wild type animals at similar developmental stages.

Supplemental Figure 1.

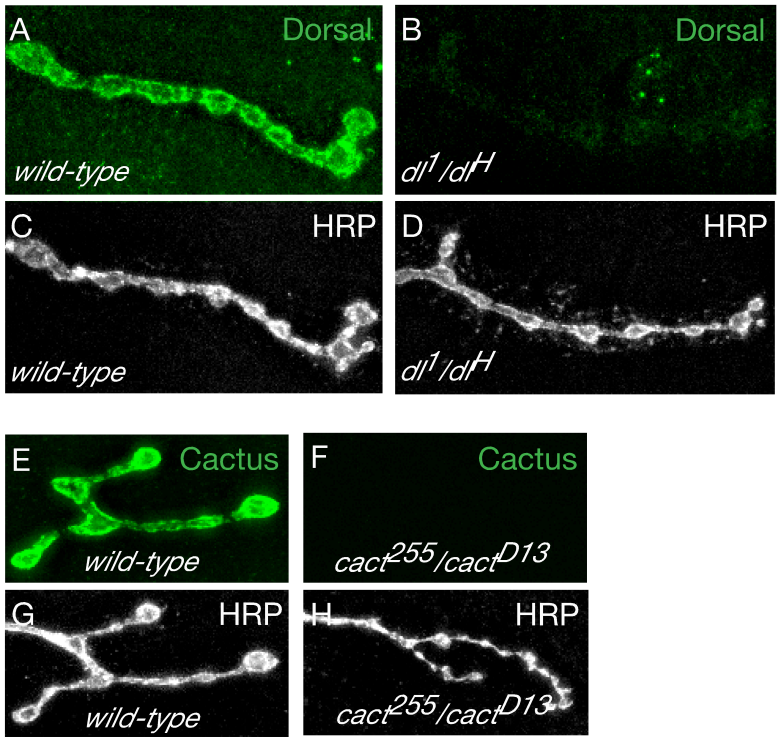

CHAPTER FOUR

pelle acts downstream of cytoplasmic Dorsal to regulate Glutamate receptor insertion

Elizabeth S. Heckscher, Stephanie D. Albin and Graeme W. Davis

SUMMARY

In this study we investigate how an NF-kB-containing complex is involved in regulation of synaptic glutamate receptors (GluR). First, we characterize a modified GluR subunit, GluRIIA$^{\alpha BT}$. Specifically we show that GluRIIA$^{\alpha BT}$ can functionally substitute for the endogenous GluRIIA subunit, and in combination with certain labeling protocols we monitor trafficking of GluRs on to and off of the membrane. In *cactus* mutants with reduced levels of synaptic GluRs, we analyze receptor internalization, and find that it is unaffected. Second, we investigated the localization of Pelle kinase within the muscle, showing it in puncate structures and surrounding nuclei. We order *pelle*, *dorsal* and *cactus* within the genetic pathway that controls GluR abundance, and show that *pelle* likely acts downstream of *dorsal* but not *cactus*. In addition, we show that reductions in GluR correlate with reductions in dN-20, an antibody raised to Pelle. Overall our data are consistent with a model in which cytoplasmic Dorsal regulates the localization or abundance Pelle within the muscle, which in turn mediates glutamate receptor insertion into the synapse.

INTRODUCTION

Changes in synaptic transmission underlie brain development and maturation, as well as learning and memory; such changes also underlie many pathological states of the central nervous. Synaptic transmission is mediated by the release of neurotransmitter onto clusters of neurotransmitter receptors. Neurotransmitter receptors, such as glutamate receptors can be dynamically transported to and from the postsynaptic membrane. It is now widely accepted that dynamic trafficking of glutamate receptors mediates certain forms of synaptic plasticity. For example, changes in surface expression of AMPA-type glutamate receptors underlie rapid synaptic modification associated with classical Hebbian forms of plasticity (Bredt and Nicoll, 2003; Malinow and Malenka 2002), though to be the cellular basis for learning and memory (Kandel, 2001). In addition, dynamic trafficking of glutamate receptors has been proposed as a mechanism for synaptic scaling that takes place in response to chronic manipulations of neural activity (Turrigiano and Nelson, 2004; Perez-Otano and Ehlers, 2005). Although the regulation of glutamate receptors has been intensively studied in the context of synaptic plasticity, similar molecular mechanisms are also likely to mediate normal synaptic development and maturation (Malinow and Malenka, 1992). Many questions remain: Which aspects of membrane trafficking are involved in regulation of neurotransmitter receptors? Which of these steps are regulated? And how is this regulation achieved?

Endocytosis and postendocytic sorting regulates surface expression of glutamate receptors. Endocytosis of glutamate receptors into early endosomes occurs via a clathrin-dependent pathway (Carroll et al., 1999; Gray et al., 2003; Lavezzari et al., 2003; Lee et

al., 2002: Man et al., 2000; Prybyloswki et al., 2005; Wang and Linden, 2000) and in response to ubiquitination (Juo and Kaplan, 2004; Burbea et al., 2002). Furthermore, constitutive endocytosis as well as activity-regulated endocytosis impact the complement of glutmate receptors found within excitatory synapses (Bredt and Nicoll, 2003; Ehlers 2000; Lin et al., 2000; Luscher et al., 1999; Luthi et al., 1999; Malinow and Malenka, 2002; Nishimune et al., 1998; Noel et al., 1999; Zhou et al., 2001). For example, Rab5, a protein associated with early endosomal transport, can be activated by plasticity-inducing stimuli (Brown et al., 2005), and overexpression of Rab5 leads to decreased amount of AMPA-type glutamate receptors on surface (Blanpeid et al., 2002, Brown et al., 2005). After glutamate receptors enter the early endosome they undergo a postendocytic-sorting event. They can associate with Hepatocyte growth factor-regulated tyrosine kinase substrate (HRS), a FYVE domain containing protein (Komada and Kitamura, 2005), which traffics receptors to the lysosome for degradation; alternatively receptors can enter the recycling endosome (Kennedy and Ehlers, 2006). Postendocytic sorting can be regulated by intracellular signaling, specific subunit composition of receptors, and activity (Alberi et al., 2005; Ehlers, 2000; Scott et al. 2004; Steiner et al., 2005). Thus, regulated endocytosis and postendocytic sorting have emerged as mechanisms responsible for various form of synaptic plasticity (Beattie et al., 2000, Kennedy and Ehlers, 2006; Malinow and Malenka, 2002) due to their effects on regulation of synaptic glutamate receptor abundance.

Trafficking from recycling endosomes and from the transgolgi nextwork also impacts the abundance glutamate receptors on the cell surface. Fast insertion of AMPA-type glutamate receptors occurs in response to plasticity-inducing stimuli (Shi et al.,

1999), and both of these processes could contribute to such an insertion event. Recycling endosomes, the destination of some receptors after postendocytic sorting, is thought to act as a reservoir for glutamate receptors (Kennedy and Ehlers, 2006; Malinow and Malenka, 2002). From this reservoir, receptors can be rapidly shuttled back to the synapse (Park et al., 2004). Indeed, expression of a dominant negative Rab11, a component of recycling endosomes (Ullrich et al. 1996), impairs insertion of AMPA-type glutamate receptors (Park et al., 2004). In addition, trafficking from the transgolgi network (TGN) to the cell surface is important for regulation of surface glutamate receptor expression (Broutman and Baudry 2001). For example, experiments using dominant negative Rab8 to block trafficking from TGN demonstrate that this biosynthetic pathway is required for delivery of AMPA-type glutamate receptors to the plasma membrane (Gerges et al 2004). Thus, both internalization and insertion regulate the abundance of synaptic glutamate receptors. An important next step, however, is to define the intracellular signaling pathways that regulate these processes.

In this study we investigate how an NF-kB-containing complex is involved in regulation of synaptic glutamate receptors (GluR). Previously we showed that mutations in *NF-kB*/*dorsal*, *IkB*/*cactus* and *IRAK*/*pelle* kinase specifically impair GluR density at the Drosophila neuromuscular junction (NMJ) (Heckscher et al., 2007). Additionally, this study showed that Dorsal, Cactus and Pelle function together in the cytoplasm to control synaptic GluRs. Although data indicated that control of GluR density occurred via a post-transcriptional mechanism, the exact cellular mechanism by which Dorsal, Cactus and Pelle regulate GluR abundance remains an open question. Here we present a two-part study addressing this question. In the first part we characterize a new tool, a

modified GluR subunit, which can be used to monitor trafficking of GluRs on to and off of the membrane at the Drosophila NMJ. Using this tool we show that receptor internalization is unaffected in *cactus* mutants. Second, we describe the localization of Pelle kinase in discrete puncta within the muscle, which are likely to be endosomal structures. We show that *pelle* acts downstream of *dorsal* but not *cactus* in regulation of GluR abundance, and suggest that Dorsal regulates the localization or abundance of *pelle* within the muscle. Overall our data are consistent with a model in which Pelle kinase, acting downstream of cytoplasmic Dorsal, mediates glutamate receptor insertion into the synapse.

Monitoring trafficking of GluRs to and from the muscle surface using a modified GluRIIA subunit

Previously we showed that Dorsal and Cactus control GluR density via a posttranscriptional mechanism (Heckscher et al., 2007). In addition, our data hinted that the cellular process affected by these proteins could be intracellular trafficking (Heckscher et al., 2007). Thus, we (Stephanie Albin) created a tool to directly assess trafficking of GluRs onto and off of the muscle surface *in vivo*. Specifically, we altered a GluRIIA subunit by inserting an extra 13 aa encoding an alpha-bungarotoxin (αBT) binding site into the extracellular, N-terminus (Figure 1A, Stephanie Albin) (GluRIIA$^{\alpha BT}$) (Katchalski-Katzir et al., 2003; Ravidn and Axelrod, 1977; Sekine-Aizawa and Huganir, 2004). To determine whether addition of the αBT tag perturbed normal trafficking or function of GluRIIA subunit we expressed *GluRIIA$^{\alpha BT}$* under the control of the endogenous *GluRIIA* promoter (Petersen et al. 1997) in a *GluRIIA* null mutant (*GluRIIA^{sp16}*). In this background, expression of *GluRIIA$^{\alpha BT}$* restores GluRIIA to the muscle surface, and significantly restores the function of the synapse (Figure 1B, wt 1.1 $\pm$ 0.4 n=11, *GluRIIA^{sp16}* 0.28 $\pm$ 0.01 n=9, *GluRIIA^{sp16}, GluRIIA$^{\alpha BT}$* ** 0.73 $\pm$ 0.4, n=11 mEPSP amplitude in mV, **p<0.01 comparisons between *GluRIIA^{sp16}* with and without *GluRIIA$^{\alpha BT}$*, data from Stephanie Albin). This demonstrates that the modified GluRIIA$^{\alpha BT}$ subunit can functionally substitute for GluRIIA.

Next, we addressed whether we could specifically label GluRIIA$^{\alpha BT}$ using αBT. Application of an alexa fluor-conjugated αBT (e.g. αBT-488) to wild type larva,

dissected open into a fillet preparation, results in essentially no background (data not shown, Stephanie Albin). Thus αBT does not bind non-specifically to the muscle surface. When I perform the same experiment using larvae that express GluRIIA$^{\alpha BT}$, I see bright synaptic staining (Figure 2A), which can be completely blocked by pretreatment with unlabeled αBT (Figure 2C). Notably, as demonstrated by lack of rhodamine dextran uptake by the muscle, I see synaptic αBT-488 staining in unpermeablized muscle (Figure 2 B). Thus, using this protocol, I can specifically label GluR receptors located on the muscle surface.

I took advantage of GluRIIA$^{\alpha BT}$ to ask whether I could directly detect an internal pool of GluR residing near the synapse. To do so, I pretreated the synapse with unlabeled αBT to block surface receptor staining. Next, I permeablized the muscle surface, demonstrated by uptake of rhodamine dextran (Figure 2F), and then added αBT-488. In this experiment, I see increased fluorescence throughout the muscle, but no specific increase near the synapse (Figure 2E). Indeed, this overall increase in fluorescence is not *GluRIIA*$^{\alpha BT}$-dependent, because I see similar increases in wild type controls (data not shown). Overall our data suggest that internal stores of GluRIIA are likely to be distributed throughout the muscle, rather than located in close proximity to the synapse. In addition, these data suggest that most, if not all GluRs present at the synapse reside on the muscle surface.

Next using GluRIIA$^{\alpha BT}$ I examined the stability of receptors within the membrane, which at the Drosophila NMJ is thought to be a slow process (Rasse et al., 2005). To monitor the internalization of receptors off the muscle surface, I labeled surface receptors with αBT as described above. I either immediately fixed half of the preps or incubated

them for an allotted period of time before fixation. Using this protocol to monitor the extent of receptor internalization that occurs over a 30 minute time period, I see no significant decrease in the amount of surface labeling (wt 0 h 99 $\pm$ 8.2 n=17, 30 min 106 $\pm$ 12.3 n=9,% 0 h αBT staining, wt 0 h 100 $\pm$ 1.9 n=17, 30 min 112 $\pm$ 6.7 n=9, % 0 h HRP staining). These data suggest there is no rapid internalization of surface receptors. In addition, we took late stage embryos just after NMJ formation which expressed the *GluRIIA*$^{\alpha BT}$ transgene, and injected αBT-488 (done by Regina Vittore). I raised these animals at 20ºC, and at the end of larval development, eight days later I dissected wandering third instar larvae. Remarkably, I see prominent synaptic αBT labeling in these animals (Figure 3A). These data are consistent with the idea that once inserted into the membrane receptors are largely stabilized.

Given the finding that GluR receptor internalization is a relatively slow process at the Drosophila NMJ, I wanted to determine whether it was feasible to use GluRIIA$^{\alpha BT}$ to monitor the trafficking of receptors onto or off of the muscle surface. I devised a two-part assay. First as described above I combined the labeling of surface receptors and subsequent incubation to monitor receptor internalization. In addition, after incubation and just prior to fixation, I applied αBT to the preps again, this time conjugated to different fluorophore (Figure 3B); in this way I monitor the receptors that were inserted into the membrane during the incubation period. In addition, instead of incubating for 30 minutes, I incubated for 8 h at 30ºC (Figure 3B). By normalizing synapses fixed immediately after initial labeling (100 $\pm$ 5.9 % of 0h labeling n=9) and fixed after an 8h incubation (8 h 25 $\pm$ 2.1** n=10 % 0 h αBT fluorescence** $p<0.01$), I find a significant internalization of initially labeled receptors (Figure 3B). In the same synapses there was

no significant change in HRP antigenicity (0 h 100 ± 6.2 n=9, 8 h 113 ± 3.5 n=10 % 0 h HRP fluorescence. In addition, when I incubate for 8 h in HL3 saline plus Ca^{2+}, I see insertion of GluRs into the synapse (Figure 3B). I do not see the same insertion of new receptors when preps are incubated in Schnieder's Drosophila Media, and currently I cannot explain this discrepancy. However, overall these data demonstrate that, at a minimum, GluRIIA$^{\alpha BT}$ can be used to monitor internalization of surface receptors in Drosophila fillet preps.

Because I hypothesized that in Drosophila muscle, Dorsal and Cactus control GluR density via receptor trafficking, I wanted to use the GluRIIA$^{\alpha BT}$ to analyze receptor trafficking in wild type and mutant larvae. Before I monitored internalization, I confirmed that even when expressing GluRIIA$^{\alpha BT}$ in these genetic backgrounds I detect differences in synaptic GluR abundance, previously detected by anti-GluRIIA staining (Heckscher et al., 2007). I show that in wild type larvae harboring several copies of the *GluRIIA$^{\alpha BT}$* transgene, surface labeling with αBT-488 almost completely co-localizes with anti-GluRIIA antibody staining (Figure 4A-B, data not shown). This demonstrates that GluRIIA$^{\alpha BT}$ is incorporated into most if not all GluR clusters. Next, I preformed the same co-labeling experiment a in *cact^{RN}* mutant background, and see a significant decrease in GluRIIA αBT abundance compared to wild type (Figure 4C-E). Indeed the percent GluRIIA reduction measured by these two different labeling methods are in excellent agreement (Figure 4E). This is consistent with prior data, showing that *cactus* disrupts a post-transcriptional mechanism to control GluRs (Heckscher, et al., 2007). Thus, these data demonstrate that there is a correlation between the abundance GluRIIA

detected on the surface using αBT -labeling, and the total GluRIIA abundance visualized by anti-GluIIA staining, in wild type and mutant backgrounds.

To test whether Cactus controls GluR density via regulation internalization of receptors, I measured the relative amount of receptor internalization in wild type and $cact^{RN}$ mutants. I monitored receptor internalization at 0h, 1h and 2h in wild type and $cact^{RN}$ mutant larvae, and find no significant difference in the amount of internalized receptor between wild type and mutant at any time point (Figure 5). Thus, it seems that in the $cact^{RN}$ mutant background, receptor internalization is not affected. Instead, these data suggest that receptor insertion could be attenuated in $cact^{RN}$ mutant backgrounds. Important next steps include directly examining receptor insertion in $cact^{RN}$ mutants, as well as conducting a similar analysis in *dorsal* and *pelle* mutants. However, taking into consideration that Dorsal and Cactus regulate GluR density via a posttranscriptional mechanism (Heckscher et al., 2007) and I find normal receptor internalization in *cactus*, I favor the idea that Cactus, and by extension Dorsal, controls GluR density via regulating receptor insertion.

Pelle localizes to distinct puncta and surrounds muscle nuclei

At the NMJ, Dorsal and Cactus are co-localized in a postsynaptic region that is rich in late endosomes (Narayanan et al. 2000). However, perturbation of these endosomes through mutation of *hook* or *deep organge* does not seem to affect GluR abundance (Narayanan et al. 2000). Since we previously implicated Pelle kinase as part of the cytoplasmic Dorsal/Cactus pathway that controls GluR density, I turned to a detailed examination of Pelle kinase localization. Previously we constructed a GFP-

tagged UAS-Pelle transgene (done with the help of Mollie Beiwald), which I used to rescue *pelle* mutant phenotypes (Heckscher et al., 2007). I noticed that overexpressed, GFP-Pelle was found diffusely throughout the muscle, and occasionally at the synapse (Figure 6A-B). More interesting to us, however, was the observation that GFP-Pelle is enriched around the nucleus and appears in punctate structures (Figure 6A-B). To determine whether this localization of GFP-Pelle was muscle specific, we expressed GFP-Pelle in S2 cell lines (done with the help of Mollie Beiwald), where I observe a similar pattern: GFP-Pelle localizes to discrete puncta, which lie outside the nucleus (Figure 6C, F). Thus in different cell types the GFP-Pelle localization pattern is qualitatively similar.

It remained possible, however, that some aspects of the GFP-Pelle localization pattern were artifacts due to overexpression. To determine the endogenous localization pattern of Pelle, I obtained a commercially available anti-Pelle antibody, dN-20. This antibody is raised against a peptide mapping at the N-terminus of Pelle, preventing us from directly testing whether dN-20 detects N-terminally tagged GFP-Pelle. However, when we label S2 cells, which endogenously express Pelle (Shen and Manely, 2002), and which we transfected with GFP-Pelle, we see a similar distribution of GFP-Pelle and dN-20 staining (Figure 6C-E). Indeed, GFP-Pelle and dN-20 immunoreactivity both surround the nucleus and highlight discrete puncta, some of which are co-labeled (Figure 6C-E, arrows). This data suggests that GFP-Pelle and dN-20 are labeling similar, if not identical subcellular structures in S2 cells. When I label wild type muscle with dN-20, I detect discrete puncta (Figure 7A) and an almost cage-like staining pattern surrounding the muscle nuclei (Figure 7C). This staining pattern closely resembles the GFP-Pelle

localization pattern (Figure 7D-E). Notably, I do not detect any synaptic staining with the dN-20 antibody (data not shown). Finally, I demonstrate that in a *pelle* null mutation (pll^{RM8}) dN-20 staining is eliminated from the muscle (Figure 7A-B), indicating that dN-20 staining depends on the presence of Pelle protein. Taken together these data suggest that the dN-20 staining pattern reflects the endogenous Pelle kinase distribution. Specifically, I suggest that endogenous Pelle kinase localizes to discrete puncta and in a domain surrounding the muscle nuclei. This localization is consistent with the idea that Pelle associates with an endosome and regulates an aspect of intracellular trafficking.

As a side note, identifying the molecular nature of the dN-20-postive punta is an important next step, because it will help determine the specific trafficking event in which Pelle participates. My preliminary data suggest that dN-20 labeled structures do not extensively co-label with the early endosomal marker, Rab5 (Figure 8A-B)(Ullrich et al., 1996). In addition, dN-20 puncta co-label with the anti-GluRIIC antibody (Figure 8C-F).

Although I see an interesting Pelle localization pattern (Figures 6, 7), it was unclear how it was relevant to the phenotypes seen in *dorsal* or *cactus* mutants. In other systems the biochemical activity of Pelle kinase is to trigger the dissociation of cytoplasmic Dorsal-Cactus protein complexes (Govind, 1999). It is hard to imagine how such a biochemical activity is consistent with the diffusely distributed, punctate localization pattern of Pelle, given that the Dorsal-Cactus complex resides at the synapse (Heckscher et al., 2007, Cantera, et al. 1999). Thus I set out to test whether the role of endogenous Pelle kinase at the NMJ was similar to the role of Pelle kinase in other contexts. If so, I expected to see an increase in co-localized, synaptic Dorsal and Cactus in *pelle* mutants compared to wild type. To test this prediction, I performed quantitative

anti-Dorsal and anti-Cactus fluorescence microscopy. In *pelle* mutants, synaptic Cactus staining is normal, and synaptic Dorsal staining is modestly, but significant reduced (Figure 9, Table 1). Since I do not find the predicted increase in staining, I think that at the NMJ endogenous Pelle kinase has a function other than to disassociate the Dorsal-Cactus complex. This would be consistent with the idea that the site of action for Pelle in the muscle is in endosomal structures, labeled by the dN-20 antibody.

Regulation of dN-20 staining

Usually, *pelle* acts upstream of *dorsal* and *cactus*, because Pelle kinase activity dissociates cytoplasmic Dorsal/Cactus complexes. At the NMJ, however, I see little evidence to suggest that this is the role of Pelle. Previous genetic studies show that *pelle*, *dorsal* and *cactus* act in the same pathway leading to GluR receptor density (Heckscher et al. 2007). Thus, we asked whether *pelle* was acting upstream of *dorsal* and *cactus* as it is in other contexts, or whether at the NMJ it could be acting downstream. To investigate this, I overexpressed a GFP-tagged Pelle transgene, which previously I used to rescue *pelle* mutant phenotypes (Heckscher et al., 2007), in *dorsal* and *cactus* mutant backgrounds. Specifically, I attempted to rescue heterozygous point mutant alleles of *dorsal* (dl^2) and *cactus* ($cact^{RN}$), which were previously demonstrated to dominantly reduce the density of synaptic GluRs (Heckscher et al., 2007). Initial experiments indicate that overexpression of *pelle* is sufficient to rescue dl^2 but not $cact^{RN}$ mutant phenotypes (Figure 11). (An important next step is to repeat a similar experiment in the *dorsal* null mutant background). These data indicate that in the context of control of GluR density *pelle* is likely acting downstream of *dorsal* but not *cactus*.

One possible mechanism by which *dorsal* could act upstream of *pelle* is by regulating the localization or stability of Pelle. Thus, I asked whether Dorsal (or Cactus) was involved in regulation of dN-20 localization or abundance in the muscle. I examined dN-20 staining in *dorsal* mutants known to have impaired GluR density (Heckscher et al., 2007), including dl^2 and a *dorsal* null allele (dl^1). In these backgrounds I see virtually no dN-20 staining surrounding the nuclei or in puncta (Figure 10). Next, I preformed a similar analysis using two previously characterized, hypomorphic *cactus* alleles, $cact^{HE}$ and $cact^{RN}$ (Heckscher et al., 2007). Again I see virtually no dN-20 staining surround the nuclei. However, in $cact^{RN}$ faint, punctate dN-20 staining remains (Figure 10). These data suggest that Dorsal, but perhaps not Cactus, is required for localization of dN-20 to puncate structures. Taken together these observations are consistent with a model in which *dorsal* acts upstream of *pelle* to regulate its localization or abundance.

As a side note, the correlation between reduced dN-20 staining and reduced GluRIIA is remarkable, especially given that examination of Cactus and Dorsal levels in these same mutant backgrounds fails to reveal any trend (Table 1). Due to this remarkable correlation, I examined the dN-20 expression in other mutant backgrounds with diminished GluRIIA levels. First, I looked in a *pelle* kinase dead allele, pll^{078}, and again a see drastic reduction in dN-20 staining (Figure 10). Second, I examined dN-20 staining in a heterozygous *GluRIIA* null mutation, which reduce levels of GluRIIA staining (70 ± 4 % wt GluRIIA n=10). I see variable dN-20 staining: sometimes it appears wild type (data not shown), and sometimes it is greatly diminished (Figure12A-C) (Table 1). Finally, when I examine dN-20 staining in homozygous *GluRIIA* nulls, staining is largely absent (Figure 12A-C). Two scenarios could account for these

findings. First, is that Dorsal and Cactus directly control the localization of dN-20, but that the localization of Dorsal and Cactus themselves are sensitive to GluRIIA levels. However, when I tested whether synaptic Cactus or Dorsal levels were altered in *GluRIIA* background, I see no difference in staining intensity (Figure 12D-H) (Table 1). Second, dN-20 may be sensitive to GluRIIA levels, and reduced dN-20 staining in *dorsal* and *cactus* mutations could be a secondary consequence of reduced GluRIIA. However, the finding that in the $cact^{RN}$ background dN-20 staining remains, although at a lower level, does not quite fit with such an idea. Thus, at the moment, I am not entirely sure how to interpret these data.

Could Dorsal, Cactus or Pelle control GluR density via translational regulation?

Although we favor the idea that Dorsal, Cactus and Pelle act to control GluR density via regulation of receptor trafficking, we also examined whether these proteins could control GluR density via regulation of translation. A previous study, which showed that at the NMJ regulation of GluRIIA can occur via local translation, showed that *GluRIIA* transcripts localize at the synapse (Sigrist et al., 2000). We entertained the possibility that Dorsal and Cactus could be involved in localizing *GluR* transcripts to the NMJ. Specifically, because a handful of reports suggest that DNA binding domains can also bind RNA (Dubnau and Struhl, 1996; Liu et al., 2003; Rivera-Pomar et al., 1996), we were interested in the idea that the DNA binding domain of Dorsal might act as an RNA binding domain in the cytoplasm. This idea predicts that there should be a Dorsal binding site the untranslated regions (UTR) of *GluRIIA*. To look for Dorsal binding sites, we used P-match analysis to examine 3' and 5' UTRs of all *GluR* subunits known to be

expressed at the NMJ (Chekmenev et al., 2005; Pan and Courey, 1992; Tisse et al., 1991). Using the least stringent criteria, we found potential binding sites in *GluRIIA*, *GluRIID*, and *GluRIIE*. Reasoning that if a binding site was of biological significance it should be conserved among different species of *Drosophilid* flies, we used a comparative genomic approach to ask which binding sites were conserved. Only the potential Dorsal binding site in the 5' UTR of *GluRIIA* was completely conserved within the *melanogaster* group (*melanogaster, simulans, sechellia, yakuba, erecta*) (Figure 13A, gray box) however, most of this UTR is highly conserved. Finally, we asked whether there was any secondary structure in the 5' UTR of *GluRIIA* mRNA that would form hairpin structures, which would almost certainly occlude binding to a DNA binding domain. Using a secondary structure prediction algorithm, we find that the potential Dorsal binding site in 5' UTR of *GluRIIA* forms a helix (Figure 13B, gray box). Taken together these data are consistent with the idea, albeit far-fetched, that Dorsal could bind to and localize *GluRIIA* mRNA to the NMJ.

We also entertained the possibility that *pelle* may be involved in local translation. Previous studies showed that aggregations of the translation initiation factor, eIF4G, and poly(A) Binding Protein (PABP) likely representing polysomes, are co-localize in the muscle near the synapse (Sigrist et al., 2000). Thus, it was possibility that dN-20 positive puncta were also associated with polysomes. However, when we labeled a muscle expressing a PABP2-GPF fusion (Clyne et al., 2003), we did not see any significant co-localization (data not shown). In addition, in the extremely limited live imaging that I have done with GFP-Pelle, occasionally I could see GFP-puncta moving (data not shown), suggesting that these structures represent transport endosomes rather than static

polysomes. Thus, we do not find any compelling data to suggest that Pelle is involved in local translation.

DISCUSSION

Glutamate receptor insertion, stability and internalization at the Drosophila NMJ

In this study we describe a new tool, GluRIIA$^{\alpha BT}$, which allows us to selectively label glutamate receptors found on the muscle surface. Using GluRIIA$^{\alpha BT}$ we monitored the dynamics of GluRs in the muscle membrane at the Drosophila NMJ. Recently another group used a modified GluRIIA subunit, in this case tagged with GFP, to examine the development of GluR receptors (Rasse et al., 2005). This study made interesting suggestions about the normal trafficking of glutamate receptors, and we were able to compare our findings with theirs. First, Rasse et al., by conducting photobleaching experiments of synaptic and extrasynaptic areas, suggested that stores of GluR receptors are distributed through out the muscle. We were able to directly test this idea using GluRIIA$^{\alpha BT}$ in combination with differential permeablization protocols. And in agreement with the conclusions of the prior study, we do not find evidence for an internal pool of GluRIIA$^{\alpha BT}$ located in close proximity to the synapse. Second, Rasse et al. suggested that internalization of receptors off the membrane was a relatively slow process. In general, our data support this conclusion: we find little evidence of rapid internalization of receptors off the surface, and we find that αBT-labeled GluRIIA$^{\alpha BT}$ on the surface of the muscle can be detected eight days after αBT administration. Thus, for the most part our data support the general conclusions made by Rasse et al.

In specifics, however, our data differ from Rasse et al. Using GluRIIA^{GFP}, they suggest that below 30% of the total number of receptors are internalized over a 24 h

period at 25ºC. In contrast, when we measure receptor internalization over an 8 h period at 30ºC, we see internalization of 75% of the total number of labeled receptors. Thus there is a discrepancy in measurement of the rate of internalization of receptors off the muscle surface. There are at least two major experimental differences that could explain such a discrepancy. First, in the Rasse study, GluRs were monitored in anesthetized, intact larvae over a period of days. In contrast, we monitored GluRs in partially dissected fillet preparations over a period of hours. Second, it is possible that different modifications made to the GluRIIA subunit, addition GFP (~100 aa, inserted into intracellular C-terminus) versus an alpha-bungarotoxin binding site (13 aa inserted into extracellular N-terminus) could have differential effects on receptor internalization. Despite these discrepancies, we consider GluRIIA$^{\alpha BT}$ to be a useful assay for comparing rates of internalization between mutant and wild type backgrounds.

Pelle kinase likely mediates surface insertion of GluRIIA

Previously we showed that *dorsal*, *cactus* and *pelle* loss of function mutations impair GluR density at the NMJ (Heckscher et al., 2007). In this study we show that GluRs found at the NMJ are located on the muscle surface. Therefore, Dorsal, Cactus and Pelle promote the surface expression of GluRs. There are two basic ways in which these proteins could promote surface expression: by inhibiting receptor internalization, or by promoting receptor insertion. We show directly that in a *cactus* mutant background, which has reduced GluR density, receptor internalization is not altered. Thus, Cactus (and by extension Dorsal and Pelle) should be acting to promote receptor insertion. A variety of cellular processes are ultimately required for proper receptor insertion: transcription,

translation and trafficking. Of these processes we favor the idea that trafficking is the relevant step. First, our previous study suggested that a posttranscriptional mechanism accounts for the control of GluRs in *dorsal* and *cactus* backgrounds (Heckscher et al., 2007). Second, in this study I find little evidence to implicate Dorsal, Cactus or Pelle in regulation of translation. Thus, by process of elimination I favor the idea that that these proteins are acting to regulate receptor insertion. An important next step is to determine the molecular identity of the Pelle-positive puncta. For example, co-localization with Rab8 would suggest that Pelle may regulate receptor trafficking from the TGN, whereas colocalization with Rab11 would suggest that Pelle may mediate recycling from the recycling endosome (Figure 14). Ultimately, this type of positive data will be required to demonstrate that Pelle specifically regulates a trafficking step.

Table 1. GluRIIA, Dorsal, Cactus, dN-20 in *GluRIIA*, *dl*, *cact*, *pll* mutants

Genotype	Antibody			
	GluRIIA	Dorsal	Cactus	dN-20
GluRIIAsp16 (null)	Absent	Normal	Normal	Absent
GluRIIAsp16/+	>50%	Normal	No data	Varies
dl1 (null)	>50%*	Absent*	<50%**	Absent
dl2	<50%*	>50%*	Normal**	Absent
cactHE	>50%*	Normal*	>50%*	Absent
cactRN	>50%*	Normal*	>50%*	<50%
pllRM8 (null)	>50%*	>50%	Normal	Absent
pll078	>50%*	>50%	Normal	Absent

*Gray box indicates this data is summarized from the previous chapter.

** Indicates data is included below:

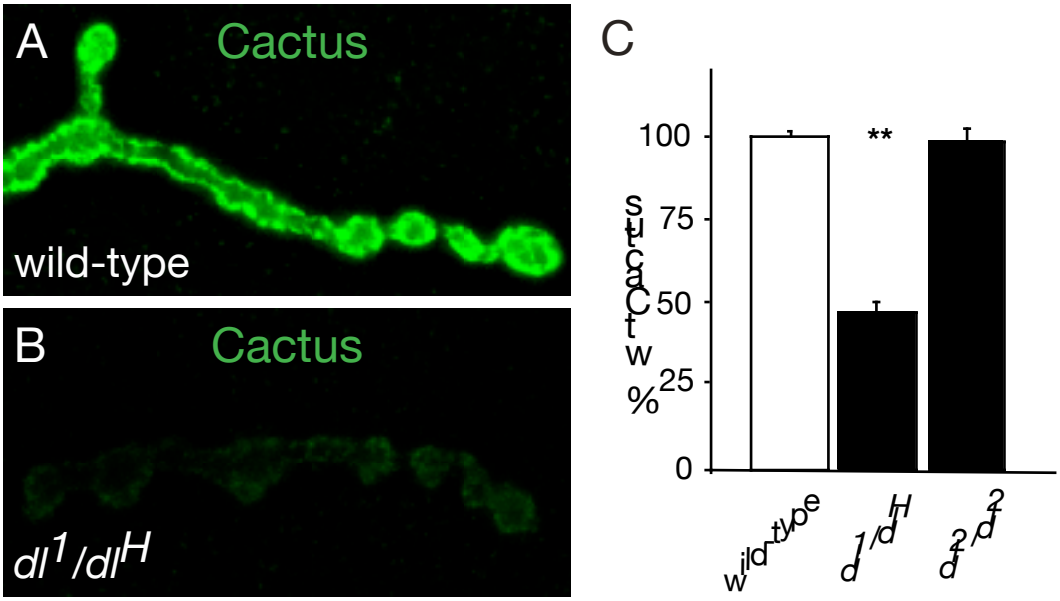

Figure 1. A modified GluRIIA subunit functionally substitutes for GluRIIA.

A) An alpha-bungarotoxin binding site was inserted into the extracellular, N-terminus of the GluRIIA receptor (GluRIIA$^{\alpha BT}$). **B)** GluRIIA staining is restored to *GluRIIA* null mutants expressing *GluRIIA*$^{\alpha BT}$. Expression of *GluRIIA*$^{\alpha BT}$ also restores synaptic function scale bar is mV/ms.

Figure 2. No internal subsynaptic pool of GluRs in Drosophila neuromuscular synapses

A-B) *GluRIIA*$^{\alpha BT}$ expressing larva were filleted; αBT-488 and rhodamine-dextran were applied. Note αBT-488 binds at the synapse, and that no rhodamine-dextran enters the muscle because it was not permeablized. **C-D)** In a similar experiment synapses were pretreated with unlabeled αBT. Note that the surface staining is completely blocked. **E-F)** In this experiment, synapse were pretreated with unlabeled αBT and permeablized before αBT-488 and rhodamine-dextran were applied. Note that there is an even distribution of fluorescence throughout the muscle, and that rhodamine-dextran enters the permeablized tissue.

Figure 3. Monitoring receptor stability, internalization and insertion using GluRIIA$^{\alpha BT}$

A) *GluRIIA*$^{\alpha BT}$ expressing late embryos were injected with αBT-488. At the end of larval development, we find synaptic labeling with αBT-488. The right panel is shown with HRP, to highlight the neuron. **B)** We show the protocol used to monitor internalization of receptors off of the muscle surface and insertion of new receptors onto the muscle surface. Sequential incubation with αBT-596 and αBT-488, with no intervening treatment shows surface receptors (labeled red); no new receptor insertion can be

detected. Using a similar protocol, we see that after 8 hours of incubation between labeling with αBT-596 and αBT-488, there was significant internalization of receptors (disappearance of red staining). During the same period, there was significant insertion of new receptors, but only when preps were incubated in saline (appearance of green staining).

Figure 4. Correlation between anti-GluRIIA staining and alpha-bungarotoxin labeling in wild type and mutant

A-B) Animals expressing *GluRIIA*$^{\alpha BT}$ were incubated with αBT-488, fixed and labeled with anti-GluRIIA. **C-D)** The same experiment was performed on animals expressing *GluRIIA*$^{\alpha BT}$ in a *cactus* mutant background. The level of αBT-488 and anti-GluRIIA labeling is reduced in comparison to wild type. **E)** Quantification of the reduction in αBT labeling and anti-GluRIIA labeling in the *cact* background versus wild type shows that the percent reduction measured by either method is similar. (*GluRIIA*$^{\alpha BT}$*/Y;; GluRIIA*$^{\alpha BT}$/+ = 100 $\pm$ 8.1 n=13, *GluRIIA*$^{\alpha BT}$*/Y; cact*^{RN}*/+; GluRIIA*$^{\alpha BT}$/+ = 68 $\pm$ 10.3* n= 9, % wt αBT staining, *GluRIIA*$^{\alpha BT}$*/Y;; GluRIIA*$^{\alpha BT}$/+ = 99 $\pm$ 4.6 *GluRIIA*$^{\alpha BT}$*/Y; cact*^{RN}*/+; GluRIIA*$^{\alpha BT}$/+ = 73 $\pm$ 5.4** % wt anti-GluRIIA staining, *GluRIIA*$^{\alpha BT}$*/Y;; GluRIIA*$^{\alpha BT}$/+ = 100 $\pm$ 3.5, *GluRIIA*$^{\alpha BT}$*/Y; cact*^{RN}*/+; GluRIIA*$^{\alpha BT}$/+ = 97 $\pm$ 6.4 % wt HRP staining, * $p<0.05$, ** $p<0.01$).

Figure 5. No defect in receptor internalization in *cact*^{RN} mutants

A) We monitored internalization of surfaced labeled GluRs in wild type (open circles) and *cactus* mutants (gray boxes) over a two-hour period. While there are significant reductions in αBT labeling in both genotypes over this time period, there is no significant difference between genotypes at any given time point. (*GluRIIA*$^{\alpha BT}$*/GluRIIA*$^{\alpha BT}$ 0 h 99 $\pm$

8.2 n=17, 1 h 85 ± 13.8 n=9, 2 h 66 ± 3.6 n=10 % 0 h wt αBT labeling, $cact^{RN}/cact^{RN}$; $GluRIIA^{\alpha BT}/GluRIIA^{\alpha BT}$ 0 h 100 ± 8.9 n= 9, 1 h 69 ± 14.7 n= 7, 2 h 61 ± 9.3 n= 9 % 0 h $cact^{RN}$ αBT labeling). **B)** In the same synapses there is no reduction in HRP staining ($GluRIIA^{\alpha BT}/GluRIIA^{\alpha BT}$ 0 h = 100 ± 1.9, 1 h 102 ± 4.6, 2 h 104 ± 2.9 % 0 h wt HRP labeling, $cact^{RN}/cact^{RN}$; $GluRIIA^{\alpha BT}/GluRIIA^{\alpha BT}$ 0 h 100 ± 1.8, 1 h 102 ± 1.0, 2 h 98 ± 2.6 % 0 h $cact^{RN}$ HRP labeling).

Figure 6. GFP-Pelle localizes to discreet puncta in larval muscle and S2 cells.

A-B) Overexpression of GFP-Pelle in muscle shows general cytoplasmic and synaptic localization. The synapse is shown by HRP labeling (B). In addition GFP-Pelle is found in punctate structures and near the nucleus (noted as N). **C-F)** This image is a single optical section of an S2 cell expressing N-terminally tagged *GFP-Pelle*, and which endogenously expresses *pelle*. GFP Pelle is found in punctate structures (arrows) (C). Staining with an antibody raised to N-terminus of Pelle, dN-20 shows a similar localization (arrows) (D). There is some colocalization of GFP-Pelle and dN-20 at brightly labeled puncta (arrows) (E). In all dimensions GFP-Pelle puncta surrounds the nucleus, highlighted by a purple DAPI staining (noted as N) (F).

Figure 7. dN-20 localizes to discreet puncta in larval muscle.

A-C) dN-20 labeling is shown in wild type and *pelle* null muscle (pll^{RM8}). In wild type (A) dN-20 labeled puncta are found throughout the muscle and surround the muscle nuclei, marked by purple DAPI staining. A high resolution, three-dimensional reconstruction of in wild type shows that dN-20 staining surrounds the nuclei in all dimensions (C). dN-20 staining is absent from *pelle* null (pll^{RM8}). **D-E)** Two different synapses are shown. One is a wild type synapse labeled with dN-20 (D); the other shows

localization of GFP-Pelle in a *pelle* mutant background (E). Note the localization patterns of dN-20 and GFP-Pelle are strikingly similar.

Figure 8. Preliminary characterization of dN-20 puncta

A-B) A synapses was co-labeled with dN-20 and the early endosome marker Rab5. There is modest co-localization in wild type (A, circle), which is background staining because it is not eliminated in *pll* null (pll^{RM8})(B, circle). **C-D)** A wild type synapse was co-labeled with dN-20 and anti-GluRIIC (C), the box indicates the region enlarged in D-F. Note there is extensive colocalization between dN-20 staining and anti-GluRIIC staining (E-F).

Figure 9. Endogenous Pelle does not negatively regulate Dorsal and Cactus abundance at the NMJ.

A-C, G) Cactus levels in *pelle* null ($pll^{25}/Df(3R)D605$) and kinase dead (pll^{078}/pll^{078}) mutants are not different than in wild type (wt 100 $\pm$ 3.2 n=29, $pll^{25}/Df(3R)D605$ 97 $\pm$ 19 n=2, pll^{078}/pll^{078} 100 $\pm$ 5.0 n=14 % wt Cactus levels). **D-E, H)** Dorsal levels are modestly reduced in *pelle* mutants in comparison to wild type (wt 100 $\pm$ 3.1 n=38, $pll^{25}/Df(3R)D605$ 82 + 2.5** n=19, pll^{078}/pll^{078} 87 + 3.6 n=20** % wt Dorsal levels, ** $p<0.01$).

Figure 10. Localization of dN-20 in *dorsal* and *cactus* mutants

dN-20 staining is shown in wild type and a variety of mutants. dN-20 nuclear and puncate staining is almost completely gone in *pelle* kinase dead (pll^{078}), *dorsal* null (dl^{1}), *dorsal* point mutant (dl^{2}), and *cactus* point mutant ($cact^{HE}$) alleles. In another *cactus* point mutant ($cact^{RN}$) dN-20 levels are greatly diminished, but puncta are still visible.

Figure 11. Expression of *pelle* rescues GluRIIA levels in dl^2 but not $cact^{RN}$ backgrounds

A-C) Synapses were stained with anti-GluRIIA and pseudocolored to visualize differences in staining intensity. Expression of *pelle* in dl^2 background (B), but not a $cact^{RN}$ background (C) can rescue the reduced GluRIIA staining phenotype. **D)** Quantification of the GluRIIA staining intensities (wt 100 $\pm$ 2.9 n=8, dl^2*/UAS-GFP-Pelle; 24B*/+ 103 $\pm$ 3.5 n=10, $cact^{RN}$*/UAS-GFP-Pelle; 24B*/+ 74 $\pm$ 3.6** n=10, % wt GluRIIA staining, ** $p<0.01$).

Figure 12. Localization of dN-20, Cactus and Dorsal in *GluRIIA* mutants

A-C) dN-20 staining is greatly diminished in heterozygous (B) and homozygous *GluRIIA* mutants (C). **D-E)** wild type and *GluRIIA* null synapses were stained with anti-Cactus and then pseudocolored to visualize difference is staining intensity. **F-H)** wild type, *GluRIIA* heterozygous and homozygous null mutants were stained with anti-Dorsal and psuedocolored. There is no difference in Cactus or Dorsal staining intensity in the GluRIIA mutant background.

Figure 13. The 5' UTR of *GluRIIA* mRNA contains a potential Dorsal binding site.

A) An alignment of the 5' UTRs of *GluRIIA* from the melanogaster group of Drosophilid flies shows that this region of the mRNA is highly conserved, including a potential Dorsal binding site (gray box). **B)** A secondary structure prediction of the 5' UTR of *GluRIIA* mRNA from *Drosophila melanogaster* shows that the potential Dorsal binding site lies in a region predicted to be helical (gray box).

Figure 14. Endosomal trafficking in Drosophila

This diagram summarizes the trafficking events known to impact glutamate receptor abundance (red arrows) (Kennedy and Ehlers, 2006), and the Drosophila molecules known to mark different endosomes (Fisher et al., 2006).

Figure 1. A modified GluRIIA subunit functionally substitutes for GluRIIA.

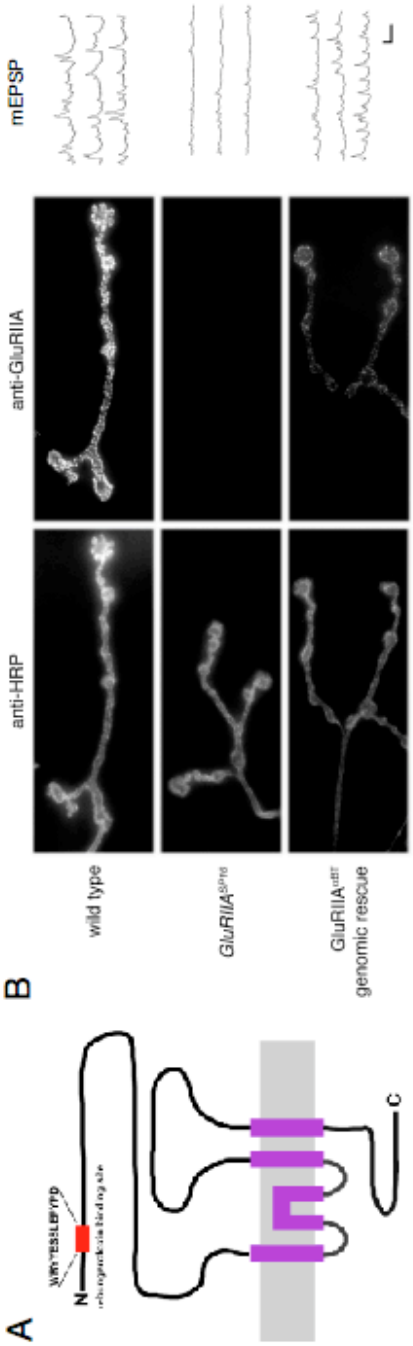

Figure 2. No internal subsynaptic pool of GluRs in Drosophila neuromuscular synapses

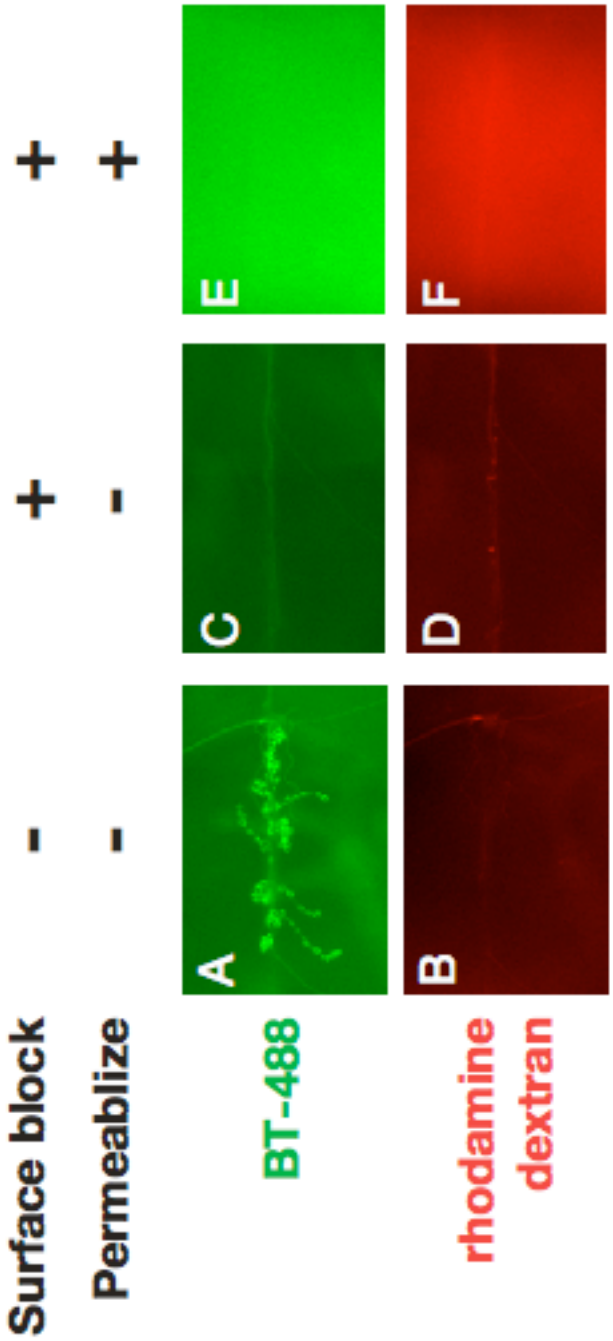

Figure 3. Monitoring receptor stability, internalization and insertion using GluRIIA$^{\alpha BT}$

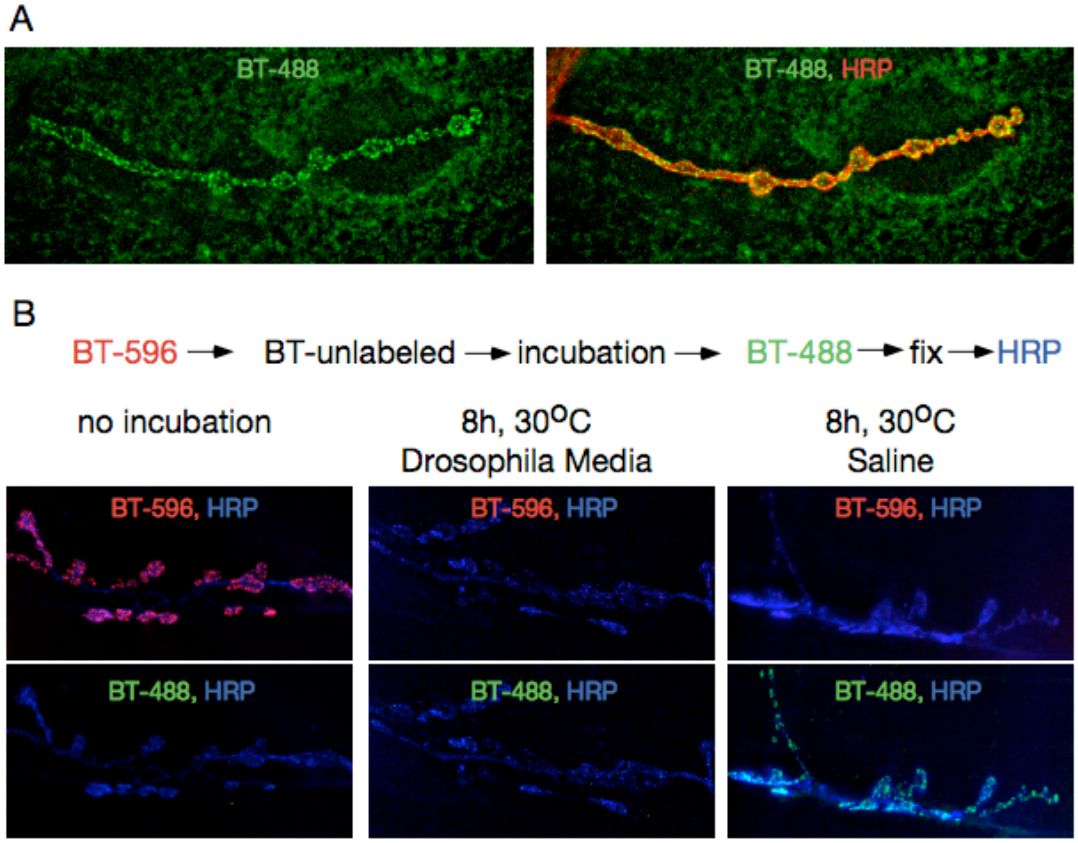

Figure 4. Correlation between anti-GluRIIA staining and alpha-bungarotoxin labeling in wild type and mutant

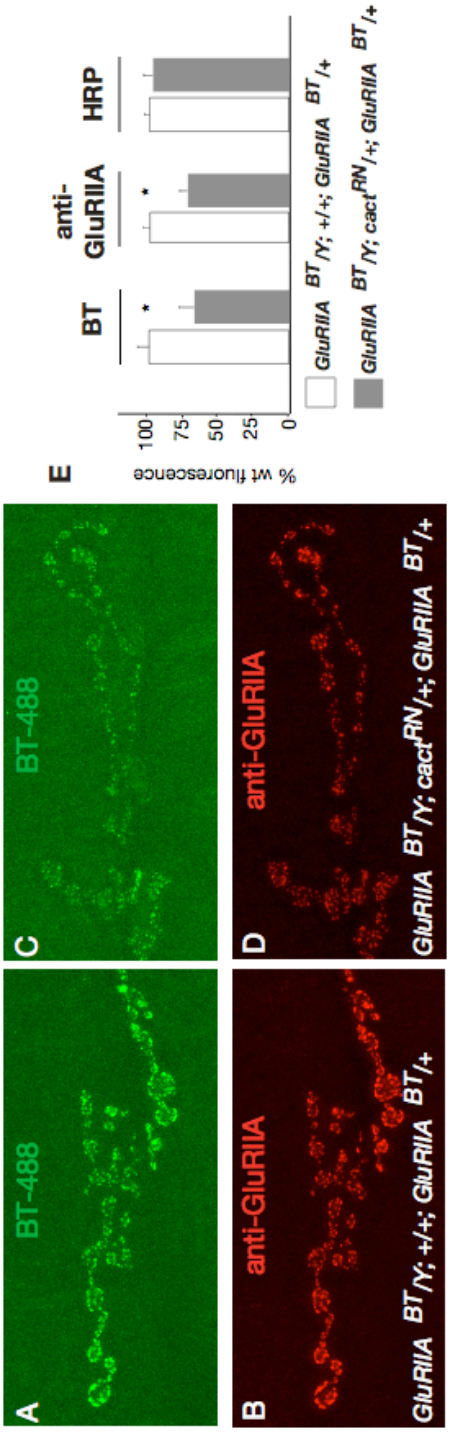

Figure 5. No defect in receptor internalization in *cact*^{RN} mutants

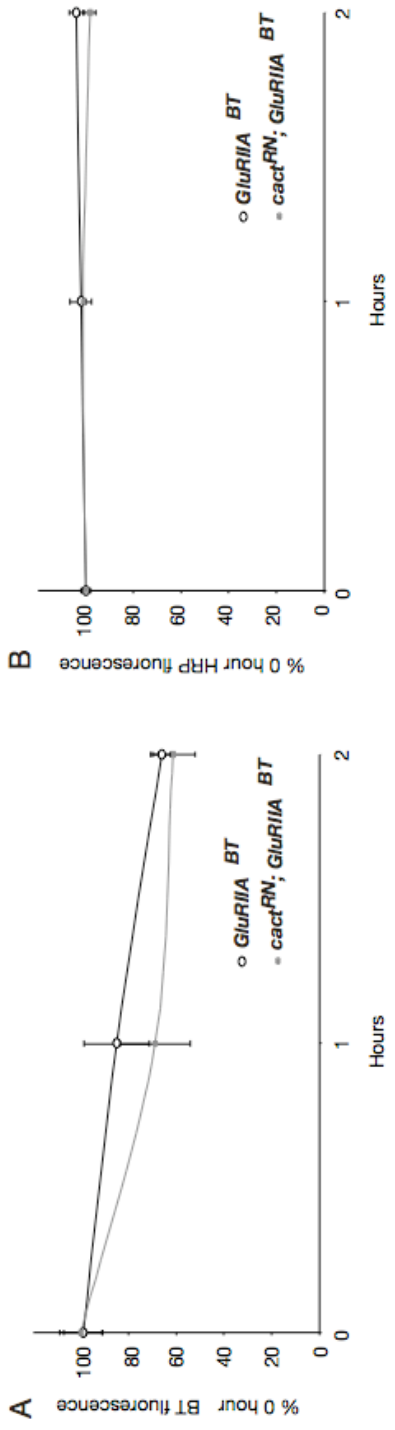

Figure 6. GFP-Pelle localizes to discreet puncta in larval muscle and S2 cells.

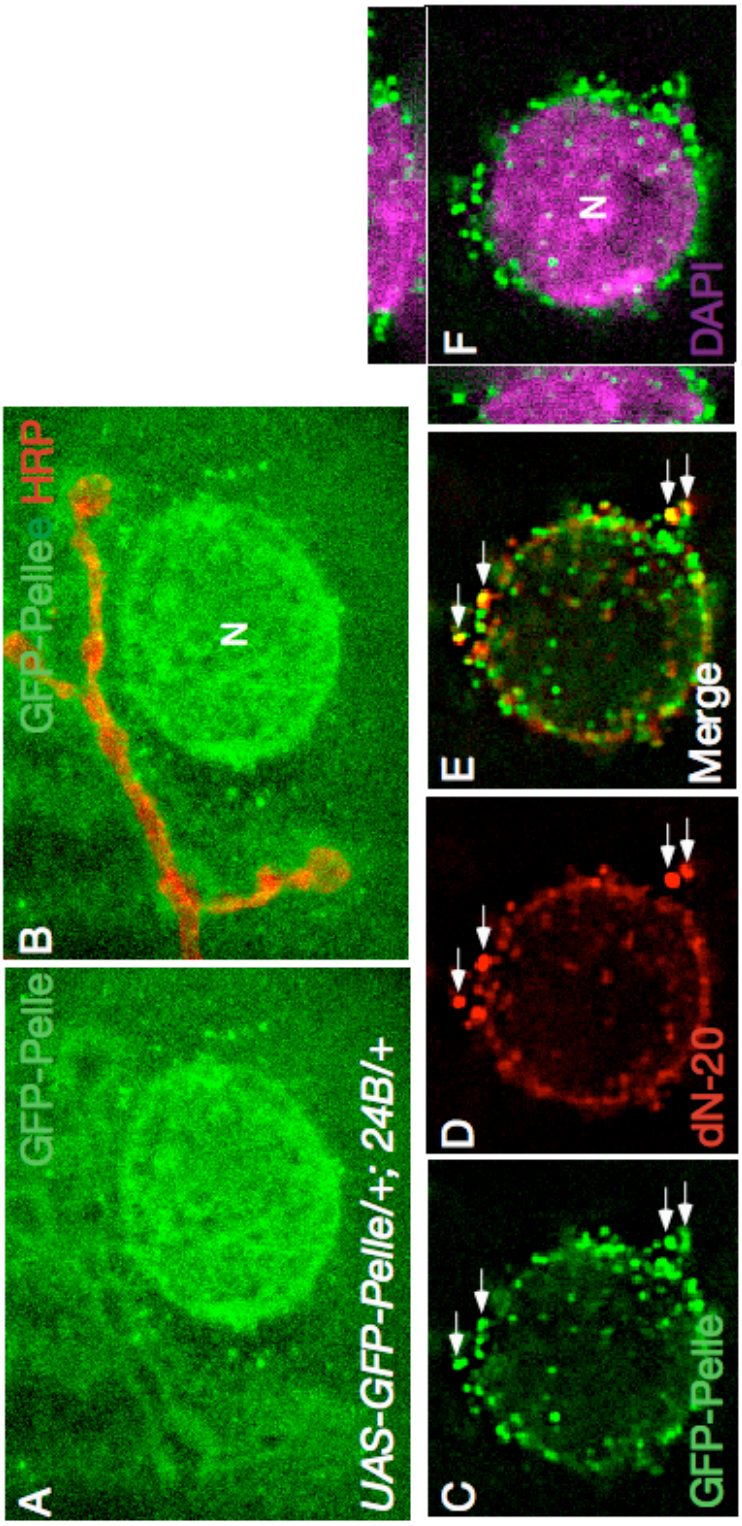

Figure 7. dN-20 localizes to discreet puncta in larval muscle.

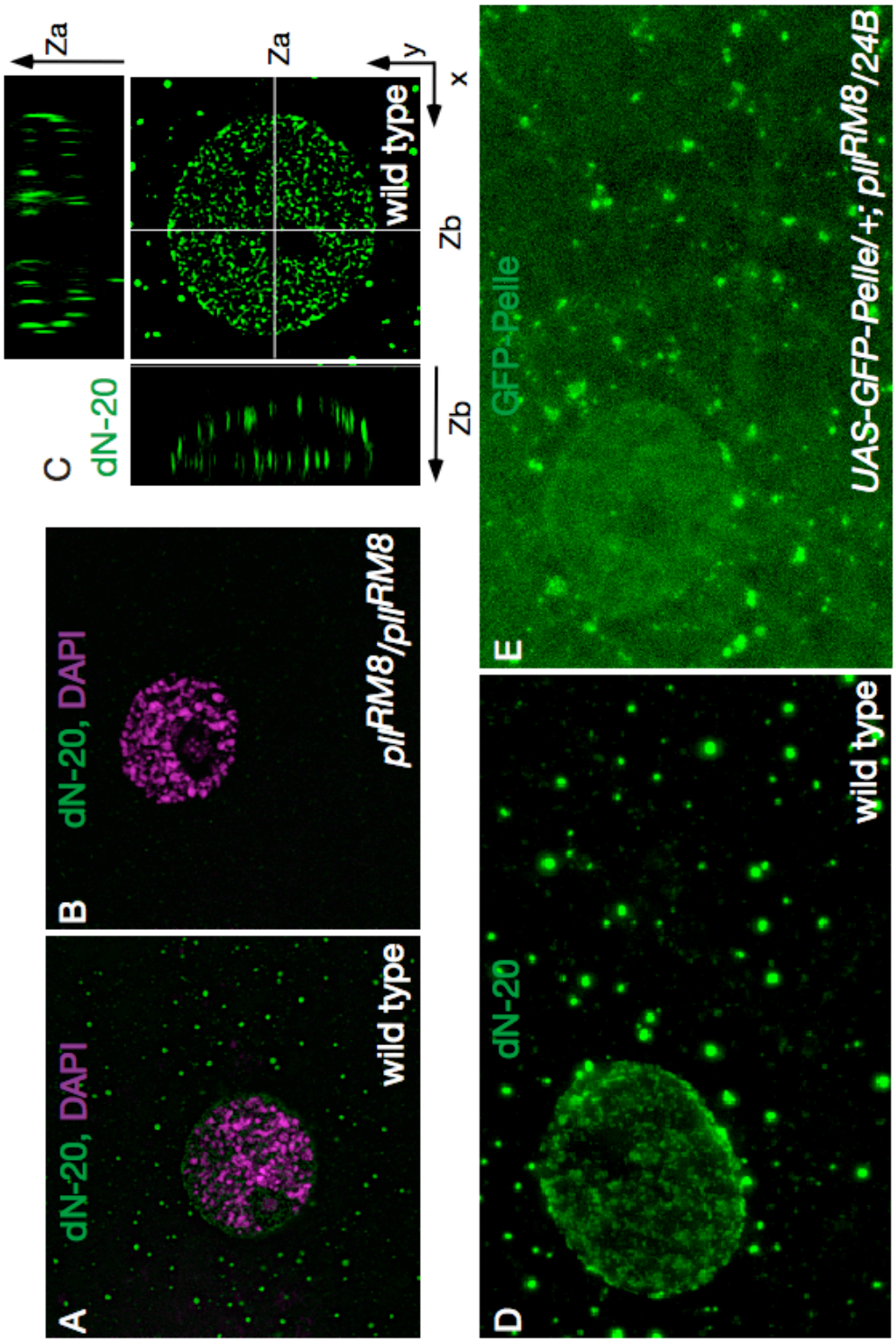

Figure 8. Preliminary characterization of dN-20 puncta

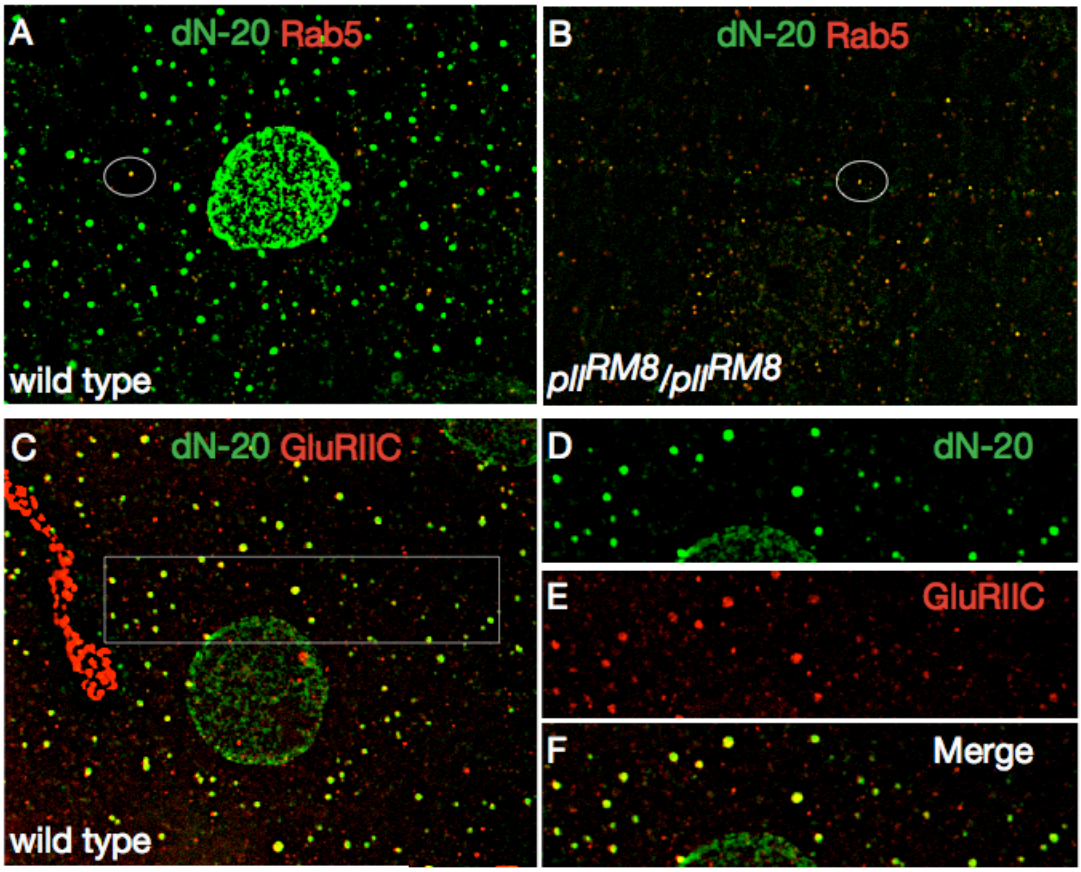

Figure 9. Endogenous Pelle does not negatively regulate Dorsal and Cactus abundance at the NMJ.

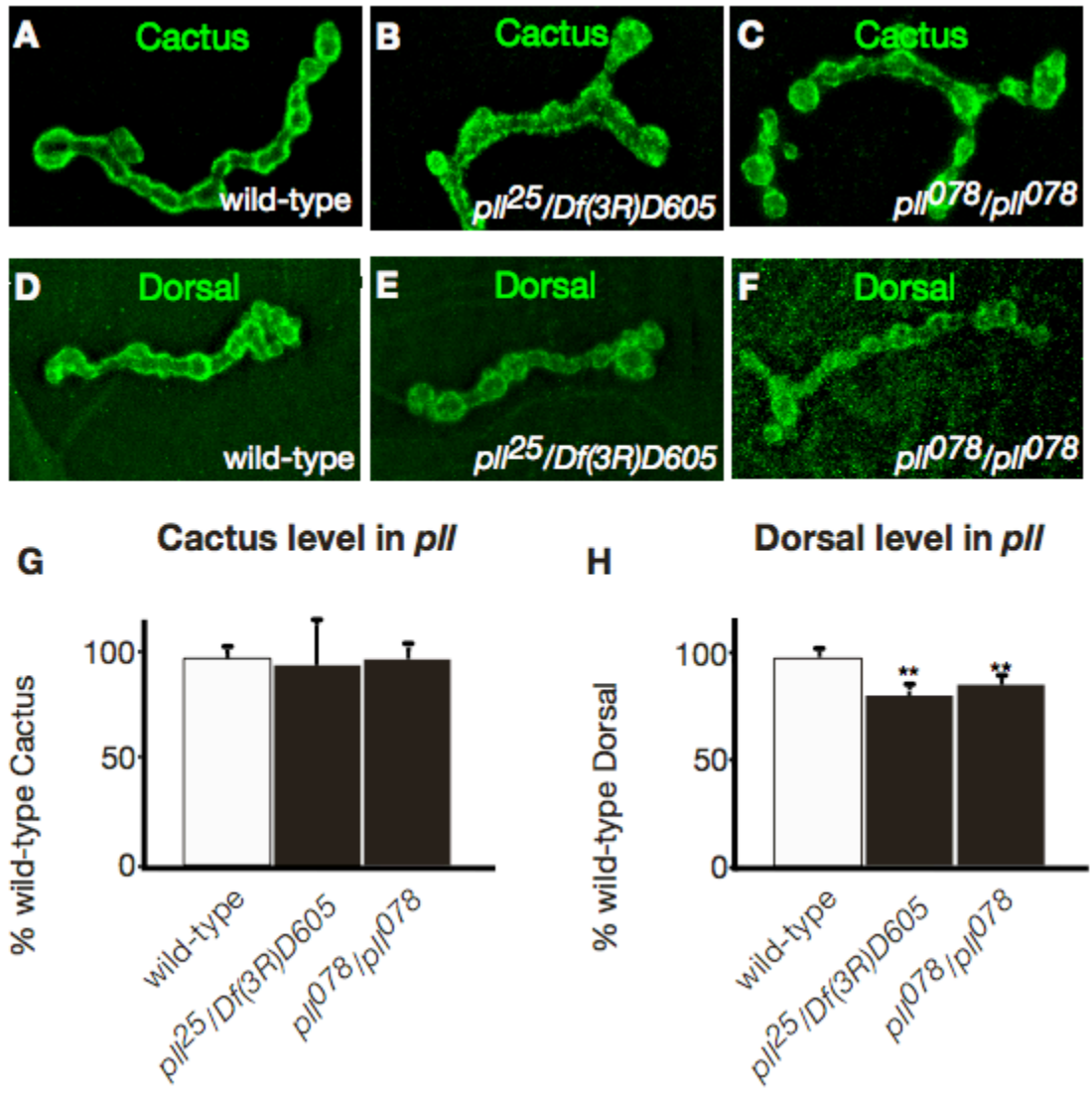

Figure 10. Localization of dN-20 in *dorsal* and *cactus* mutation

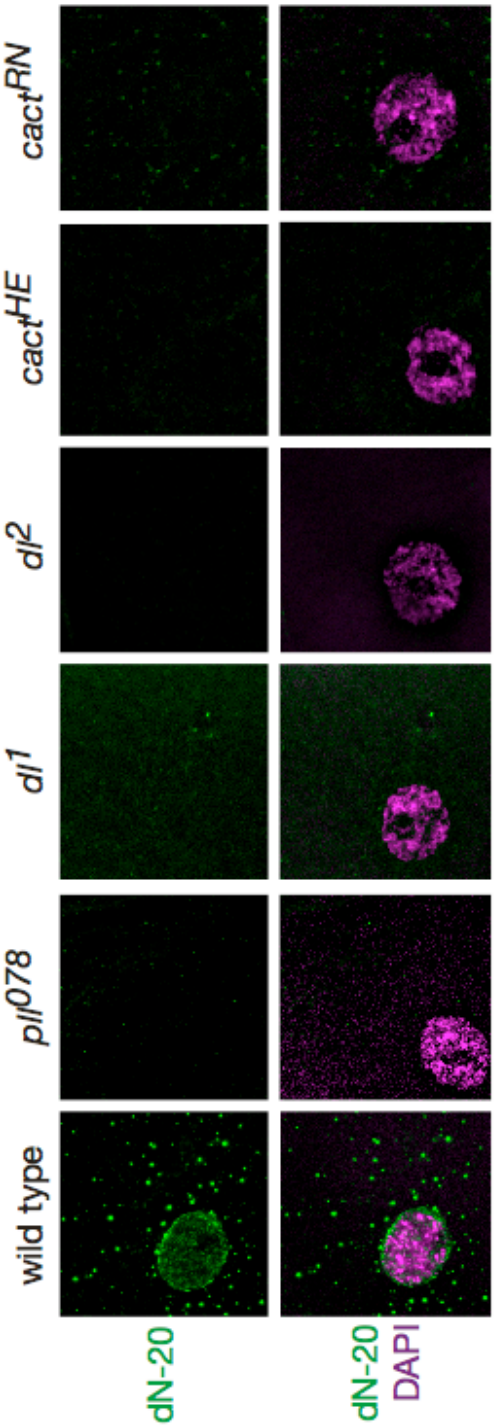

Figure 11. Expression of *pelle* rescues GluRIIA levels in dl^2 but not $cact^{RN}$ backgrounds

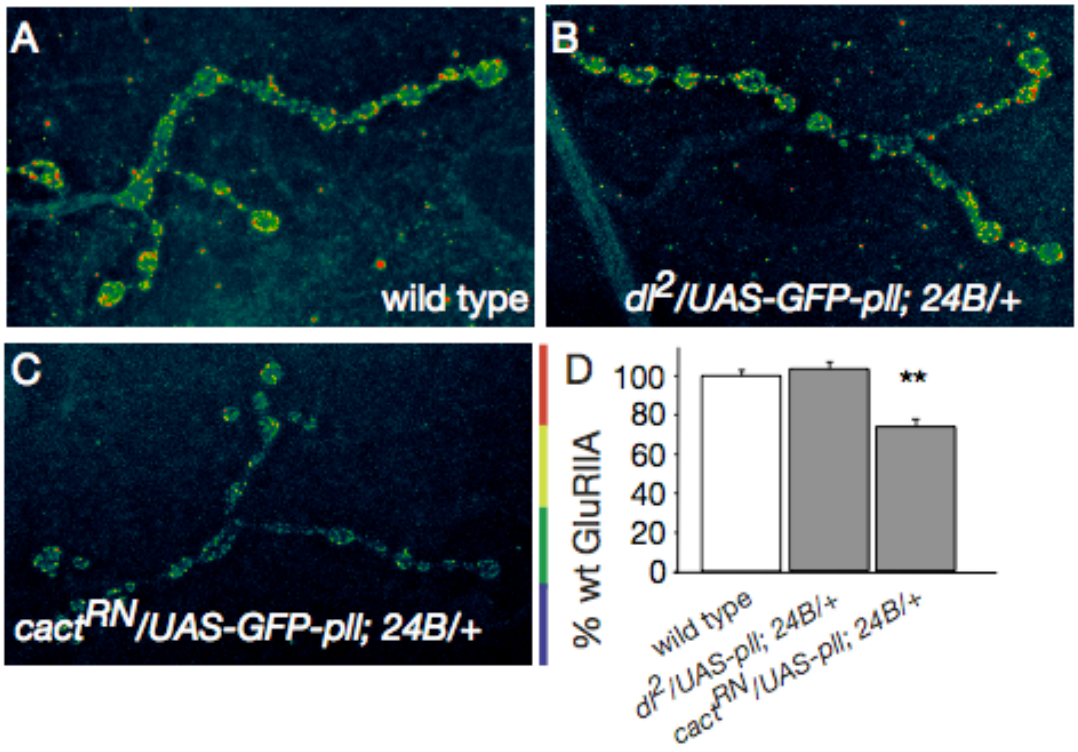

Figure 12. Localization of dN-20, Cactus and Dorsal in *GluRIIA* mutants

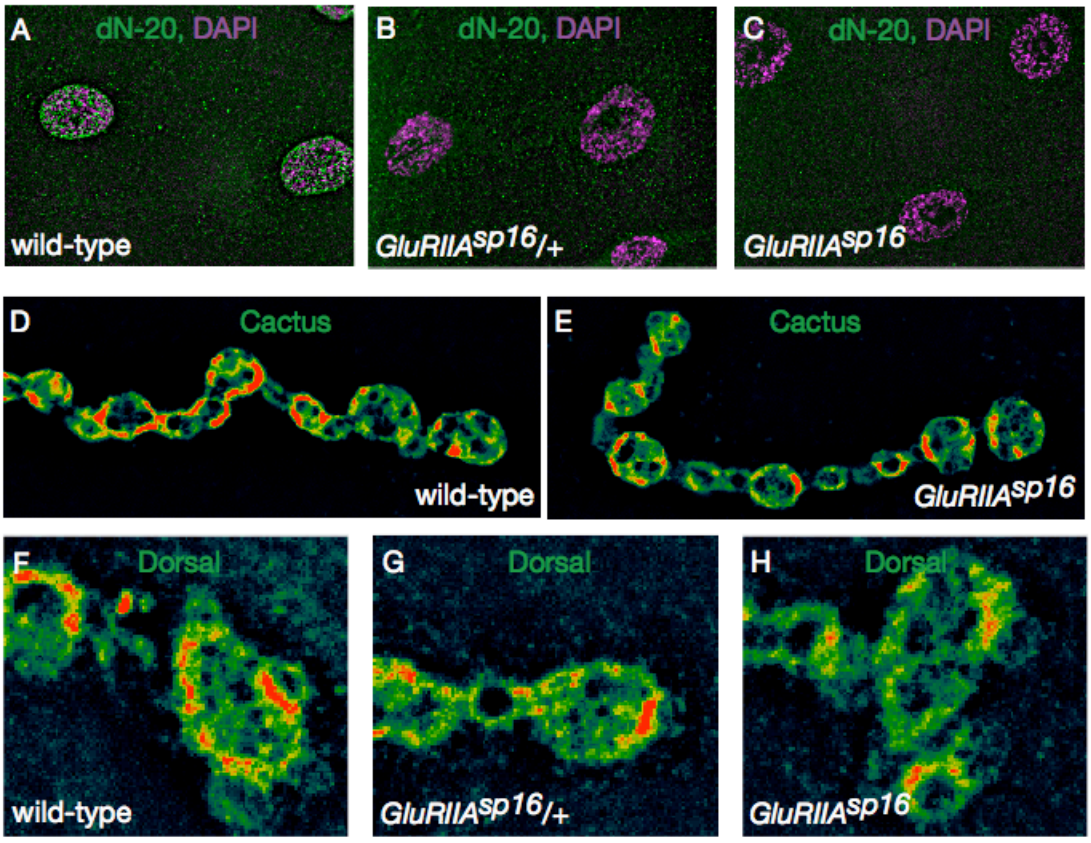

Figure 13. The 5’ UTR of *GluRIIA* mRNA contains a potential Dorsal binding site

A

```
Simulans          AGTAGGCGTGCGAAGCGCTCCAAGACTGGGTGCTTCCGTTGCGTGAAAATAAATTGTGAA 60
sechellia         AGTAGGCGTGCGAAGCGCTCCAAGACTGGGTGCTTCCGTTGCGTGAAAATAAATTGTGTA 60
melanogaster      AGTAGGCGTGCGAAGCGCTCCAAGACTGGGTGCTTCCGTTGCGTGAAAATAAATTGTGAA 60
yakuba            AGTAGCCGTGCAAAGCGCTCCAAGACTGGGTGCTTCCGTTGCGTGAAAATAAATTGTGAA 60
erecta            AGTAGCCGTGCGCAGCGCTCCAAGACTGGGTGCTTCCGTTGCGTGAAAATAAATTGTGAA 60
                  ***** *****  ********************************************* *

Simulans          GAAGAAAGACGGCACTTTGTATCTGCTAGTTTTGAATTATTTTTTTTCTGTGGCAGTCTG 120
sechellia         GAAGAAAGACGGCACTTTGTATCTGCTAGTTTTGAATTCTTTTTTTTCTGTGGCAGTCTG 120
melanogaster      GAAGAAAGACGGCACTTTGTATCTGCTCGTTTTGAATT-TTTTTTTTCTGTGGCAGTCTG 119
yakuba            GAAGA----CAGCACTTTGTATCTGCTCGTTTC--ATAGTTTTTTTTTGTGAGGCAGTCTG 114
erecta            CCAGA----CAGCACTTTGTATCTGCTAGTTTTCATATTTCTTGTTTCTGTGACAGTCTG 116
                    ***    * *************** ****       * ** *** ** * *******

Simulans          TGTGTGGGTCTGTAGATATAGATTTGTACATATGCAGCTGGGAAGTGAACACGAAATGG- 179
sechellia         TGTGTGCGTCTGTAGATATAGATTTGTACATATGCAGCTGGGAAGTGAACACGAAATGGC 180
melanogaster      TGTGCG--TCTGTAGATATAGATTTGTACATATGCAGTTGGGAAGTGAACACGAAATGGC 177
yakuba            TGTGTGCGGCAGTAGATATAGATTTGTACATATGCAGCTGAGAAGTGAACACGAAATGGC 174
erecta            TGTGCG--GCTGTAGATATAGATTTGTACATATGCAGCTGAGAAGTGAACACGAAATGGC 174
                  **** *   * ************************** ** ******************

Simulans          TGCTGCATTTAGAAAATTCAATTAGTTTCGAGTGTGTTGAGGTAAACGAAAAA 232
sechellia         TGCTGCATTTAGAAAATTCAATTAGTTTCGAGTGTGTTGAGGTAAACGAAAAA 233
melanogaster      TGCTGCATTTAGAAAATTCAATTAGTTTCGAGTGTGTTGAGGTAAACGAAAAA 230
yakuba            TGCTGCATTTAGAAAATTCAATTAGTTTCGAGTGTGTTGAGGTAAACG----- 222
erecta            TGCTGCATTTAGAAAATTCAATTAGTTTCGAGTGTGCTGAGGTGAACG----- 222
                  ************************************ ****** ****
```

B

Figure 14. Endosomal trafficking in Drosophila

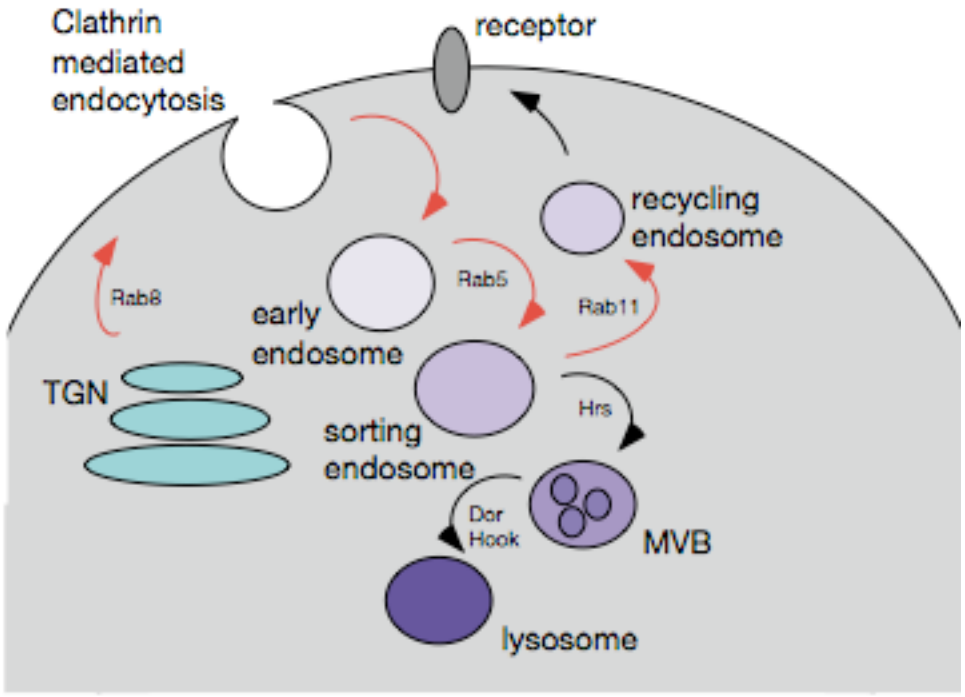

EXPERIMENTAL PROCEDURES

CHAPTER ONE (*NERVE-WRACKED*)

Fly Stocks

Jack Roos (UCSF) provided: *EP(2)2490*, EP(2)2490^{145}, *EP(2)2490^{21}*. Bloomington stock center provided: *k13215*, *Df(2)TW1*, *Dup (2) 2*, *Df(3L)Cat*. Craig Woodard (Mount Hollyoke College, South Hadley, MA) provided *FTZ-F1^{ex17}* and *FTZ-F1^{ex19}*.

Antibody staining

Unless otherwise noted, wandering third instar larvae were fixed in 3.7% formaldehyde in PBS for seven minutes before antibody treatment. Monoclonal antibodies were obtained from the Developmental Hybridoma Bank. Dilutions and original sources are listed in parentheses: CSP or DCSP-2 (6D6) (1:10, Seymour Benzer, Cal Tech, Zinsmaier et al., 1994), Fas II or ID4 (1:10, Corey Goodman, UC, Berkeley), Syt or 3H2 2D7 (1:10, Kai Zinn, UCLA). Rabbit-anti-Dap-160 (1:500) was provided by Reg Kelly, UCSF (Roos and Kelly, 1998). For information on myc, syn and DLG antibodies as well as secondary antibodies see Material and Methods in Chapter 3.

Bouton counts and Synaptic length

Bouton counts were done as reported in Chapter 3. Synaptic length was quantified using DeltaVision Video Management software. All type I synapses on muscle four stained with anti-HRP were included in analysis.

Pathfinding analysis

FasII staining was done using previous published protocols (Lin and Goodman, 1994), pathfinding analysis was preformed using previoius published protocols (Krueger et al., 1996).

Nothern analysis

Northern analysis was done as described in Chapter 3.

RT PCR

cDNA was prepared as described in Chapter 2. To probe the 5' end of *DHR39* I used eh148 (GCTAGAGCGGTTGTGGAATC) and eh150 (CCAGTTGGGATTTCACGTTT). To probe the 3' end of *DHR39* I used eh131 (TTTTCAACACATCGTTCATGG), eh132 (AATGCGCCTAGAGGGAAAAT), eh145 (GGCAAGGAGATGTTGACGAT), eh152 (GAGCTTTTGCTACGCATTCC).

Cloning of UAS-GFP-DHR39

EcoRI and BglII sites were added to eGFP by PCR amplification of eGFP with the following primers: eh177 (TCGAATTCTGCAGTCGACGG) and eh178 (TTTAGATCTCTTGTACAGCTCGTCCATGCCGAG). A BglII site was added the EST LD45021, using eh179 (GCAGATCTATGCCAAACATGTCCAGCATCAAGCG) and Sp6 primers. The GFP and DHR39 coding sequence were then cloned into pUAST.

CHAPTER TWO (*BAD HAIR DAY*)

Genetics

KG2636 and *KG766* were produced by the Drosophila Gene Disruption Project (Bellen et al., 2004). *K14029*$^{J1.1}$ was provided by David Huen (University of Cambridge). For a complete list of fly lines used for this project see Table 1.

P-element excision

A line harboring a deficiency (+/*Y; Df(2L)TW1/CyO)* was crossed to a to marked, balanced stock with a transpose source on the third chromosome ($y^{-}w^{-}$*; Sb/CyO; Dr Δ2-3/TM6B)*. In the next generation the resulting progeny, $y^{-}w^{-}$*/Y; Df(2L)TW1/CyO; Dr Δ2-3*/+ were crossed to the P-element line to be excised, y^{-}*; KG2636*. Note that KG elements are marked by both *white*$^{+}$ and *yellow*$^{+}$ (Roseman, et al., 1995). In the next generation flies containing the P-element and deficiency in the presence of transposase, y^{-}*/Y; KG2636/Df(2L)TW1; Dr Δ2-3*/+ were crossed to y^{-} w^{-}. The resulting progeny were screened for yellow-bodied flies. 3482 flies were screened, and of these 162 lines were selected for further analysis. Molecular characterization of these lines was carried out, using the primers eh28 cttcaagcatctgcaggagtg, in first exon, and eh166 gcaagtcccttagctcagga, in second exon, and eh161ctcgcacttattgcaagcat, in P-element, and eh163 caagcaaacgtgcactgaat, in P-element. This generated 24 precise excisions and five small deletions, none larger than 15 bp.

Male recombination

The P-element line, *KG2636* was crossed to flies carrying a multiply marked, second chromosome with a transposase source on the third chromosome: *dp b cn bw; Dr Δ2-3/TM6B*. The resulting flies, *KG2636/dp b cn bw; Dr Δ2-3*/+ were crossed to a line

multiply marked on the second, *dp b cn bw*. Male recombinant chromosomes that may have deleted *CG8677* coding sequence were selected, specifically: *KG2636 cn bw/dp b cn bw*, which look white-eyed. 59 white-eyed lines were generated and screened by PCR as described above. Unfortunately, this did not yield any lines with deleted genomic sequence.

P-element replacement

The balanced P-element line, *KG2636; MKRS/TM6B* was crossed to a donor P-element line *WeeP-GFP phase 3*/+ (Clyne et al., 2003), which resided on the third chromosome. The resulting progeny, *+/Y; KG2636/+; WeeP-GFP phase 3/MKRS* were crossed to a marked, transposase source: $y^{-}w^{-}$*; Sp/CyO; Dr Δ2-3/MKRS*. Flies harboring the original P-element, the donor P-element and the transposase source were then selected and crossed to a stock balanced on the second chromosome, (*KG2636 /CyO; WeeP-GFP phase 3/Dr Δ2-3 x* $y^{-}w^{-}$*; Gla/SM6a)*. In the following generation, lines with P-element replacement events were selected: Dropped, red-eyed, yellow-bodied flies. 3242 flies were screened, and 32 lines were selected for further analysis. PCR primers: JbseqE catggtcctgctggagttcg, eh166, JbseqF accactaccagaagaacac, IPCR10 cttgtacagctcgtccatgc, all of which are in *WeeP-GFP*, eh171 ccaggcaagaaagtaggttga, in *KG2636*, eh175 cttcttatttgagagatagt, in genomic DNA, were used for molecular characterization. 75% of all lines tested were the correct genotype, *KG2636→WeeP-GFP(*w^{+}*,* GFP^{-}*)*. Next, to remove the *white* gene in the *WeeP-GFP* P-element, *KG2636→WeeP-GFP(*w^{+}*,* GFP^{-}*)* was crossed to the marked, flipase-containing chromosome, *hsFlp/Y; Sp/CyO; MKRS/TM6B*. A 24 h egg lay was grown for one day then heat shocked for 1 h at 37ºC, every other day of larval development. Adults were screened for mosaic eye color. These

were outcrossed to the balancer chromosome, *w⁻; Sco/CyO*, and *w⁻; KG2636→WeeP-GFP (GFP⁺)/CyO* flies were recovered for analysis.

Intron/exon boundary determination

Genomic DNA was prepared using Quick Fly Genomic DNA Prep (BDGP--Inverse PCR and Protocol). Samples were sent to Elim Biopharmaceuticals, Inc. (Hayward, CA) for sequencing. The following EST-primer pairs were used for determination of intron/exon boundaries of *CG8677* splice forms: SD19239 (eh109 gtcacattctcctgcatctc in exon 6, eh110 gtttattatagtttaaacac in exon 8), SD26839 (eh111 caaaatcgaaatgtttgattg , eh112 gggtcctcgacttcctcctg), RE54795 (eh42 tcggagtatctgcctcctgt, in exon 9), LD41783 (eh028 cttcaagcatctgcaggagtg in exon 1, eh30 ctctcccgagcaagaggatc, in exon 2), GH21171 (eh32 cactcgcacccgtggtcgccg in exon 5, eh33 caccagcgcgacatgcaact in exon 6, eh35 catccgcaacaggaacagca in exon 8, eh69 cttcaaccctaacagcaag in exon 5, eh70 cttctacgcccactactacgac in exon 6).

RT-PCR determination of CG8677 larval splice forms

Third instar *yw* larvae were collected and RNA was extracted using Trizol (Invitrogen). An oligo dT- and random hexamer- primed cDNA library was synthesized using the Thermoscript RT-PCR system (GibcoBRL/Invitrogen). To probe for *CG8677-l* isoform I used eh133 gctggaccacgtggatattc, in exon 8 and eh135 tcgcccattgttgttgaata in exon 9; for *CG8677-s* I used eh133 and eh134 tcatcctgttgcgagctaaa in exon 8.

RT-PCR etermination of polyA site of CG8677-long isoform

Third instar, *yw* larvae were collected and RNA was extracted using Trizol (Invitrogen). Then then a modified First Strand cDNA Synthesis (Gibco) reaction was carried out with one of the following gene specific primers: eh23 ggccacgcgtcga ctagtactaccatt

tgcggctccttct, eh24 ggccacgcgtcga ctagtacgcgta atattaaattgata, eh25 ggccacgcgtcgac tagtacactgaat tctagataaatgt, eh26 ggccacgcgtcg actagtacagcat tttcagccttcgctt, eh27 ggccacgcgtcg actagtacttacac gactgcggcgctct. Next, two rounds of PCR were preformed with intron spanning primers, specific for the long isoform of *CG8677*, eh40 atcactcggttcccactttg in exon 8 and eh41 cggtatactctcgctcctgcc in exon 9. Only the cDNA with primed eh27 produced a band of expected size.

Northern analysis

Using a Cellector Tissue Sieve (Bellco Glass Inc., Vineland NJ) approximately 200-300 µl of third instar larvae (~1 bottle) were collected, and then rinsed with water. RNA was extracted using Trizol (Invitrogen, Carlsbad, CA), (~1 bottle of larvae per 1 ml of Trizol). For each genotype a total of four bottles were used, pooling RNA at the end Trizol extraction. Note that for RNA isolation with Trizol, the extra steps called for in the "proteoglycan and polysaccharide contamination" in the Troubleshooting section were used. The the quality of RNA was asses on a gel, and quantity by UV spec. ~ 1 mg of total RNA per genotype was PolyA selected using Oligotex Kit (Qiagen). The polyA-selected RNA was eluted in 80 µl. 10 µl was used to assess quantity and quality of RNA. Expected yield was ~25 µg polyA-selected RNA. A Formaldehyde Agarose gel was run according to instructions in Oligotex instruction manual, Appendix E. 30µl/lane of sample was loaded in each land, representing anywhere from 4 ug to 15 µg. As a standard the 0.24-9.5 kb RNA Ladder (Gibco) was used. Transfer was done using Standard SSC transfer methods, and then the RNA was UV cross linked to the membrane. Probe preparation was preformed follow directions included in the Prime-It II Random Primer Labeling Kit (Stratagene). Probes were prepared as followed: for

DHR39 (template EST LD45021, primers eh86, ctcgcacttattgcaagcat, eh87 catgcgatatttgccgactt, in first codin exon), for *CG8677* (template EST LD1783, primers eh06-eh07, in exon 4), for *CG31626* (template EST RE11840, primers eh05 tactggtagcccgactccac, eh116 agagcttgccaaagcaaatc, first coding exon), for RP49 (RP49pGEMT, primers rp49-S catccgcccagcatacag, rp49-AS aaatgtgtattccgaccagg). Probes were purified using MicroSping G-25 Columns (Amersham Pharmacia Biotech). Before addition to prehyb probes were denatured. Hybridization was done using standard protocols in Rapid Hyb buffer (Ambersham).

RNAi

dsRNA production was done by amplifying DNA via PCR reactions: Using template EST LD41783 with eh82 taatacgactcac tatagggagaccata tcggaggagtgcaag, eh83 taatacgactcactat agggagacttttgat cctcttgctcgg (exon 1-2), eh06 taatacgactcacta tagggagagatgac gatcctaccctgga and eh07 taatacgactcac tatagggagaaacttc tcgcttacggctga (exon 4). Using template EST GH221171 with eh84 taatacgactcacta tagggagaggcttaac gagtatgacgac and eh85 taatacgactca ctatagggagag cttaggtgttttct ggcg (exon 5), or eh127 taatacgactcacta tagggagaatactgg tagcccgactccac and eh128 taatacgactcacta tagggagaactct tcgtcttcgctgtgtg) or (exon 9/*CG31626*). RNA was transcribed using the T7 MEGAscript kit (Ambion). dsRNA was delivered by embryonic injection for RNA produced with eh06-eh07, or by soaking with the others (Eaton et al., 2002).

In situ hybridization

Probe production was done using MAXIscript kit (Ambion) with one of the following templates: EST LD41783 cut with EcoRI, and transcribed with SP6, GH21171 cut with NheI and transcribed with Sp6 or cut with XhoI transcribed with T7. A 24h collection of

embryos was hybridized using previous published protocols (http://www.fruitfly.org/methods/RNAinsitu.html).

Antibody construction

Two peptides corresponding to 297-316 aa and 322-341 aa of dRSF were synthesized and co-injected into rabbits (#5128, #5129) by (Alpha Diagnostics International).

Polytene chromosome preparation

Polytene chromosomes were prepared according to published protocol : "Preparation and Immunostaing of Polytene Chromosome Squashes" C.H. James, P.W. Badenhrost and B.M. Turner. Staining was done with RB-anti-MSL (1:200) in 1% BSA block for 1 h at 37ºC. The MSL antibody was provided by Katie Worringer, Panning LabUCSF.

Immunohisotchemistry

All experiments were done on fillet preps of wandering third instar larvae. Animals were fixed in 3.7% formaldehyde in PBS for 7 minutes at room temperature unless otherwise noted. Secondary antibodies and antibodies directly conjugated to HRP are described elsewhere (Chapter 3). Synapsin, GluRIIA, Cactus and Dorsal staining was done as described elsewhere (Chapter 3). FasII, Syt, and DAP-160 was done as described elsewhere (Chapter 1). The following monoclonal antibodies 22c10 (1:10) (Fujita et al., 1982) and nc82 (1:10) (Wagh et al. 2006) were obtained from the Developmental Studies Hybridoma Bank developed under the auspices of the NICHD and maintained by The University of Iowa, Department of Biological Sciences, Iowa City, IA 52242. Rb-anti-Dliprin (1:1000), was a gift of David Van Vactor (Harvard University) (Kaufmann et al., 2002). Image capture was done as described elsewhere (Chapter 3).

CHAPTER THREE (CYTOPLASMIC NF-KAPPAB)

Genetics

Drosophila mutant stocks were obtained from the following sources: *Df(3R)D605*, dl^{1} and dl^{UY2278} from the Bloomington Stock Center (Bloomington, IN); pll^{RM8}, pll^{078}, dl^{H}, dl^{2}, dl^{PZ}, dl^{U5}, $cact^{D13}$, $cact^{255}$, and $cact^{HE}$ from the Max-Planck-Institut (Tuebingen, Germany); pll^{25} from Steve Wasserman (University of California, San Diego); *HSP70-dl* and $cact^{RN}$ from Ruth Steward (Rutgers University); D4 and -920twi/lacZ from Albert Courey (University of California, Los Angeles); DD1 from Marika Olcot (Oregon State University); dlg^{M52} from Vivian Budnik (University of Massachusetts, Medical School). Flies for experiments involving dl^{2}, dl^{PZ}, $cact^{RN}$ *and* $cact^{HE}$ were incubated at 29ºC, as were the *wild-type* controls.

Larval over-expression of *dorsal* was achieved by using a heat shock inducible *dorsal* transgene (*HSP70-dl*); vials were immersed in a 37ºC water bath for one hour, three times on each day of larval development. Muscle specific over-expression was achieved by crossing dl^{UY2278}, a *UAS*-containing P-element (Nicolai et al., 2003), to muscle specific Gal4 drivers. *UAS-GFP-Pelle* was constructed by inserting the coding sequence of *pelle* into the GW (N-terminal EGFP tag) Gateway vector using TOPO TA Cloning Kit for entry into Gateway Technology (Invitrogen, Carlsbad, CA).

Immunohistochemistry

Unless otherwise noted wandering third-instar larva were dissected and stained according to previously published methods (Albin and Davis, 2004). The following antibodies were obtained from the Developmental Studies Hybridoma Bank (University of Iowa, Department of Biological Sciences, Iowa City): anti-myc (9E 10) (Evan et al., 1985), anti-

GluRIIA (8B4D2; 1:10)(Schuster CM, 1991), and mAb-Dlg (1:1000) (Corey Goodman, University of California, Berkeley). We obtained mouse anti-Synapsin (1:10) from Erich Buchner (University of Würzburg), rabbit anti-GluRIIC (1:2500) from Aaron DiAntonio (Washington University School of Medicine, St. Louis MO), rabbit anti-Cactus (1:1000) and rabbit anti-Dorsal (1:500) from Steve Wasserman (University of California, San Diego). Secondary antibodies (FITC labeled, TRITC labeled, Cy5 labeled) anti-mouse, and anti-rabbit as well as the FITC-, TRITC- and Cy5-conjugated anti-HRP antibodies were provided by Jackson Immunoresearch Laboratories and used at 1:200. For LacZ staining, larvae were fixed in 4% paraformaldehyde (Sigma, St. Louis, MO) for seven minutes. 12.5μl of 8% X-gal and 0.5 ml staining solution (Drosophila Protocols, William Sullivan, Editor) was incubated at 65ºC and then added to the larva in a 1.5 mL microfuge tube, and incubated at 37ºC until staining was complete. Animals were washed in PBT and cleared in glycerol for further analysis and imaging.

Imaging

Unless otherwise noted, all images were acquired using a Zeiss 2000M inverted microscope, 100x 1.4nA lens and CoolSnap HQ cooled CCD camera. Image capture and analysis were performed using Intelligent Imaging Innovations (3I) software. For comparisons of fluorescent intensities across genotypes, samples from different genotypes were dissected and fixed identically, processed in the same vial and imaged at identical exposures and light intensities. For quantification of GluR fluorescence intensity, the synaptic region of interest was defined by first imaging co-stained anti-HRP. GluR fluorescence intensity was quantified by measuring the average GluR intensity across this

region of interest in a 2D confocal projection image as done previously (Albin and Davis, 2004).

Electrophysiology

Recordings were preformed as described in (Albin and Davis, 2004). Wandering third-instar larvae were selected after leaving the food. Larvae were dissected in HL3 saline in 0.5 mM Ca^{2+}. Whole-muscle recordings were made from muscle 6, abdominal segment A3, as described previously (Davis et al., 1996). Quantal content was calculated by dividing the average maximal EPSP amplitude by the average amplitude of the spontaneous miniature release events (mEPSP) for each recording and multiple recordings were averaged per genotype. Measurements of maximal EPSP and input resistance were done by hand using the cursor option in Clampfit (Molecular Devices). Measurements of spontaneous miniature release events were semi-automated using MiniAnalysis software (Synaptosoft, Decatur, GA). For each recording, 100-300 mEPSP events were averaged to determine the average mEPSP amplitude.

Real-time reverse transcription-PCR

Real-time reverse transcription-PCR assays were performed using an iCycler (Bio-Rad) with SYBR Green fluorescence. Real-time PCR amplification was performed after an initial denaturation of 8 min at 95°C, followed by 50 cycles of 20 sec denaturation at 95°, 30 sec annealing at 60°C, and 30 sec extension at 72°C. Fluorescent detection was performed at the annealing stage as previously described (Albin and Davis, 2004).

Electron microscopy

Larvae were prepared for electron microscopy and analysis was performed as previously described (Pielage et al., 2005).

CHAPTER FOUR (TRAFFICKING AND PELLE)

Fly stocks

All of the fly stocks used in this chapter were described in the Chapter 3.

Imaging and Immunofluorescence

Image capture and quantification were described Chapter 3. GluRIIA, GluRIIC, Cactus, Dorsal and secondary antibodies and DAPI are described Chapter 3. dN-20 (1:50) is an affinity purified goat polyclonal antibody (Santa Cruz Biotechnology, Inc.). Rb-anti-Rab5 (Calbiochem, 1:50). For dN-20 co-localization experiments, fixation was done for five minutes at RT in 3.7% formaldehyde with the following secondary antibodies were used: DK-anti-RB-TRITC (1:250) or GT-anti-RB-alexa-fluor-488 (1:600) and RB-anti-GT-FITC (1:1000) or DK-anti-GT-TRITC (1:200) (Jackson ImmunoResearch).

GluRIIA$^{\alpha BT}$ construction and electrophysiology

See Stephanie Albin's thesis.

Surface blockade and premablization protocols

General precautions for αBT label include: conduct the entire procedure in the cold room (4ºC), and store all solutions on ice before use. Pin head and tail; carefully dissect in HL3 saline; do not stretch the prep! For incubations longer than 10 minutes, the solution was agitated every ten minutes by gentle pipetting. Use fresh aliquots of αBT (Molecular Probes/Invitrogen), and avoid exposure to light. For preblock: use 50 μg/mL unlabeled αBT in HL3 for 30 minutes. Wash 4X in HL3. For unpermeablized staining: add 10 μg/mL αBT-488 and 10 μl/mL rhodamine-dextran (Molecular Probes/Invitrogen) in HL3 for 30 minutes. Wash 4X in HL3. Stretch the prep, then fix in 4% paraformaldehyde (PFA) in PBS, for 8 minutes. For permeablization: incubate for one hour in 0.1% Triton

X-100, 2% normal goat serum, 2% bovine serum albumin in PBS. Then add αBT-488/rhodamine-dextran and fix as described above. Preps were put into 70% glycerol in PBS plus Vectasheild (Vectorlabs) for 1 h at RT before mounting and imaging.

Receptor internalization/insertion assay

Follow the general precautions listed above. Incubate in10 μg/mL αBT-596 in HL3 for 30 minutes. Wash 4X in HL3. Incubate in 50 μg/mL in unlabeled αBT. Wash 4X in HL3. Incubate at 30ºC for allotted period of time (e.g. 0 h, 30 min, 1 h, 2h, 8h) in Schneider's Drosophila media, or HL3 plus 0.5 mM Ca^{2+} and 20 μl/mL fetal calf serum. Preps were shielded from light and incubated in humidified chambers. Wash 4X in HL3. Incubate in 10 μg/mL αBT-488 in HL3 for 30 minutes. Wash 4X in HL3. Stretch, fix as described above. Add anti-HRP-Cy3 (Jackson ImmunoResearch) (1:200) for 1 h at RT. Wash 4X in PBT. Preps were processed for mounting as described above.

Embryonic aBT injections

An one hour collection of embryos containing $GluRIIA^{sp16}$, $GluRIIA^{aBT11\text{-}6}$ chromosome were aged for 24 h at room temperature. They were injected with 500 μg/ml αBT-488 in saline. Embryos were incubated for 8 days at 20ºC, dissected, fixed in 4% PFA for 7 minutes and then incubated with anti-HRP-TRITC. Preps were processed for mounting as described above.

Transfection of S2 cells

S2 cells stabling expressing Gal4 were transfected using Cellfectin (Invitrogen). Cells were fixed, stained and imaged using standard protocols.

REFFERENCES

Aberle H, Haghighi AP, Fetter RD, McCabe BD, Magalhaes TR, Goodman CS. wishful thinking encodes a BMP type II receptor that regulates synaptic growth in Drosophila.Neuron. 2002 Feb 14;33(4):545-58.

Alberi S, Boda B, Steiner P, Nikonenko I, Hirling H, Muller D. The endosomal protein NEEP21 regulates AMPA receptor-mediated synaptic transmission and plasticity in the hippocampus. Mol Cell Neurosci. 2005 Jun;29(2):313-9.

Albensi, B. C., and Mattson, M. P. (2000). Evidence for the involvement of TNF and NF-kappaB in hippocampal synaptic plasticity. Synapse *35*, 151-159.Aasland R, Gibson TJ, Stewart AF. The PHD finger: implications for chromatin-mediated transcriptional regulation. Trends Biochem Sci. 1995 Feb;20(2):56-9.

Albin SD, Davis GW. Coordinating structural and functional synapse development: postsynaptic p21-activated kinase independently specifies glutamate receptor abundance and postsynaptic morphology. J Neurosci. 2004 Aug 4;24(31):6871-9.

Atwood HL, Govind CK, Wu CF. Differential ultrastructure of synaptic terminals on ventral longitudinal abdominal muscles in Drosophila larvae. J Neurobiol. 1993 Aug;24(8):1008-24.

Ayer S, Walker N, Mosammaparast M, Nelson JP, Shilo BZ, Benyajati C. Activation and repression of Drosophila alcohol dehydrogenase distal transcription by two steroid hormone receptor superfamily members binding to a common response element. Nucleic Acids Res. 1993 Apr 11;21(7):1619-27.

Baghdiguian, S., Martin, M., Richard, I., Pons, F., Astier, C., Bourg, N., Hay, R. T., Chemaly, R., Halaby, G., Loiselet, J., *et al.* (1999). Calpain 3 deficiency is associated with myonuclear apoptosis and profound perturbation of the IkappaB alpha/NF-kappaB pathway in limb-girdle muscular dystrophy type 2A. Nat Med *5*, 503-511.

Bakalkin, G., Yakovleva, T., and Terenius, L. (1993). NF-kappa B-like factors in the murine brain. Developmentally-regulated and tissue-specific expression. Brain Res Mol Brain Res *20*, 137-146.

Baker, S. J., and Reddy, E. P. (1998). Modulation of life and death by the TNF receptor superfamily. Oncogene *17*, 3261-3270.

Baldwin, A. S., Jr. (1996). The NF-kappa B and I kappa B proteins: new discoveries and insights. Annu Rev Immunol *14*, 649-683.

Beattie EC, Carroll RC, Yu X, Morishita W, Yasuda H, von Zastrow M, Malenka RC. Regulation of AMPA receptor endocytosis by a signaling mechanism shared with LTD. Nat Neurosci. 2000 Dec;3(12):1291-300.

Bellen HJ, Levis RW, Liao G, He Y, Carlson JW, Tsang G, Evans-Holm M, Hiesinger PR, Schulze KL, Rubin GM, Hoskins RA, Spradling AC The BDGP gene disruption project: single transposon insertions associated with 40% of Drosophila genes. Genetics. 2004 Jun;167(2):761-81.

Belvin, M. P., Jin, Y., and Anderson, K. V. (1995). Cactus protein degradation mediates Drosophila dorsal-ventral signaling. Genes Dev *9*, 783-793.

Bergmann, A., Stein, D., Geisler, R., Hagenmaier, S., Schmid, B., Fernandez, N., Schnell, B., and Nusslein-Volhard, C. (1996). A gradient of cytoplasmic Cactus degradation establishes the nuclear localization gradient of the dorsal morphogen in Drosophila. Mech Dev *60*, 109-123.

Beumer KJ, Rohrbough J, Prokop A, Broadie K. A role for PS integrins in morphological growth and synaptic function at the postembryonic neuromuscular junction of Drosophila. Development. 1999 Dec;126(24):5833-46.
Bienz M. The PHD finger, a nuclear protein-interaction domain. Trends Biochem Sci. 2006 Jan;31(1):35-40.
Blanpied TA, Scott DB, Ehlers MD. Dynamics and regulation of clathrin coats at specialized endocytic zones of dendrites and spines. Neuron. 2002 Oct 24;36(3):435-49.
Bredt DS, Nicoll RA. AMPA receptor trafficking at excitatory synapses.Neuron. 2003 Oct 9;40(2):361-79
Broadie K, Sink H, Van Vactor D, Fambrough D, Whitington PM, Bate M, Goodman CS. From growth cone to synapse: the life history of the RP3 motor neuron. Dev Suppl. 1993;:227-38.
Broadie K, Bate M. Innervation directs receptor synthesis and localization in Drosophila embryo synaptogenesis. Nature. 1993a Jan 28;361(6410):350-3.
Broadie K, Bate M. Activity-dependent development of the neuromuscular synapse during Drosophila embryogenesis. Neuron. 1993b Oct;11(4):607-19.
Broutman G, Baudry M. Involvement of the secretory pathway for AMPA receptors in NMDA-induced potentiation in hippocampus. J Neurosci. 2001 Jan 1;21(1):27-34.
Brown TC, Tran IC, Backos DS, Esteban JANMDA receptor-dependent activation of the small GTPase Rab5 drives the removal of synaptic AMPA receptors during hippocampal LTD. Neuron. 2005 Jan 6;45(1):81-94.
Budnik V, Koh YH, Guan B, Hartmann B, Hough C, Woods D, Gorczyca M. Regulation of synapse structure and function by the Drosophila tumor suppressor gene dlg. Neuron. 1996 Oct;17(4):627-40.
Budnik V, Zhong Y, Wu CF. Morphological plasticity of motor axons in Drosophila mutants with altered excitability. J Neurosci. 1990 Nov;10(11):3754-68.
Burbea M, Dreier L, Dittman JS, Grunwald ME, Kaplan JM. Ubiquitin and AP180 regulate the abundance of GLR-1 glutamate receptors at postsynaptic elements in C. elegans. Neuron. 2002 Jul 3;35(1):107-20.
Cai, D., Frantz, J. D., Tawa, N. E., Jr., Melendez, P. A., Oh, B. C., Lidov, H. G., Hasselgren, P. O., Frontera, W. R., Lee, J., Glass, D. J., and Shoelson, S. E. (2004). IKKbeta/NF-kappaB activation causes severe muscle wasting in mice. Cell *119*, 285-298.
Cantera R., Kozlova, T., Barillas-Mury C, Kafatos FC (1999a). Muscle Structure and Innveravtion Are Affected by Loss of Dorsal in the Fruit Fly, Drosophila melanogaster. Molecular and Cellular Neuroscience *13*, 131-141.
Cantera R., Roos, E., Engstrom Y (1999b). DIF and Cactus are colocalized in the larval nervous system of Drosophila melanogaster. J Neurobiol *38*, 16-26.
Carroll RC, Beattie EC, Xia H, Luscher C, Altschuler Y, Nicoll RA, Malenka RC, von Zastrow M. Dynamin-dependent endocytosis of ionotropic glutamate receptors. Proc Natl Acad Sci U S A. 1999 Nov 23;96(24):14112-7.
Chekmenev DS, Haid C, Kel AE. P-Match: transcription factor binding site search by combining patterns and weight matrices. Nucleic Acids Res. 2005 Jul 1;33

Clyne PJ, Brotman JS, Sweeney ST, Davis G. Green fluorescent protein tagging Drosophila proteins at their native genomic loci with small P elements. Genetics. 2003 Nov;165(3):1433-41.
Collins CA, Wairkar YP, Johnson SL, DiAntonio A. Highwire restrains synaptic growth by attenuating a MAP kinase signal. Neuron. 2006 Jul 6;51(1):57-69.
Coyle IP, Koh YH, Lee WC, Slind J, Fergestad T, Littleton JT, Ganetzky B. Nervous wreck, an SH3 adaptor protein that interacts with Wsp, regulates synaptic growth in Drosophila. Neuron. 2004 Feb 19;41(4):521-34.
Davis, G. W. (2006). Homeostatic Control of Neural Activity: From Phenomenology to Molecular Design. Annu Rev Neurosci. *29*, 307-323.
Davis, G. W., DiAntonio, A., Petersen, S. A., and Goodman, C. S. (1998). Postsynaptic PKA controls quantal size and reveals a retrograde signal that regulates presynaptic transmitter release in Drosophila. Neuron *20*, 305-315.
Davis, G. W., Schuster, C. M., and Goodman, C. S. (1996). Genetic dissection of structural and functional components of synaptic plasticity. III. CREB is necessary for presynaptic functional plasticity. Neuron *17*, 669-679.
Davidson B, Trope' CG, Wang TL, Shih IeM. Expression of the chromatin remodeling factor Rsf-1 is upregulated in ovarian carcinoma effusions and predicts poor survival. Gynecol Oncol. 2006 Dec;103(3):814-9.
Denk, A., Wirth, T., and Baumann, B. (2000). NF-kappaB transcription factors: critical regulators of hematopoiesis and neuronal survival. Cytokine Growth Factor Rev *11*, 303-320.
Deuring R, Fanti L, Armstrong JA, Sarte M, Papoulas O, Prestel M, Daubresse G, Verardo M, Moseley SL, Berloco M, Tsukiyama T, Wu C, Pimpinelli S, Tamkun JW. The ISWI chromatin-remodeling protein is required for gene expression and the maintenance of higher order chromatin structure in vivo. Mol Cell. 2000 Feb;5(2):355-65.
Dickman DK, Lu Z, Meinertzhagen IA, Schwarz TL. Altered synaptic development and active zone spacing in endocytosis mutants. Curr Biol. 2006 Mar 21;16(6):591-8.DiAntonio A, Haghighi AP, Portman SL, Lee JD, Amaranto AM, Goodman CS. Ubiquitination-dependent mechanisms regulate synaptic growth and function. Nature. 2001 Jul 26;412(6845):449-52.
Dubnau and Struhl RNA recognition and translational regulation by a homeodomain protein Nature, Vol 379, 22 February 1996
Eaton BA, Davis GW. (2005) LIM Kinase1 controls synaptic stability downstream of the type II BMP receptor. Neuron. *47*, 695-708.
Eaton BA, Fetter RD, Davis GW. Dynactin is necessary for synapse stabilization. Neuron. 2002 May 30;34(5):729-41.
Edwards, D. N., Towb, P., and Wasserman, S. A. (1997). An activity-dependent network of interactions links the Rel protein Dorsal with its cytoplasmic regulators. Development *124*, 3855-3864.
Ehlers MD. Reinsertion or degradation of AMPA receptors determined by activity-dependent endocytic sorting. Neuron. 2000 Nov;28(2):511-25.
Evan, G. I., Lewis, G. K., Ramsay, G., and Bishop, J. M. (1985). Isolation of monoclonal antibodies specific for human c-myc proto-oncogene product. Mol Cell Biol *5*, 3610-3616.

Featherstone, D.E., Rushton, E., Rohrhough J, Liebl F, Karr J, Sheng Q, Rodesch C, Broadie K (2005). An Essential Drosophila Glutamate Receptor Subuint that Functions in Both Central Neuropil and Neuromusclar Junction. J. Neurosci *25*, 399-3208.

Fischer JA, Eun SH, Doolan BT. Endocytosis, endosome trafficking, and the regulation of Drosophila development. Annu Rev Cell Dev Biol. 2006;22:181-206.

Flores-Saaib, R. D., Jia, S., and Courey, A. J. (2001). Activation and repression by the C-terminal domain of Dorsal. Development *128*, 1869-1879.

Fortier, T.M., Vasa, P.P., Woodard, C.T. (2003). Orphan nuclear receptor betaFTZ-F1 is required for muscle-driven morphogenetic events at the prepupal-pupal transition in Drosophila melanogaster. Dev. Biol. 257(1): 153--165.

Franco B, Bogdanik L, Bobinnec Y, Debec A, Bockaert J, Parmentier ML, Grau Y. Shaggy, the homolog of glycogen synthase kinase 3, controls neuromuscular junction growth in Drosophila. J Neurosci. 2004 Jul 21;24(29):6573-7.Johansen J, Halpern ME, Johansen KM, Keshishian H. Stereotypic morphology of glutamatergic synapses on identified muscle cells of Drosophila larvae. J Neurosci. 1989 Feb;9(2):710-25.

Fraser, C. C. (2006). Exploring the positive and negative consequences of NF-kappaB inhibition for the treatment of human disease. Cell Cycle *5*, 1160-1163.

Fujita, S.C., Zipursky, S.L., Benzer, S., Ferrus, A., and Shotwell, S.L. (1982). Monoclonal antibodies against the Drosophila nervous system. Proc. Natl. Acad. Sci. USA 79, 7929-7933.

Furukawa, K., and Mattson, M. P. (1998). The transcription factor NF-kappaB mediates increases in calcium currents and decreases in NMDA- and AMPA/kainate-induced currents induced by tumor necrosis factor-alpha in hippocampal neurons. J Neurochem *70*, 1876-1886.

Gerges NZ, Backos DS, Esteban JA. Local control of AMPA receptor trafficking at the postsynaptic terminal by a small GTPase of the Rab family. J Biol Chem. 2004 Oct 15;279(42):43870-8.

Ghosh, S., May, M. J., and Kopp, E. B. (1998). NF-kappa B and Rel proteins: evolutionarily conserved mediators of immune responses. Annu Rev Immunol *16*, 225-260.

Gillespie, S. K., and Wasserman, S. A. (1994). Dorsal, a Drosophila Rel-like protein, is phosphorylated upon activation of the transmembrane protein Toll. Mol Cell Biol *14*, 3559-3568.

Govind, S. (1996). Rel signalling pathway and the melanotic tumour phenotype of Drosophila. Biochem Soc Trans *24*, 39-44.

Govind, S. (1999). Control of development and immunity by rel transcription factors in Drosophila. Oncogene *18*, 6875-6887.

Guan B, Hartmann B, Kho YH, Gorczyca M, Budnik V. The Drosophila tumor suppressor gene, dlg, is involved in structural plasticity at a glutamatergic synapse. Curr Biol. 1996 Jun 1;6(6):695-706.

Guerrero G, Reiff DF, Agarwal G, Ball RW, Borst A, Goodman CS, Isacoff EY. Heterogeneity in synaptic transmission along a Drosophila larval motor axon. Nat Neurosci. 2005 Sep;8(9):1188-96.

Guttridge, D. C., Mayo, M. W., Madrid, L. V., Wang, C. Y., and Baldwin, A. S., Jr. (2000). NF-kappaB-induced loss of MyoD messenger RNA: possible role in muscle decay and cachexia. Science *289*, 2363-2366.

Hacker, H., and Karin, M. (2006). Regulation and function of IKK and IKK-related kinases. Sci STKE *2006*, re13.

Halfon, M. S., Hashimoto, C., and Keshishian, H. (1995). The Drosophila toll gene functions zygotically and is necessary for proper motoneuron and muscle development. Dev Biol *169*, 151-167.

Halfon, M. S., and Keshishian, H. (1998). The Toll pathway is required in the epidermis for muscle development in the Drosophila embryo. Dev Biol *199*, 164-174.

Heckscher ES, Fetter RD, Marek KW, Albin SD and Davis GW. Cytoplasmic NF-kB, I-kB and IRAK Control Glutamate Receptor Density at the Drosophila NMJ. Submitted

Hecht, P. M., and Anderson, K. V. (1993). Genetic characterization of tube and pelle, genes required for signaling between Toll and dorsal in the specification of the dorsal-ventral pattern of the Drosophila embryo. Genetics *135*, 405-417.

Hennessy BT, Nanjundan M, Cheng KW, Nolden L, Mills GB. Identification of remodeling and spacing factor 1 (rsf-1, HBXAP) at chromosome 11q13 as a putative oncogene in ovarian cancer. Eur J Hum Genet. 2006 Apr;14(4):381-3.

Horner MA, Chen T, Thummel CS. Ecdysteroid regulation and DNA binding properties of Drosophila nuclear hormone receptor superfamily members. Dev Biol. 1995 Apr;168(2):490-502.

Horner MA, Thummel CS. Mutations in the DHR39 orphan receptor have no effect on viability. DIS, 80 (1997):35-36.

Huet F, Ruiz C, Richards G. Puffs and PCR: the in vivo dynamics of early gene expression during ecdysone responses in Drosophila. Development. 1993 Jun;118(2):613-27.

Jackman, R. W., and Kandarian, S. C. (2004). The molecular basis of skeletal muscle atrophy. Am J Physiol Cell Physiol *287*, C834-843.

Johansen J, Halpern ME, Johansen KM, Keshishian H. Stereotypic morphology of glutamatergic synapses on identified muscle cells of Drosophila larvae. J Neurosci. 1989 Feb;9(2):710-25.

Juo P, Kaplan JM. The anaphase-promoting complex regulates the abundance of GLR-1 glutamate receptors in the ventral nerve cord of C. elegans. Curr Biol. 2004 Nov 23;14(22):2057-62.

Inoue H, Imamura T, Ishidou Y, Takase M, Udagawa Y, Oka Y, Tsuneizumi K, Tabata T, Miyazono K, Kawabata M. Interplay of signal mediators of decapentaplegic (Dpp): molecular characterization of mothers against dpp, Medea, and daughters against dpp. Mol Biol Cell. 1998 Aug;9(8):2145-56.

Isoda, K., and Nusslein-Volhard, C. (1994). Disulfide cross-linking in crude embryonic lysates reveals three complexes of the Drosophila morphogen dorsal and its inhibitor cactus. Proc Natl Acad Sci U S A *91*, 5350-5354.

Isoda, K., Roth, S., and Nusslein-Volhard, C. (1992). The functional domains of the Drosophila morphogen dorsal: evidence from the analysis of mutants. Genes Dev *6*, 619-630.

Kambris, Z., Hoffmann, J. A., Imler, J. L., and Capovilla, M. (2002). Tissue and stage-specific expression of the Tolls in Drosophila embryos. Gene Expr Patterns *2*, 311-317.

Kandel ER. The molecular biology of memory storage: a dialogue between genes and synapses. Science. 2001 Nov 2;294(5544):1030-8

Katchalski-Katzir E, Kasher R, Balass M, Scherf T, Harel M, Fridkin M, Sussman JL, Fuchs S (2003) Design and synthesis of peptides that bind alpha-bungarotoxin with high affinity and mimic the three-dimensional structure of the binding-site of acetylcholine receptor. Biophys Chem 100:293-305.

Kaufmann N, DeProto J, Ranjan R, Wan H, Van Vactor D. Drosophila liprin-alpha and the receptor phosphatase Dlar control synapse morphogenesis. Neuron. 2002 Mar 28;34(1):27-38.

Kauppila, S., Maaty, W. S., Chen, P., Tomar, R. S., Eby, M. T., Chapo, J., Chew, S., Rathore, N., Zachariah, S., Sinha, S. K., *et al*. (2003). Eiger and its receptor, Wengen, comprise a TNF-like system in Drosophila. Oncogene *22*, 4860-4867.

Kennedy MJ, Ehlers MD. Organelles and trafficking machinery for postsynaptic plasticity. Annu Rev Neurosci. 2006;29:325-62

Keshishian H, Broadie K, Chiba A, Bate M. The drosophila neuromuscular junction: a model system for studying synaptic development and function. Annu Rev Neurosci. 1996;19:545-75.

Keshishian H, Kim YS. Orchestrating development and function: retrograde BMP signaling in the Drosophila nervous system. Trends Neurosci. 2004 Mar;27(3):143-7.

Khodosh R, Augsburger A, Schwarz TL, Garrity PA. Bchs, a BEACH domain protein, antagonizes Rab11 in synapse morphogenesis and other developmental events. Development. 2006 Dec;133(23):4655-65.

Kidd, S. (1992). Characterization of the Drosophila cactus locus and analysis of interactions between cactus and dorsal proteins. Cell *71*, 623-635.

Koh TW, Verstreken P, Bellen HJ. Dap160/intersectin acts as a stabilizing scaffold required for synaptic development and vesicle endocytosis. Neuron. 2004 Jul 22;43(2):193-205.

Koh YH, Popova E, Thomas U, Griffith LC, Budnik V. Regulation of DLG localization at synapses by CaMKII-dependent phosphorylation. Cell. 1999 Aug 6;98(3):353-63.

Komada M, Kitamura N. The Hrs/STAM complex in the downregulation of receptor tyrosine kinases. J Biochem (Tokyo). 2005 Jan;137(1):1-8

Krueger NX, Van Vactor D, Wan HI, Gelbart WM, Goodman CS, Saito H. The transmembrane tyrosine phosphatase DLAR controls motor axon guidance in Drosophila. Cell. 1996 Feb 23;84(4):611-22.

Ladner, K. J., Caligiuri, M. A., and Guttridge, D. C. (2003). Tumor necrosis factor-regulated biphasic activation of NF-kappa B is required for cytokine-induced loss of skeletal muscle gene products. J Biol Chem *278*, 2294-2303.

Lahey T, Gorczyca M, Jia XX, Budnik V. The Drosophila tumor suppressor gene dlg is required for normal synaptic bouton structure.Neuron. 1994 Oct;13(4):823-35.

Lavezzari G, McCallum J, Lee R, Roche KW. Differential binding of the AP-2 adaptor complex and PSD-95 to the C-terminus of the NMDA receptor subunit NR2B regulates surface expression. Neuropharmacology. 2003 Nov;45(6):729-37.

Lazzaro MA, Picketts DJ.Cloning and characterization of the murine Imitation Switch (ISWI) genes: differential expression patterns suggest distinct developmental roles for Snf2h and Snf2l. J Neurochem. 2001 May;77(4):1145-56.
Lee SH, Liu L, Wang YT, Sheng M. Clathrin adaptor AP2 and NSF interact with overlapping sites of GluR2 and play distinct roles in AMPA receptor trafficking and hippocampal LTD. Neuron. 2002 Nov 14;36(4):661-74.
Li H, and Cooper, RL. Effects of the ecdysoneless mutant on synaptic efficacy and structure at the neuromuscular junction in Drosophila larvae during normal and prolonged development. Neuroscience 2001 Sept;106(1):193-200.
Li TR, White KP. Tissue-specific gene expression and ecdysone-regulated genomic networks in Drosophila. Dev Cell. 2003 Jul;5(1):59-72.
Lin DM, Goodman CS. Ectopic and increased expression of Fasciclin II alters motoneuron growth cone guidance. Neuron. 1994 Sep;13(3):507-23.
Lin JW, Ju W, Foster K, Lee SH, Ahmadian G, Wyszynski M, Wang YT, Sheng M. Distinct molecular mechanisms and divergent endocytotic pathways of AMPA receptor internalization. Nat Neurosci. 2000 Dec;3(12):1282-90.
Liebl FL, Werner KM, Sheng Q, Karr JE, McCabe BD, Featherstone DE. Genome-wide P-element screen for Drosophila synaptogenesis mutants. J Neurobiol. 2006 Mar;66(4):332-47
Loyola, A.; Huang, J.-Y.; LeRoy, G.; Hu, S.; Wang, Y.-H.; Donnelly, R. J.; Lane, W. S.; Lee, S.-C.; Reinberg, D. Functional analysis of the subunits of the chromatin assembly factor RSF. Molec. Cell. Biol. 23: 6759-6768, 2003.
Liu W, Seto J, Sibille E, Toth M. The RNA Binding Domain of Jerky Consists of Tandemly Arranged Helix-Turn-Helix/Homeodomain-like Motifs and Binds Specific Sets of mRNAs Mol and Cel. Biol, June 2003, Vol 23, No 12, pp 4083-93
Luscher C, Xia H, Beattie EC, Carroll RC, von Zastrow M, Malenka RC, Nicoll RA. Role of AMPA receptor cycling in synaptic transmission and plasticity. Neuron. 1999 Nov;24(3):649-58.
Luthi A, Chittajallu R, Duprat F, Palmer MJ, Benke TA, Kidd FL, Henley JM, Isaac JT, Collingridge GL.Hippocampal LTD expression involves a pool of AMPARs regulated by the NSF-GluR2 interaction. Neuron. 1999 Oct;24(2):389-99.
Malinow R, Malenka RC. AMPA receptor trafficking and synaptic plasticity. Annu Rev Neurosci. 2002;25:103-26
Man HY, Wang Q, Lu WY, Ju W, Ahmadian G, Liu L, D'Souza S, Wong TP, Taghibiglou C, Lu J, Becker LE, Pei L, Liu F, Wymann MP, MacDonald JF, Wang YT. Activation of PI3-kinase is required for AMPA receptor insertion during LTP of mEPSCs in cultured hippocampal neurons. Neuron. 2003 May 22;38(4):611-24.
Mao TL, Hsu CY, Yen MJ, Gilks B, Sheu JJ, Gabrielson E, Vang R, Cope L, Kurman RJ, Wang TL, Shih IeM. Expression of Rsf-1, a chromatin-remodeling gene, in ovarian and breast carcinoma. Hum Pathol. 2006 Sep;37(9):1169-75.
Marie B, Sweeney ST, Poskanzer KE, Roos J, Kelly RB, Davis GW. Dap160/intersectin scaffolds the periactive zone to achieve high-fidelity endocytosis and normal synaptic growth. Neuron. 2004 Jul 22;43(2):207-19.
Marques G, Bao H, Haerry TE, Shimell MJ, Duchek P, Zhang B, O'Connor MB. The Drosophila BMP type II receptor Wishful Thinking regulates neuromuscular synapse morphology and function. Neuron. 2002 Feb 14;33(4):529-43.

Marrus S.B., Portman, S.L., Allen, M.J., Moffat, K.G., and DiAntonio, A. (2004). Differential Localization of Glutamate Receptor Subunits at the Drosophila Neuromuscular Junction. The Journal of Neuroscience *24*, 1406-1415.

Mattson, M. P., and Camandola, S. (2001). NF-kappaB in neuronal plasticity and neurodegenerative disorders. J Clin Invest *107*, 247-254.

Mattson, M. P., Culmsee, C., Yu, Z., and Camandola, S. (2000a). Roles of nuclear factor kappaB in neuronal survival and plasticity. J Neurochem *74*, 443-456.

Mattson, M. P., Culmsee, C., and Yu, Z. F. (2000b). Apoptotic and antiapoptotic mechanisms in stroke. Cell Tissue Res *301*, 173-187.

Mattson, M. P., and Meffert, M. K. (2006). Roles for NF-kappaB in nerve cell survival, plasticity, and disease. Cell Death Differ *13*, 852-860.

McCabe BD, Hom S, Aberle H, Fetter RD, Marques G, Haerry TE, Wan H, O'Connor MB, Goodman CS, Haghighi AP. Highwire regulates presynaptic BMP signaling essential for synaptic growth. Neuron. 2004 Mar 25;41(6):891-905.

McCabe BD, Marques G, Haghighi AP, Fetter RD, Crotty ML, Haerry TE, Goodman CS, O'Connor MB. The BMP homolog Gbb provides a retrograde signal that regulates synaptic growth at the Drosophila neuromuscular junction. Neuron. 2003 Jul 17;39(2):241-54.

Meberg, P. J., Kinney, W. R., Valcourt, E. G., and Routtenberg, A. (1996). Gene expression of the transcription factor NF-kappa B in hippocampus: regulation by synaptic activity. Brain Res Mol Brain Res *38*, 179-190.

Meffert, M. K., and Baltimore, D. (2005). Physiological functions for brain NF-kappaB. Trends Neurosci *28*, 37-43.

Meffert, M. K., Chang, J. M., Wiltgen, B. J., Fanselow, M. S., and Baltimore, D. (2003). NF-kappa B functions in synaptic signaling and behavior. Nat Neurosci *6*, 1072-1078.

Menon KP, Sanyal S, Habara Y, Sanchez R, Wharton RP, Ramaswami M, Zinn K.The translational repressor Pumilio regulates presynaptic morphology and controls postsynaptic accumulation of translation factor eIF-4E. Neuron. 2004 Nov 18;44(4):663-76.

Mellor J. It takes a PHD to read the histone code. Cell. 2006 Jul 14;126(1):22-4.

Moon R.T., Bowerman, B., Boutros, M., Perrimon, N. (2002) The promise and perils of Wnt signaling through beta-catenin. Science *296*,1644-6.

Narayanan R, Kramer H, Ramaswami M. Drosophila endosomal proteins hook and deep orange regulate synapse size but not synaptic vesicle recycling. J Neurobiol. 2000 Nov 5;45(2):105-19.

Nicolai, M., Lasbleiz, C., and Dura, J. M. (2003). Gain-of-function screen identifies a role of the Src64 oncogene in Drosophila mushroom body development. J Neurobiol *57*, 291-302.

Nicolas, E., Reichhart, J.M., Hoffmann, J.A., Lemaitre B. (1998) In vivo regulation of the IkappaB homologue cactus during the immune response of Drosophila. J Biol Chem *273*, 10463-9.

Nilsson EE, Skinner MK. Role of transforming growth factor beta in ovarian surface epithelium biology and ovarian cancer. Reprod Biomed Online. 2002 Nov-Dec;5(3):254-8.

Nishimune A, Isaac JT, Molnar E, Noel J, Nash SR, Tagaya M, Collingridge GL, Nakanishi S, Henley JM. NSF binding to GluR2 regulates synaptic transmission. Neuron. 1998 Jul;21(1):87-97.
Noel J, Ralph GS, Pickard L, Williams J, Molnar E, Uney JB, Collingridge GL, Henley JM.Surface expression of AMPA receptors in hippocampal neurons is regulated by an NSF-dependent mechanism. Neuron. 1999 Jun;23(2):365-76.
Norris, J. L., and Manley, J. L. (1992). Selective nuclear transport of the Drosophila morphogen dorsal can be established by a signaling pathway involving the transmembrane protein Toll and protein kinase A. Genes Dev *6*, 1654-1667.
Nose, A., Van Vactor, D., Auld, V., and Goodman, C. S. (1992). Development of neuromuscular specificity in Drosophila. Cold Spring Harb Symp Quant Biol *57*, 441-449.
Ohno CK, Petkovich M. FTZ-F1 beta, a novel member of the Drosophila nuclear receptor family. Mech Dev. 1993 Jan;40(1-2):13-24
Ohno CK, Ueda H, Petkovich M. The Drosophila nuclear receptors FTZ-F1 alpha and FTZ-F1 beta compete as monomers for binding to a site in the fushi tarazu gene. Mol Cell Biol. 1994 May;14(5):3166-75.
O'Mahony, A., Raber, J., Montano, M., Foehr, E., Han, V., Lu, S. M., Kwon, H., LeFevour, A., Chakraborty-Sett, S., and Greene, W. C. (2006). NF-kappaB/Rel regulates inhibitory and excitatory neuronal function and synaptic plasticity. Mol Cell Biol *26*, 7283-7298.
O'Riordan, K. J., Huang, I. C., Pizzi, M., Spano, P., Boroni, F., Egli, R., Desai, P., Fitch, O., Malone, L., Ahn, H. J., *et al*. (2006). Regulation of nuclear factor kappaB in the hippocampus by group I metabotropic glutamate receptors. J Neurosci *26*, 4870-4879.
Pan D, Courey AJ. The same dorsal binding site mediates both activation and repression in a context-dependent manner. EMBO J. 1992 May;11(5):1837-42.
Parnas D, Haghighi AP, Fetter RD, Kim SW, Goodman CS. Regulation of postsynaptic structure and protein localization by the Rho-type guanine nucleotide exchange factor dPix. Neuron. 2001 Nov 8;32(3):415-24.
Paradis S, Sweeney ST, Davis GW.Homeostatic control of presynaptic release is triggered by postsynaptic membrane depolarization. Neuron. 2001 Jun;30(3):737-49.
Park M, Penick EC, Edwards JG, Kauer JA, Ehlers MDRecycling endosomes supply AMPA receptors for LTP. Science. 2004 Sep 24;305(5692):1972-5.
Perez-Otano I, Ehlers MD. Homeostatic plasticity and NMDA receptor trafficking. Trends Neurosci. 2005 May;28(5):229-38
Petersen, S. A., Fetter, R. D., Noordermeer, J. N., Goodman, C. S., and DiAntonio, A. (1997). Genetic analysis of glutamate receptors in Drosophila reveals a retrograde signal regulating presynaptic transmitter release. Neuron 19, 1237-1248.
Pielage J, Fetter RD, Davis GW. A postsynaptic spectrin scaffold defines active zone size, spacing, and efficacy at the Drosophila neuromuscular junction. J Cell Biol. 2006 Nov 6;175(3):491-503.
Prybylowski K, Chang K, Sans N, Kan L, Vicini S, Wenthold RJ. The synaptic localization of NR2B-containing NMDA receptors is controlled by interactions with PDZ proteins and AP-2. Neuron. 2005 Sep 15;47(6):845-57.
Qin G., Schwarz, T., Kittel R.J., Schmid A., Rasse T.M., Kappei D., Ponimaskin E., Heckmann M., Sigrist S.J. (2005). Four Different Subunits Are Essential for

Expressing the Synaptic Glutamate Receptor at Neuromusclar Junctions of Drosophila. J. Neurosci *25*, 3209-3218.
Qiu, P., Pan, P. C., and Govind, S. (1998). A role for the Drosophila Toll/Cactus pathway in larval hematopoiesis. Development *125*, 1909-1920.
Rasse TM, Fouquet W, Schmid A, Kittel RJ, Mertel S, Sigrist CB, Schmidt M, Guzman A, Merino C, Qin G, Quentin C, Madeo FF, Heckmann M, Sigrist SJ. Glutamate receptor dynamics organizing synapse formation in vivo. Nat Neurosci. 2005 Jul;8(7):898-905.
Ravdin P, Axelrod D (1977) Fluorescent tetramethyl rhodamine derivatives of alpha-bungarotoxin: preparation, separation, and characterization. Anal Biochem 80:585-592.
Rawson JM, Lee M, Kennedy EL, Selleck SB. Drosophila neuromuscular synapse assembly and function require the TGF-beta type I receptor saxophone and the transcription factor Mad. J Neurobiol. 2003 May;55(2):134-50.
Reach, M., Galindo, R.L., Towb, P., Allen, J.L., Karin, M., Wasserman, S.A. (1996). A Gradient of Cactus Protein Degradation Establishes Dorsoventral Polarity in the Drosophila Embryo. Developmental Biology *180*, 353-364.
Reiss M. TGF-beta and cancer. Microbes Infect. 1999 Dec;1(15):1327-47
Rheuben MB, Yoshihara M, Kidokoro Y. Ultrastructural correlates of neuromuscular junction development. Int Rev Neurobiol. 1999;43:69-92.
Rivera-Pomar R, Niessing D, Schmidt-Ott U, Gehring WJ, Jackle H.. RNA binding and translational suppression by bicoid Nature, Vol 379, 22 February 1996
Rohrbough J, Grotewiel MS, Davis RL, Broadie K. Integrin-mediated regulation of synaptic morphology, transmission, and plasticity. J Neurosci. 2000 Sep 15;20(18):6868-78.
Rollenhagen A, Lubke JH.The morphology of excitatory central synapses: from structure to function. Cell Tissue Res. 2006 Nov;326(2):221-37.
Roos J, Kelly RB. Dap160, a neural-specific Eps15 homology and multiple SH3 domain-containing protein that interacts with Drosophila dynamin. J Biol Chem. 1998 Jul 24;273(30):19108-19.
Rorth P, Szabo K, Bailey A, Laverty T, Rehm J, Rubin GM, Weigmann K, Milan M, Benes V, Ansorge W, Cohen SM. Systematic gain-of-function genetics in Drosophila. Development. 1998 Mar;125(6):1049-57.
Roseman RR, Johnson EA, Rodesch CK, Bjerke M, Nagoshi RN, Geyer PK. A P element containing suppressor of hairy-wing binding regions has novel properties for mutagenesis in Drosophila melanogaster. Genetics. 1995 Nov;141(3):1061-74.
Roth, S., Hiromi, Y., Godt, D., and Nusslein-Volhard, C. (1991). cactus, a maternal gene required for proper formation of the dorsoventral morphogen gradient in Drosophila embryos. Development *112*, 371-388.
Saitoe M, Tanaka S, Takata K, Kidokoro Y. Neural activity affects distribution of glutamate receptors during neuromuscular junction formation in Drosophila embryos. Dev Biol. 1997 Apr 1;184(1):48-60.
Saitoe M, Koshimoto H, Hirano M, Suga T, Kidokoro Y. Distribution of functional glutamate receptors in cultured embryonic Drosophila myotubes revealed using focal release of L-glutamate from caged compound by laser. J Neurosci Methods. 1998 Apr 30;80(2):163-70.

Saitoe M, Schwarz TL, Umbach JA, Gundersen CB, Kidokoro Y. Absence of junctional glutamate receptor clusters in Drosophila mutants lacking spontaneous transmitter release. Science. 2001 Jul 20;293(5529):514-7.
Schmidt-Ullrich, R., Memet, S., Lilienbaum, A., Feuillard, J., Raphael, M., and Israel, A. (1996). NF-kappaB activity in transgenic mice: developmental regulation and tissue specificity. Development *122*, 2117-2128.
Schupbach, T., Wieschaus, E. (1989). Female Sterile mutations on the second chromosome of Drosophila Melanogaster I. Maternal effect mutations. Genetics *121*, 101-117.
Schupbach, T. Wieschaus, E. E. (1991). Female Sterile Mutations on the Second Chromosome of Drosophila Melanogaster. II. Mutations Blocking Ogenesis or Altering Egg Morphology. Genetics *129*, 1119-1136.
Schuster CM, Davis GW, Fetter RD, Goodman CS. Genetic dissection of structural and functional components of synaptic plasticity. II. Fasciclin II controls presynaptic structural plasticity. Neuron. 1996a Oct;17(4):655-67.
Schuster CM, Davis GW, Fetter RD, Goodman CS. Genetic dissection of structural and functional components of synaptic plasticity. I. Fasciclin II controls synaptic stabilization and growth. Neuron. 1996b Oct;17(4):641-54.
Schuster, C.M., Ultsch, A., Schloss. P., Cox, J.A., Schmitt, B., Betz, H. (1991). Molecular cloning of an invertebrate glutamate receptor subunit expressed in Drosophila muscle. Science *254*, 112-114.
Scott DB, Michailidis I, Mu Y, Logothetis D, Ehlers MD. Endocytosis and degradative sorting of NMDA receptors by conserved membrane-proximal signals. J Neurosci. 2004 Aug 11;24(32):7096-109.
Sekine-Aizawa Y, Huganir RL (2004) Imaging of receptor trafficking by using alpha-bungarotoxin-binding-site-tagged receptors. Proc Natl Acad Sci U S A 101:17114-17119.
Shamay, M.; Barak, O.; Doitsh, G.; Ben-Dor, I.; Shaul, Y. Hepatitis B virus pX interacts with HBXAP, a PHD finger protein to coactivate transcription. J. Biol. Chem. 277: 9982-9988, 2002.
Shamay, M.; Barak, O.; Shaul, Y. HBXAP, a novel PHD-finger protein, possesses transcription repression activity. Genomics 79: 523-529, 2002.
Sen, R., and Baltimore, D. (1986). Inducibility of kappa immunoglobulin enhancer-binding protein Nf-kappa B by a posttranslational mechanism. Cell *47*, 921-928.
Shen, B., and Manley, J. L. (1998). Phosphorylation modulates direct interactions between the Toll receptor, Pelle kinase and Tube. Development *125*, 4719-4728.
Shen B, and Manley, J. L. (2002). Pelle kinase is activated by autophosphorylation during Toll signaling in Drosophila. Development *129*, 1925-1933.
Sherwood NT, Sun Q, Xue M, Zhang B, Zinn K.Drosophila spastin regulates synaptic microtubule networks and is required for normal motor function. PLoS Biol. 2004 Dec;2(12):e429.
Shi SH, Hayashi Y, Petralia RS, Zaman SH, Wenthold RJ, Svoboda K, Malinow R. Rapid spine delivery and redistribution of AMPA receptors after synaptic NMDA receptor activation. Science. 1999 Jun 11;284(5421):1811-6.
Shih, I.-M.; Sheu, J. J.-C.; Santillan, A.; Nakayama, K.; Yen, M. J.; Bristow, R. E.; Vang, R.; Parmigiani, G.; Kurman, R. J.; Trope, C. G.; Davidson, B.; Wang, T.-L. :

Amplification of a chromatin remodeling gene, Rsf-1/HBXAP, in ovarian carcinoma. Proc. Nat. Acad. Sci. 102: 14004-14009, 2005.
Shirokawa, J. M., and Courey, A. J. (1997). A direct contact between the dorsal rel homology domain and Twist may mediate transcriptional synergy. Mol Cell Biol *17*, 3345-3355.
Sigrist SJ, Reiff DF, Thiel PR, Steinert JR, Schuster CM. Experience-dependent strengthening of Drosophila neuromuscular junctions. J Neurosci. 2003 Jul 23;23(16):6546-56.
Sigrist SJ, Thiel PR, Reiff DF, Lachance PE, Lasko P, Schuster CM. Postsynaptic translation affects the efficacy and morphology of neuromuscular junctions. Nature. 2000 Jun 29;405(6790):1062-5.
Steiner P, Alberi S, Kulangara K, Yersin A, Sarria JC, Regulier E, Kasas S, Dietler G, Muller D, Catsicas S, Hirling H. Interactions between NEEP21, GRIP1 and GluR2 regulate sorting and recycling of the glutamate receptor subunit GluR2. EMBO J. 2005 Aug 17;24(16):2873-84Sanyal S, Kim SM, Ramaswami M. Retrograde regulation in the CNS; neuron-specific interpretations of TGF-beta signaling. Neuron. 2004 Mar 25;41(6):845-8.
Stellwagen, D., Beattie, E. C., Seo, J. Y., and Malenka, R. C. (2005). Differential regulation of AMPA receptor and GABA receptor trafficking by tumor necrosis factor-alpha. J Neurosci *25*, 3219-3228.
Stellwagen, D., and Malenka, R. C. (2006). Synaptic scaling mediated by glial TNF-alpha. Nature *440*, 1054-1059.
Sweeney ST, Davis GW. Unrestricted synaptic growth in spinster-a late endosomal protein implicated in TGF-beta-mediated synaptic growth regulation.Neuron. 2002 Oct 24;36(3):403-16.
Thisse C., Perrin-Schmitt F., Stoetzel C., Thisse B. Sequence-specific transactivation of the Drosophila twist gene by the dorsal gene product. Cell 65:1191-1201 (1991)
Thomas U, Kim E, Kuhlendahl S, Koh YH, Gundelfinger ED, Sheng M, Garner CC, Budnik V. Synaptic clustering of the cell adhesion molecule fasciclin II by discs-large and its role in the regulation of presynaptic structure. Neuron. 1997 Oct;19(4):787-99.
Torroja L, Packard M, Gorczyca M, White K, Budnik V. The Drosophila beta-amyloid precursor protein homolog promotes synapse differentiation at the neuromuscular junction. J Neurosci. 1999 Sep 15;19(18):7793-803.
Towb, P., Bergmann, A., Wasserman, S.A. (2001) The protein kinase Pelle mediates feedback regulation in the Drosophila Toll signaling pathway. *Development* 128, 4729-36.
Turrigiano GG, Nelson SB. Homeostatic plasticity in the developing nervous system. Nat Rev Neurosci. 2004
Ullrich O, Reinsch S, Urbe S, Zerial M, Parton RG. Rab11 regulates recycling through the pericentriolar recycling endosome. J Cell Biol. 1996 Nov;135(4):913-24.
van Roessel P, Elliott DA, Robinson IM, Prokop A, Brand AH. Independent regulation of synaptic size and activity by the anaphase-promoting complex. Cell. 2004 Nov 24;119(5):707-18.
Wagh DA, Rasse TM, Asan E, Hofbauer A, Schwenkert I, Durrbeck H, Buchner S, Dabauvalle MC, Schmidt M, Qin G, Wichmann C, Kittel R, Sigrist SJ, Buchner E. Bruchpilot, a protein with homology to ELKS/CAST, is required for structural

integrity and function of synaptic active zones in Drosophila. Neuron. 2006 Mar 16;49(6):833-44.
Wan HI, DiAntonio A, Fetter RD, Bergstrom K, Strauss R, Goodman CS. Highwire regulates synaptic growth in Drosophila. Neuron. 2000 May;26(2):313-29.
Wang YT, Linden DJ. Expression of cerebellar long-term depression requires postsynaptic clathrin-mediated endocytosis. Neuron. 2000 Mar;25(3):635-47.
Wu C, Wairkar YP, Collins CA, DiAntonio A. Highwire function at the Drosophila neuromuscular junction: spatial, structural, and temporal requirements. J Neurosci. 2005 Oct 19;25(42):9557-66.
Xiao H, Sandaltzopoulos R, Wang HM, Hamiche A, Ranallo R, Lee KM, Fu D, Wu C. Dual functions of largest NURF subunit NURF301 in nucleosome sliding and transcription factor interactions. Mol Cell. 2001 Sep;8(3):531-43.
Yoshihara M, Rheuben MB, Kidokoro Y. Transition from growth cone to functional motor nerve terminal in Drosophila embryos. J Neurosci. 1997 Nov 1;17(21):8408-26.
Zhou Q, Xiao M, Nicoll RA. Contribution of cytoskeleton to the internalization of AMPA receptors. Proc Natl Acad Sci U S A. 2001 Jan 30;98(3):1261-6
Zito K, Parnas D, Fetter RD, Isacoff EY, Goodman CS. Watching a synapse grow: noninvasive confocal imaging of synaptic growth in Drosophila. Neuron. 1999 Apr;22(4):719-29.
Zinsmaier KE, Eberle KK, Buchner E, Walter N, Benzer S. Paralysis and early death in cysteine string protein mutants of Drosophila. Science. 1994 Feb 18;263(5149):977-80.
Zito K, Parnas D, Fetter RD, Isacoff EY, Goodman CS. Watching a synapse grow: noninvasive confocal imaging of synaptic growth in Drosophila. Neuron. 1999 Apr;22(4):719-29.

Publishing Agreement

It is the policy of the University to encourage the distribution of all theses and dissertations. Copies of all UCSF theses and dissertations will be routed to the library via the Graduate Division. The library will make all theses and dissertations accessible to the public and will preserve these to the best of their abilities, in perpetuity.

I hereby grant permission to the Graduate Division of the University of California, San Francisco to release copies of my thesis or dissertation to the Campus Library to provide access and preservation, in whole or in part, in perpetuity.

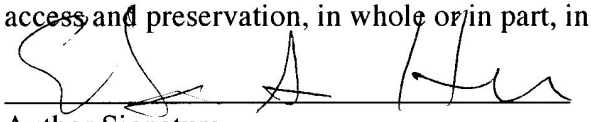

Author Signature

3/28/07

Date